PREPARATION OF Al-Ti-ALLOY CLOSED-CELL METAL FOAMS VIA FOAMING OF POWDER COMPACTS

A Thesis Submitted to
the Graduate School of Engineering and Sciences of
İzmir Institute of Technology
in Partial Fulfillment of the Requirements for the Degree of

MASTER OF SCIENCE

in Mechanical Engineering

by
Nurettin Deniz KARSU

January 2008
İZMİR

We approve the thesis of **Nurettin Deniz KARSU**

_____
Prof. Dr. Mustafa GÜDEN
Supervisor

_____
Prof. Dr. Muhsin ÇİFTÇİOĞLU
Committee Member

_____
Assoc. Prof. Dr. Sedat AKKURT
Committee Member

16 January 2008
Date

_____
Assoc. Prof. Dr. Metin TANOĞLU
Head of the Mechanical Engineering Department

_____
Prof. Dr. Hasan BÖKE
Dean of the Graduate School
of Engineering and Science

ACKNOWLEDGEMENTS

I would like to express my deepest thanks to my advisor Prof. Dr. Mustafa GÜDEN for his guidance and endless support. Besides I am also grateful to Sinan YÜKSEL for his patience at training period for the manufacturing steps of this study and for his help and friendship throughout. Lastly, I am thankful to the support from TUBİTAK (Project MAG 106M186).

ABSTRACT

PREPARATION OF Al-Ti-ALLOY CLOSED-CELL METAL FOAMS VIA FOAMING OF POWDER COMPACTS

The foaming behavior of 5 wt% 30-45, 45-56, 56-90, 90-106, 106-160 and 160-200 μm size spherical Ti6Al4V particle-added Al powder compacts were investigated for determining the effects of wetted particles on the expansion and stability of Al powder compacts. In order to determine the effect of particle-addition on the foaming behavior, Al compacts without particle addition prepared with same method were also foamed. Foaming experiments were performed using an in-situ foam expansion measuring system at 700-730 ºC. Small compression test samples were further core drilled from Ti6Al4V-Al foam samples and tested at quasi-static strain rates.

Al compacts showed the characteristic expansion-time curve, composing of 4 distinct regions. The expansion of 5 wt% Ti6Al4V-added compacts was found to be relatively low at small size particle additions, but increased with increasing particle size. Measurements of foam expansions of 30-45 μm size Ti6Al4V-added compacts with various weight percentages of particles showed that when the wt% of particles is lower than 2 wt%, the expansion behavior of the compacts became very similar to that of pure Al. Microscopic studies have further shown that Ti6Al4V addition reduced the drainage as compared with pure Al compacts. In foaming of Ti6Al4V-Al compacts, the liquid Al reacted with Ti6Al4V particles and formed $TiAl_3$ particles. In relatively small size particle-added foams, $TiAl_3$ particles dispersed through cell walls and cell edges, but at increased particle size, these particles were found next to the Ti6Al4V particles. The reduced drainage and lower foam expansions in the foaming of Ti6Al4V-added compacts were discussed based on the foam stabilization models in the literature. The reduced foamability of the compacts in small particle size Ti6Al4V addition was attributed to relatively high viscosities, due to higher cumulative surface area of the particles and higher rate of reaction between liquid Al and Ti6Al4V. The lower compression strength measured in Ti6Al4V-added foams was attributed to small specimen sizes, which could not show the mechanical properties of the bulk material.

ÖZET

TOZ KOMPAKT KÖPÜKLEŞTİRME YÖNTEMİ İLE Al-Ti ALAŞIMLI KAPALI HÜCRE METAL KÖPÜKLERİN HAZIRLANMASI

Al toz kompaktların köpükleştirilmesinde, ıslatılmış parçacık etkisinin uzamaya ve köpük kararlılığına etkilerini belirlemek için ağırlıkça %5 oranında 30–45, 45–56, 56–90, 90–106, 106–160 ve 160–200 μm boyutlu küresel Ti6Al4V tozu içeren Al kompaktların köpükleşme davranışları gözlemlenmiştir. Parçacık etkisini belirlemek için, parçacık içermeyen Al kompaktlar da hazırlanıp, köpükleştirilmiştir. Köpükleşme deneyleri deney esnasında uzamayı ölçebilecek bir sistemle 700–730 ºC'de yapılmıştır. Köpükleşen kompaktlardan göbek delme yöntemi ile elde edilen küçük numuneler statik hızlarda basma testine tabi tutulmuşlardır.

Al kompaktlar 4 bölgeden oluşan karakteristik uzama göstermişlerdir. Ağırlıkça %5 oranında Ti6Al4V içeren kompaktlarda küçük parçacık boyutlarında, uzamanın nispi olarak az olduğu ve uzamanın, parçacık boyutunun artması ile arttığı bulunmuştur. Ağırlık oranınca farklı, 30–45 μm boyutunda Ti6Al4V içeren kompaktlarla yapılan köpükleştirme deneylerinde, ağırlıkça %2'den daha az oranda Ti6Al4V içeren kompaktların Al kompaktlara benzer uzamalar gösterdiği bulunmuştur. Mikroskobik çalışmalar, Ti6Al4V katkısının drenajı azalttığını göstermiştir. Köpükleşme esnasında sıvı Al ile Ti6Al4V reaksiyona girerek $TiAl_3$ parçacıkları oluşturmuştur. Nispeten küçük boyutlu parçacıklar içeren kompaktlarda reaksiyon tabakası hücre duvar ve köşelerine dağılım gösterirken, büyük parçacık içeren kompaktlarda ise bu tabaka parçacığa bağlı kalmıştır. Ti6Al4V içeren kompaktlarda düşük drenaj ve azalan köpükleşme, literatürdeki mevcut kararlılık modelleri kullanılarak tartışılmıştır. Köpükleşmenin küçük parçacık içeren kompaktlarda azalması, toplam parçacık yüzey alanı yüksek olması ve daha fazla $TiAl_3$ parçacık oluşumu ile artan viskoziteye bağlanmıştır. Ti6Al4V içeren kompaktlarda ölçülen düşük basma mukavemetinin, kullanılan küçük boyutlu test numunelerinin kaba malzemenin özelliklerini göstermemesinden kaynaklanmaktadır.

TABLE OF CONTENTS

LIST OF FIGURES

Figure **Page**

LIST OF TABLES

Table **Page**

CHAPTER 1

INTRODUCTION

Foams are characterized by regularly distributed arrays of cells. The cells are formed by the liquid phase while the gas phase, in most cases air, fills the space in between the cells. This way of structuring of liquid and gas phases is also referred as cellular and often observed in natural materials such as bone and wood. If the cell material is replaced with a solid metal, the resultant structure is usually referred as "metal foam" or "foamed metal". Metal foams have unique mechanical and physical properties, which make them attractive in structural and functional applications. They are very light, possessing densities as low as one tenth of the density of the metal of which they are made. They crush under compressive loads almost at a constant load until about very large strains, allowing the absorption of a great deal of deformation energy. The energy absorbing capabilities of metal foams make them attractive materials to be potentially used in crash and blast protections. One scenario is to use metal foams as cores in between metal plates to make foam sandwich structures for blast protection of buildings and military vehicles. Another one is the filling of the bumpers and empty spaces in the car body to prevent shock wave passage through the passenger compartment in accidents involving collisions.

The mechanical properties of the metal foams are mainly dictated by the distribution of the cell material in the cell walls (surface), edges and nodes. In open cells, the metal phase is distributed at the cell edges and vortex, where 3 and 4 cells meet, respectively. While in the closed cell foams, additional metal phase forms the cell walls, where two cells meet. The closed cell metal foams behave very much similar to the open cell foams since the cell walls are much thinner than cell edges. The final foam structure including the relative distribution of the metal phase in the cell walls, edges and nodes is resulted by the foaming process, which is usually conducted in liquid state at relatively elevated temperatures. The structure of liquid foams changes constantly over time by various types of events including drainage, cell wall rupture and coarsening. If the change in the foam structure is relatively slow, the foam is said to be kinetically stable. In other words, a stable foam shows negligible changes in the structure with time. The foam stabilization plays an important role in forming of

controllable homogeneous foam structures. In aqueous foams, the stabilization is achieved by (a) surfactants and (b) small particles which act as elastic separator between the cells. It is noted that only the latter can be used for the metal foam stabilization.

Al closed-cell foams are currently manufactured by several different processes, in which the liquid foam is stabilized by the addition of ceramic particles to the liquid metal either in-situ or ex-situ. In Alcan Foaming Process, in which the liquid metal is foamed by gas injection, the liquid foam stabilization is achieved by adding SiC particles (Banhart 2000). In the Alporas process, the viscosity of the liquid metal is adjusted by Ca-addition into the melt, which results in the formation of oxide particles by internal oxidation (Miyoshi, et al. 2000). In foaming of powder compact process, foam stabilization was is ascribed the metal oxide filaments, which are remnants of the thin oxide layer on the aluminum powders (Banhart 2000). The ceramic particle addition in the foaming of powder compact process was subjected to several studies and the results of these investigations may be summarized as follows. TiB_2 addition, increased the plateau stresses of Al foams, however it was not effective in long-term foam stabilization (Kennedy and Asavavisitchai 2004). Contrary to TiB_2-addition, SiC_p-addition of 3 wt% was shown to improve the foam stability of Al powder compacts (Kennedy and Asavavisithchai 2004). These showed that ceramic particle addition was effective.

In the present thesis, the effects Ti6Al4V particle addition on the foaming and quasi-static crushing behavior of Al powder compacts were investigated. Ti6Al4V powders are known to be wetted by the liquid Al and therefore are good models for studying the effect of wetted particles on the foamability of Al powder compacts. In addition, Ti particles react with liquid Al, forming precipitates which increase the viscosity of the foam in-situ. The effect of Ti6Al4V-addition on the foaming behavior was determined by comparing the expansions of the Al compacts processed under the same conditions. Compression testing on the prepared composite and Al foams was conducted in order to determine the effect of Ti6Al4V-addition on the crushing behavior.

CHAPTER 2

MANUFACTURING METHODS, MECHANICAL PROPERTIES AND APPLICATION AREAS OF CLOSED-CELL ALUMINUM FOAMS

2.1. Manufacturing Methods of Closed-Cell Aluminum Foams

Aluminum closed-cell foam processing methods can be divided into two major groups: direct and indirect foaming. Designed open cell structures are commercially manufactured via continuous or batch type casting methods, e.g. cell forming mould removal method used by Duocel for the production of open cell Al and Al alloy foams (Gibson 2000). Self forming structures are manufactured via direct method either by gas injection through (Alcan/Cymat) or gas forming element addition (Alporas) into the liquid metal. In indirect approach, designed structures are manufactured by melting or partial melting of powder compacts that contain a gas evolving element (e.g.TiH_2) (Banhart 2000, Banhart 2006).

2.1.1. Direct Foaming

Metallic melts must be enough stable during the foaming process to form an effective cellular structure. Ceramic powders and/or alloying elements are added to the liquid metal to increase the stability of the bubbles produced. The first manufacturing method for foams of aluminum and aluminum alloy melts is based on gas injection into molten metal (Banhart 2000). The method is currently used by Alcan N. Hydro Aluminum in Norway and Cymat Corporations in Canada for the production of composite SiC/Al foams. The process is shown schematically in Figure 2.1.

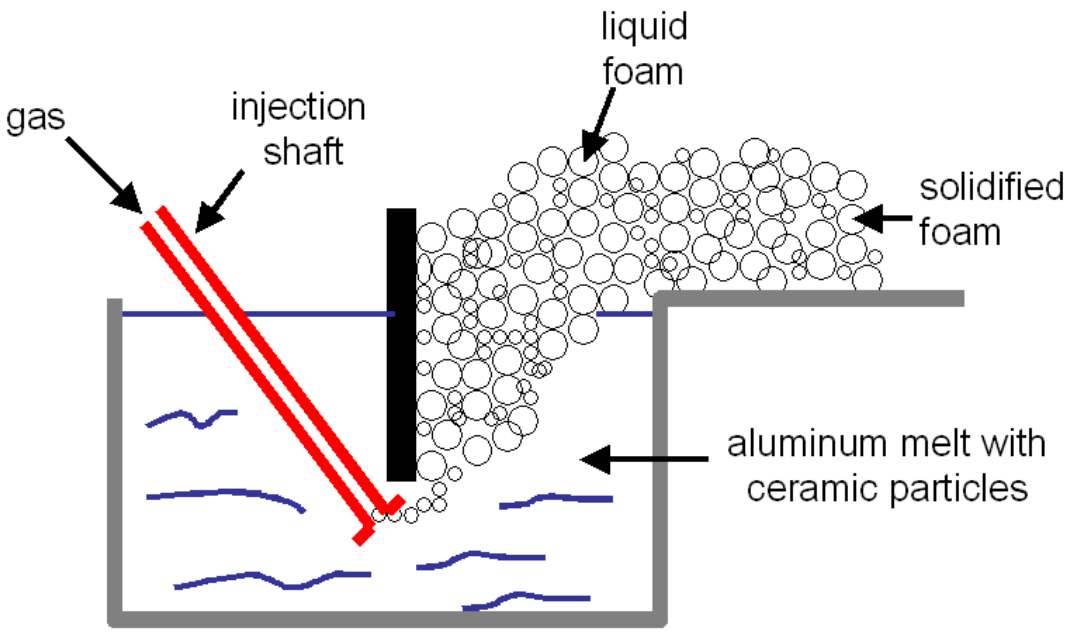

Figure 2.1. Schematic of direct foaming by gas injection

Ceramic particles such as silicon-carbide, aluminum-oxide, or magnesium-oxide are added to the liquid metal to enhance the viscosity of the melt. The size of the particles ranges between 5 and 20 micrometers, while the weight percentages of the particles vary between 10% and 20% (Raj and Daniel 2007). In the second stage, air, argon or nitrogen gas is injected into aluminum melt by specially designed rotating impellers or vibrating nozzles, introducing and distributing gas bubbles through the melt. The gas bubbles stabilized by ceramic particles rise and collect at the surface of the melt where the liquid foam is pulled by a conveyor belt. Finally, the foam is cooled down below the melting point of the metal matrix composite. The solidified foam can be used directly or cut into desired shape. The hard particles in the foam matrix may make the cutting process difficult.

This foaming process has the capability for the continuous production of closed-cell foams of 1 m wide to 0.2 m thick slabs. Typical density, average cell size and cell wall thickness of the Al foam produced by this method are 0.069-0.54g/cm^3, 3-25 mm, and 50-85 μm, respectively (Kenny 1996). Average cell size, average cell wall thickness and density depend on the changeable processing parameters such as gas injection rate and rotating shaft speed. The conveyor belt used to carry the liquid foam from the melt surface creates shearing forces, leading to the formation of elongated cells (Beals and Thompson 1997).

Another way of foaming a liquid metal directly is to add a blowing agent (e.g. TiH_2 for Al foam) to the molten metal. As the foaming agent decomposes, the released gas (e.g. hydrogen from TiH_2) drives the foaming process (Miyoshi, et al. 2000). This method is known as ALPORAS foaming process and has been used since 1986 by Shinko Wire Co. (Japan). Before foaming by TiH_2 addition, 1.5 wt% calcium metal is added into the liquid Al at 680 ºC as thickening agent and then the melt is stirred quickly (Figure 2.2). The viscosity of the melt increases with increasing stirring time because of the formation of oxide and/or metallic compounds (calcium oxide, calcium-aluminum oxide, or Al_4Ca intermetallic), which thickens the metallic melt (Miyoshi, et al. 2000). Both the volume fraction of calcium addition and stirring rate affect the viscosity of Al melt (Figure 2.3). In a later stage of the process, after adjusting the viscosity of the liquid metal, TiH_2 with an amount of 1.6 wt % is added into the melt, which releases hydrogen gas according to the following reaction:

$$TiH_2\ (s) \rightarrow Ti\ (s) + H_2\ (g)$$

Above reaction results in the expansion of the liquid metal and foamed metal fills foaming vessel at a constant pressure. Finally, the liquid foam is cooled down below the melting point of the foamed alloy quickly and the solidified Al foam is further processed for specific applications.

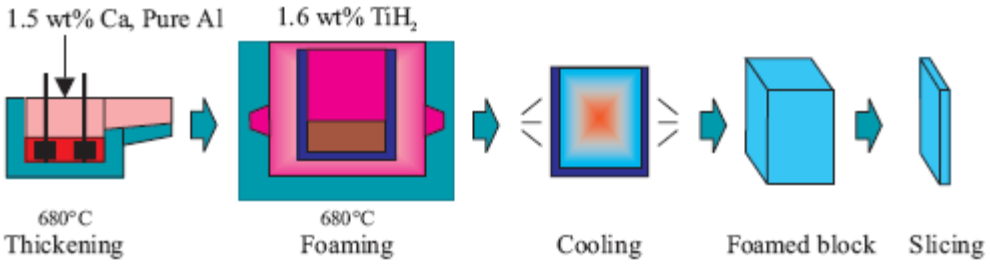

Figure 2.2. Schematic of direct foaming by blowing agents
(Source: Miyoshi, et al. 2000)

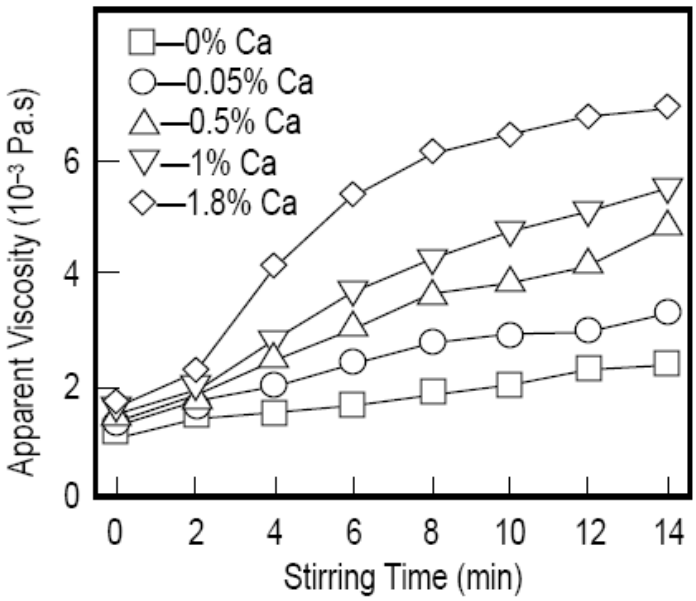

Figure 2.3. Effect of particle volume fraction and stirring time on the viscosity of Al melt (Source: Banhart 2000)

Typical densities of the foams produced by this method vary between 0.18 g/cm^3 and 0.24 g/cm,^{3} with an average cell size ranging from 1 mm to 13 mm (Miyoshi, et al. 2000). The viscosity of the molten Al can also be adjusted by injecting oxygen, air and other gas mixtures through the melt, which cause formation of Al_2O_3 particles and by adding viscosity enhancing additives directly such as Al_2O_3 and SiC. Complicated temperature cycles, difficulty in adjustment of the variables and the need for secondary processing (machining) are the disadvantages of the process.

2.1.2. Indirect Foaming

Basically, indirect foaming implies a heat treatment of a metal precursor containing blowing agent inside. Indirect foaming of powder compacts starts with mixing of metal powders containing blowing agent which upon heat treatment releases a foaming gas (Figure 2.4) (Kunze, et al. 1993). Metal powder-blowing agent mixture is then compressed to a dense, semi-finished foamable product via metal forming processes such as hot compaction, extrusion and rolling (Figure 2.4). In the final step, the semi-finished product is heated to the melting point of the metal. During heating, the blowing agent decomposes and subsequently releases gas, leading to the expansion of the molten or mushy metal and forming a highly porous structure.

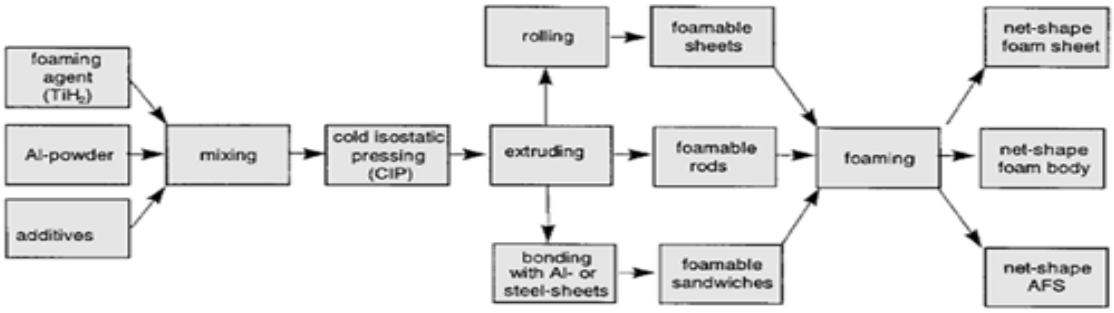

Figure 2.4. Manufacturing of aluminum foams via powder metallurgy technique (Source: Baumgartner, et al. 2000)

Besides metal hydrides (e.g., TiH_2), carbonates (e.g., calcium carbonate, potassium carbonate, sodium carbonate and sodium bicarbonate), hydrates (e.g., aluminum sulphate hydrate and aluminum hydroxide) or substances that evaporate quickly (e.g., mercury compounds or pulverized organic substances) can also be used as blowing agent depending on the melting point of the precursor.

For an efficient foaming process, it is very important to form a gas-tight semi-finished product in which the blowing agent is entrapped fully in the metallic matrix. Therefore, the temperature and the pressure of hot compaction must be high enough to bond the individual metal powder particles and form a gas-tight seal around the blowing agent particles avoiding from early decomposition of the blowing agent and the escape of H_2 gas before the melting of semi-finished product. In compaction by rolling, a temperature range between 350 ºC and 400 ºC is sufficient for the diffusion between the particles especially in the surface layers (Baumeister and H.Schrader 1992).

The weight ratio of blowing agent for forming of aluminum foam and its alloys has been found to be small. Calculations have shown that a foamable Al compact which contains 0.6 wt% TiH_2 would give an expansion factor of 17; a value almost 4 times higher than the expansion factor (4-5) experimentally found (Baumgartner, et al. 2000). This presents that, only 25% of the released hydrogen is effective in forming pores, and the rest is lost during foaming.

The time needed for maximum expansion of the semi-finished product depends on the temperature and size of the precursor and ranges from a few seconds to several minutes. The process is not only restricted to Al and its alloys, but also tin, zinc, brass, lead, gold, and some other metals and alloys can also be foamed using appropriate blowing agents and processing parameters (Yu, et al. 1998).

If a piece of foamable precursor is foamed in a furnace, the result will be a lump of metal foam with an undefined shape unless the expansion is limited. This is done by inserting the semi-finished foamable precursor into a mold having the desired shape of product and allowing expansion by heating. This process results in near-net shaped parts with a closed and dense outer skin and a highly porous cellular core. Complicated parts can be manufactured by pouring the expanding liquid foam into a mold (Figure 2.5.a). Sandwich panels consisting of a foamed metal core and two metal face sheets can be manufactured by bonding the face sheets to a piece of foam with adhesives. Another way is to roll clad Al or steel sheets onto a sheet of foamable material and allow the foamable core to expand while the face sheets remain dense (Figure 2.5.b). By this method, Al foam structures can be combined with steel or titanium face sheets as well as with Al face sheets. In the latter case, Al sheets with melting points that are higher than the core material must be used to avoid melting of the face sheets during foaming.

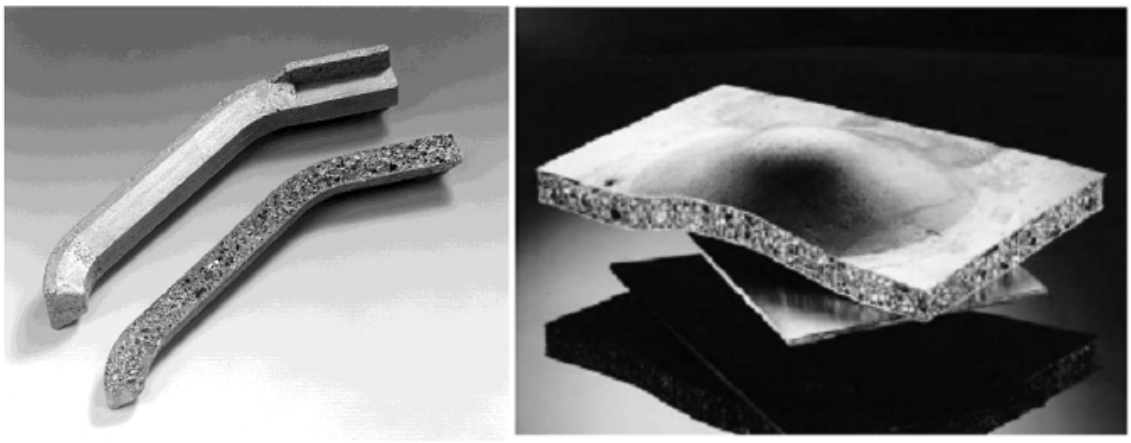

(a) (b)

Figure 2.5. (a) complicated foam parts (b) sandwich foam panel
(Source: Banhart 2000)

By applying suitable heating, it is possible to produce bodies that have continuously or discontinuously changing densities over the cross sections with this process. If the foaming process is stopped after a certain time at a constant temperature, a certain density will be obtained and if the foaming process is continued further, a higher density will be reached. As an example, structures having higher foam densities on the locations exposed to higher external loads could be manufactured by this method. If the hot compaction process is performed inside a mold, the powder mixture will be surrounded completely or partially by a blowing agent free metal powder. Upon

foaming, a dense or less porous layer and a highly porous foam core can be formed. This offers advantages for joining similar or different structures and for the production of foam core structures that require a dense cover such as car doors and frames.

Foaming of powder compacts process has been recently adjusted by incorporating TiH_2 particles directly into an Al melt instead of using powders to prepare a foamable precursor material. To prevent premature H_2 evolution, the melt should be quickly cooled down below its melting point after mixing or the blowing agent has to be passivated with the purpose of preventing it from releasing gas before solidification. The former technique, called FOAMCAST is carried out in a die-casting machine and the powdered hydride is injected into the die simultaneously with the melt (Banhart 2000). The resulting cast part is virtually dense and could be foamed by remelting in analogy to foaming from powder compacts; however, achieving a homogeneous distribution of TiH_2 powders in the die is difficult. The latter route requires that TiH_2 powders be subjected to a heat treatment cycle that forms an oxide layer on each particle, which delays the decomposition of TiH_2. TiH_2 is then added to the melt and the melt can be cooled at comparatively slow rates after stirring. Melts containing SiC particles are used to obtain stable foams. The name FORMGRIP has been given to this process which is an acronym of foaming of reinforced metals by gas release in precursors (Banhart 2000).

Accumulative Roll-Bonding Technique (ARB) has been proposed by Kitazono et al. (2004) and based on the dispersion of foaming agent into bulk metal sheets through sequential rolling. The stages of ARB are schematically illustrated in Figure 2.6.a. Two metal strips are stacked together with blowing agent powder (TiH_2) between them. The stacked strips are then roll-bonded by the reduction of thickness. The bonded strips are then cut and after surface treatment, they are stacked again and roll-bonded. After several roll-bonding cycles, rolled foamable precursor composite in which the blowing agent particles dispersed uniformly in a metal matrix is obtained (Figure 2.6.b). The composite is used as the starting material for the following high temperature foaming process.

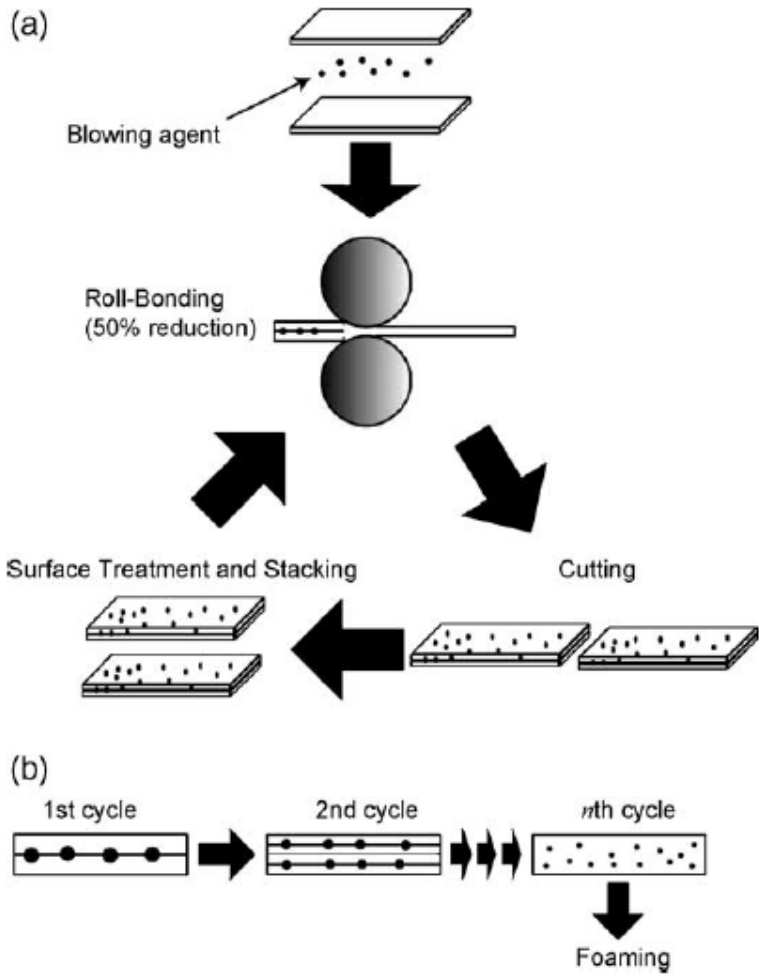

Figure 2.6. (a) Schematic of the manufacturing process of a perform sheet through ARB process (b) prediction of gradual distribution of added blowing agent particles (Source: Kitazono, et al. 2004)

The microstructure of the manufactured preform using ARB method is the same as the precursor produced by P/M process. Closed-cell aluminum foams with about 40% porosity were successfully produced through the ARB process. This process has the potential to produce a large scale sandwich structure comprising a foam core and skin plates using conventional cladding techniques.

Laser Assisted Indirect Foaming of Aluminum was proposed by Kathuria (2001). The basic principle of laser assisted foaming is shown schematically in Figure 2.7. The precursor material with blowing agent, prepared by P/M process, is foamed by heating it up to its melting point by a high power laser beam irradiation. The uni-directional expansion of the foamable precursor material can be observed during the

entire foaming process in the irradiation direction. The expansion in the other directions is small.

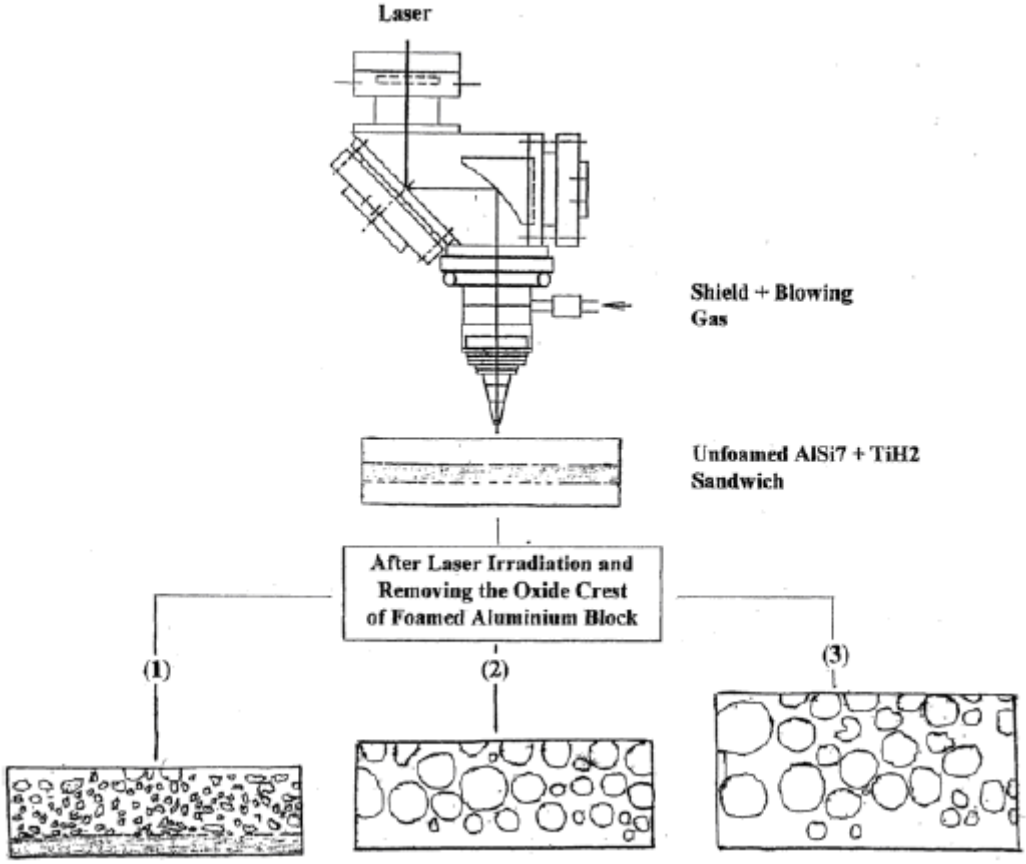

Figure 2.7. The block diagram of laser assisted AlSi7 foaming for three processing speeds, in decreasing order (1) > (2) > (3) (Source: Kathuria 2001)

Besides H_2 evolution and foaming, the shield gas Ar makes an additional help for the porosity formation and may also become trapped inside the solidified foam. In the conventional thermal melting process, the average temperature gradient of the interface varies as the bulk temperature decreases. This is accompanied by a slow cooling rate and hence a long time for the stabilization of the pores to occur. However, in the case of laser process the average temperature gradient of the interface is much higher; thus, a faster cooling rate results in the pore stabilization. Figure 2.7 also illustrates, as to how the processing speed could affect the cell morphology and the expansion ratio of the buildup foam.

The foamable Al-alloy sandwich samples fabricated according to the P/M procedure are used in this technique. Porous structures with relative densities of 0.33-0.39 and porosity of 61-67% can be fabricated.

Al-Ni intermetallic foams can be produced by mixing aluminum and nickel powders with Ti, B_4C and TiC additives (Kobashi and Kanetake 2002). After blending and compacting the precursor is heated to above the melting point of Al where a self propagating exothermal reaction takes place between the components (Figure 2.8). The oxide-hydrate in the powder surfaces leads to the formation of the blowing gas in this case. Quite uniform foams with porosities ranging up to 85% have been obtained.

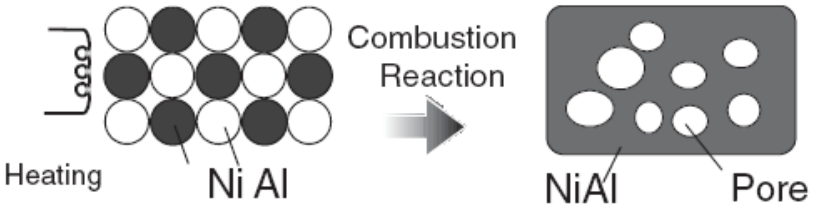

Figure 2.8. Schematic illustration of the Combustion Reaction of NiAl
(Source: Kobashi and Kanetake 2002)

Indirect Foaming by Space Holder Method are schematically presented in Figure 2.9. The process starts with mixing of metal powders with a suitable space holder material, followed by a compaction step (e.g. uniaxial and isostatic pressing) that produces metal powder-space holder mixture compact. The compacted mixture is then heat treated at a relatively low temperature to release the space holder, resulting in an unfired open cell foam metal structure. Finally, the compact is sintered at relatively high temperatures to provide structural integrity. This method allows a direct near net-shape fabrication of foamed implant components with a relatively homogeneous pore structure and a high level of porosity (60-80%) (Ryan, et al. 2006).

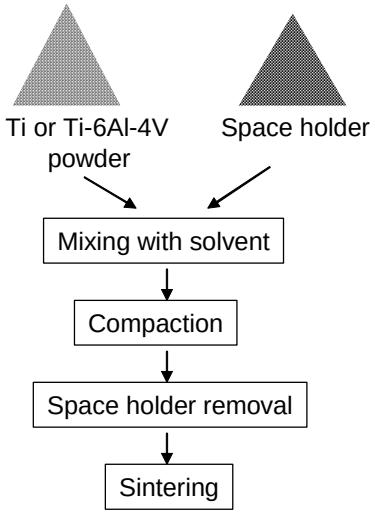

Figure 2.9. Processing steps of space holder method

2.2. Mechanical Properties of Closed-Cell Aluminum Foams

Mechanical properties of Al closed cell foams have been subjected to many studies and can be found in (Baumeister, et al. 1997, Simone and Gibson 1997, Gibson 2000, Banhart 2003, Mukai, et al. 2006). The deformation under compressive loads, elastic deformation, collapse or plateau stress, indentation and energy absorption are among the widely studied foam properties. Note that mechanical properties given below can also be applied to the other metallic foams.

Closed-cell Al foam shows a characteristic stress-strain curve under compression. As shown in Figure 2.10, the typical compression stress-strain curve consists of three distinct regions: linear elastic, collapse and densification. In linear elastic region, the deformation is controlled by cell wall bending and/or stretching depending on the structure of the cells i.e. open or closed cell. This region is followed by a plateau (collapse) region comprising several different mechanisms: elastic buckling and brittle crushing of cell walls and formation of plastic hinges. Deformation in this region is highly localized and proceeds by the spreading of the deformation from localized to undeformed regions of the sample. Since the deformation is localized, large oscillations in stress occur due to the repetitive nature of the process of cell collapse and densification can be seen in the collapse regions in Figure 2.10. Collapse region proceeds with a stress plateau either with a constant value or increasing slightly with strain. At a critical strain, known as densification strain (ε_d), the cell walls start to touch each other and, as a result of this, the material densifies (densification region). The

stress in this region increases sharply and approaches to the strength of the bulk Al metal.

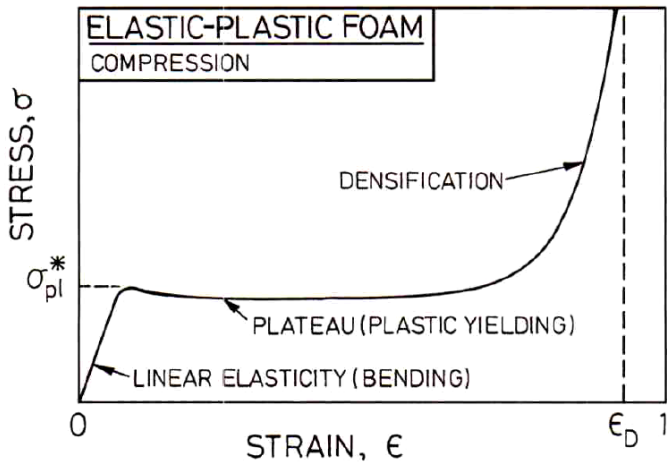

Figure 2.10. Schematic presenting characteristics of stress strain curves for metal foams (Source: Gibson and Ashby 1997)

Compressive mechanical properties of Al foams depend on their density, yield strength of the alloy of which they are made and the defects in the cell walls and edges. Compressive stress or plateau stress generally increases with increasing density (Figure 2.11) and yield strength of the foam material, while defects on the cell walls have detrimental effects on the mechanical properties.

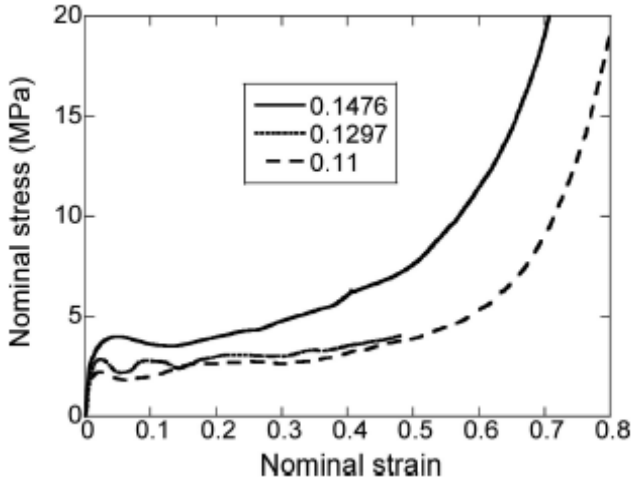

Figure 2.11. Compression stress-strain curves of 10% SiC_p/Al foams (Source: Guden and Yuksel 2006)

2.2.1. Elastic Properties

Gibson and Ashby (1997), using the simple cubic models of beams (Figure 2.12), derived the following equations.

$$\frac{E^*}{E_s} = \alpha_1 \rho \tag{2.1}$$

and

$$\frac{E^*}{E_s} = \alpha_2 \rho^2 \tag{2.2}$$

for ideal closed-cell and open cell foams, respectively. In these equations, E^* and E_s are the Elastic Modulus of the foam and cell wall material, respectively. The relative density; ρ, is defined as

$$\rho = \frac{\rho^*}{\rho_s} \tag{2.3}$$

where ρ^* and ρ_s are the densities of foam and cell wall material, respectively. The values of coefficients α_1 and α_2 depend on the geometric arrangement of cells. The value of α_1 is calculated 1/3 for isotropic closed-cell foams and 0.32 for tetrakaidecahedral cells (Simone and Gibson 1998, Kraynik, et al. 1999, Gibson 2000).

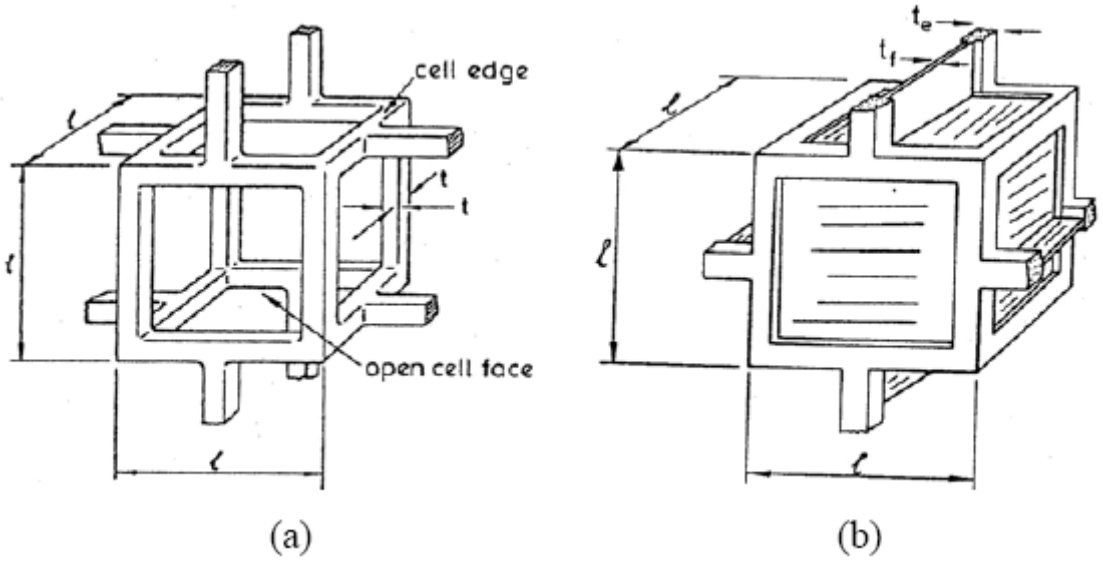

Figure 2.12. Cubic models of (a) open-cell and (b) closed-cell foams
(Source: Gibson and Ashby 1997)

Experimental elastic moduli values of Al closed-cell foams are lower than those calculated using Equation 2.1 especially at relatively low foam densities. The moduli degradation is partly due to the thicker regions on cell edges as compared to cell walls because surface tension tends to draw liquid metal to the intersections during foaming process. Gibson and Ashby (1997) proposed the following equation for the modulus of imperfect closed-cell foams:

$$\frac{E^*}{E_s} = C_1 \phi^2 \rho^2 + C_2 (1 - \phi) \rho \qquad (2.4)$$

Here, ϕ is the fraction of the material contained on cell edges and C_1 and C_2 are geometrical coefficients, similar to α_1 and α_2. The first and the second terms of the Equation 2.4 are due to cell edge bending and cell wall stretching, respectively. A high value of ϕ is generally found in commercial Al closed-cell foams and therefore the experimentally measured moduli data of closed-cell foams are usually fitted to the following general equation:

$$\frac{E^*}{E_s} = \alpha \rho^n \qquad (2.5)$$

Curved, wrinkled and missing cell walls, voids on the cell edges and cell walls and non-uniform densities are the further imperfections degrading mechanical properties of closed-cell Al foams. Foams may also show anisotropy in mechanical properties resulting from ellipsoidal cell shape. The shear stress between conveyer belt and liquid foam induces an ellipsoidal cell shape in Cymat foams. The effect of enclosed gas pressure on mechanical properties is usually ignored for Al closed-cell foams because cell walls crush during compression. Therefore, the enclosed gas escapes through the cell walls

2.2.2. Plastic Collapse and Densification

The collapse stress or plateau stress (average stress in collapse region of Figure 2.10) is an indication for the progression of the inelastic and inhomogeneous deformation and it determines the amount and the efficiency of plastic energy absorption. For an ideal closed cell structure, plastic collapse is expected to occur by the cell wall stretching in a direction perpendicular to compression axis and the plateau stress is given as (Gibson and Ashby 1997)

$$\frac{\sigma_{pl}^{*}}{\sigma_{ys}} = C\rho \tag{2.6}$$

where, σ_{pl} is the plateau stress, σ_{ys} is the yield strength of the alloy and C is a geometrical constant. In the case of cell buckling and membrane stretching, the plateau stress is given as (Gibson and Ashby 1997)

$$\frac{\sigma_{pl}^{*}}{\sigma_{ys}} = C_5 \left(\phi \frac{\rho^{*}}{\rho_s}\right)^{3/2} + C_6^{''}(1 - \phi) \frac{\rho^{*}}{\rho_s} \tag{2.7}$$

where, C_5 and C_6 are geometrical coefficients. If cell walls are thin, the strength will be dominated by the cell edge bending, approaching to the strength of open cell foams, if not, they will stretch at right angle to loading direction and may significantly contribute to plateau stress of the foam.

2.2.3. Indentation

During the indentation of a foam, an additional energy is consumed as the indenter tears the foam around the perimeter. The region under the indenter collapses at a stress of plateau stress. The tear energy added to the plateau stress determines the indentation pressure (Ramamurty and Kumaran 2004).

$$\frac{F}{\pi a^2} = \bar{P} = \sigma_{pl}^{*} + \frac{2\gamma}{a} \tag{2.8}$$

where, F, P, γ and a are the total force applied, indentation pressure, tear energy and indenter radius, respectively. The indentation pressure is the function of indenter size and foam density.

2.2.4. Energy Absorption

Foams can convert much of the impact energy into plastic deformation energy and keep the peak force exerted on the object below the level, which causes damage. This characteristic is a potential for foams to be used as impact absorbers to protect people and fragile devices from impact. Compared to bulk metals, foams absorb more energy at a constant load. The energy absorption is simply the area under the load-deformation curve (Figure 2.10) up to certain length. Al foams are widely studied as filling materials for Al and steel tubes. The results of these studies have shown that on specific energy base foam filled tubes absorb more energy than non-filled ones due to the interaction effect resulting from foam filling (Hanssen, et al. 1999). Figure 2.13 shows this effect: the force necessary to deform foam filled tube is higher than sum of the forces necessary to deform tube alone and foam alone. The foam-filled tubes also form higher number of folds than empty tubes, which results in an increased energy absorption (Kavi, et al. 2006). The interaction effect was also observed for the foam-filled tubes compressed in transverse direction (Kavi, et al. 2006). In this direction foam deforms laterally and resists the crushing of the tube. One of the potential applications of foams as energy-absorbing filling materials is in car crash boxes inserted between bumper and chassis in order to reduce the extent of damage in the chassis up to the crash velocities of 15 km/h (Banhart 2003).

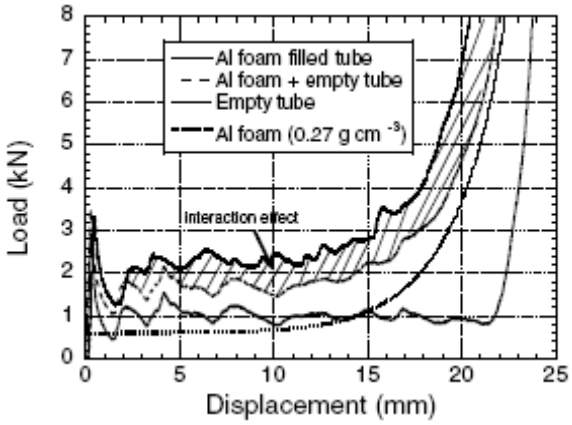

Figure 2.13. Interaction effect in Al foam (0.27 g/cm^3) filled tube
(Source: Kavi, et al. 2006)

2.3. Applications of Closed-Cell Aluminum Foams

The properties of aluminum foams including high mechanical energy absorption per unit volume, high stress and stiffness to weight ratio, constancy over time, temperature and moisture range, good acoustic, vibration and electromagnetic insulation, recyclability make them usable materials in various applications. Aluminum foams have become popular with the potential applications in

- energy absorbing systems,
- acoustic, thermal and vibration insulators,
- light-weight construction,

2.3.1. Aluminum Foam as Energy Absorber

Aluminum Foams have relatively high collapse strength compared to polymeric foams and very long plateau stress and therefore they are identified as very efficient energy absorbers. The dynamic deformation of aluminum foam (high strain rate) starts at the impact face and continues through the foam until the densification strain (Gama, et al. 2001). They are very suitable materials to be used in cashboxes of automobiles (Figure 2.14.a) and in composite armor as the intermediate layer which increase the stress wave passage to backing composite plate (Gama, et al. 2001). The other important properties of metallic foams such as non-inflammability and good sound absorbability are the additional advantages for their use in transport industry. Other

application areas of these materials include railway and ship constructions and space vehicle landing pads. The shapability of the metallic foams is a key factor for replacing the honeycomb components in existing helicopter designs (Banhart 2001).

2.3.2. Aluminum Foam as Acoustic, Thermal and Vibration Insulator

By the means of the lower modulus of elasticity of the metallic foam compared to the bulk metal which the foam is made of, the resonance frequency is lower and the metal foam behaves as a better damping system in designs (Banhart, et al. 1996). This makes them suitable materials to be used in machine construction when the damping of vibration is needed as an engine mount where less vibration of the car engine is transmitted through the chassis. (Figure 2.14.b).

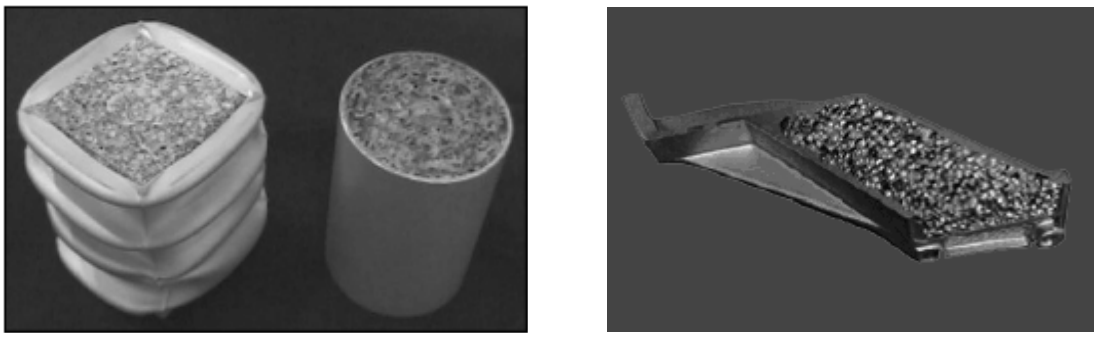

(a) (b)

Figure 2.14. (a) Prototypes of foam filled tubes designed as energy absorbers, (b) Prototype of a part of an engine mount consisting of foam core and cast shell (Source: Banhart 2003)

Because of the porous structure, metal foams have higher loss factor than the ordinary bulk material. This situation makes the sound wave partially entering and damped out while the other part is reflected back. Figure 2.15 shows the foam panel use under an elevated viaduct. These panels absorb the noise and therefore reduce the amount of noise produced in viaducts. Properties as fire resistance and no dangerous gas existence in case of a fire can further make the metal foams preferred but the sound insulating properties of metal foams are note to be worse than existing polymer based foams or glass wool.

Figure 2.15. Foam layer used under an elevated viaduct as a noise insulator (Source: Miyoshi, et al. 2000)

2.3.3. Aluminum Foam in Light-Weight Construction

Aluminum foam may be used in aerospace vehicles and all the other mechanisms where light-weight is an important factor. Aluminum foam cores are currently used in the tailbooms of helicopters (Banhart 2001). They are also used in elevator systems where reduction of weight can make a significant effect while absorbing more energy than the ordinary bulk material in case of an impact. Naturally, aluminum foam can be used in sporting equipments such as helmet or bicycle frame. Balconies in buildings made of metal foam can be safer in case of an earthquake.

CHAPTER 3

FOAM STABILITY AND MECHANICAL PROPERTIES OF CLOSED-CELL ALUMINUM FOAMS

In the foaming of metals, the metal should be in the liquid state; otherwise, the foaming process cannot take place due to high viscosity. Just after the expansion of the liquid metal starts, several different mechanisms become operative quickly in the molten metal and change the cell structure of the foam continuously. Although the expansion is a function of several parameters such as the rate of gas evolution, the viscosity and microstructure of the melt, the stability is a different phenomenon. It emphasizes the cell structures, which do not change significantly over the time. It should be noted that the currently produced Al foams are considered to be stable, at least exhibit kinematical stability. This means that, for a period of time, the liquid foam is stable. The basic principles of the liquid metal stabilization will be analyzed in different foaming processes in this section.

3.1 Basics of Metal Foam Stability

In order to understand the foam stability, the forces acting on the liquid foam within the foaming process should be known. The forces are categorized in two groups: driving forces and tensile force (Kaptay 2003, Asavavisithchai and Kennedy 2006, Banhart 2006). Driving forces consist of gravitational forces and capillary forces while the tensile force is formed by the atmospheric pressure and the pressure of the blowing gas. These forces are effective in the stability of the liquid foams and lead to several different events to occur in the liquid foam.

The flow of liquid metal from cell walls to the cell edges (Figure 3.1) is known as drainage. Drainage leads to thinner cell walls, thicker cell edges and a dense layer at the bottom of the foam (Figure 3.2). It occurs by the action of gravitational force and capillary forces. The diffusion of the gases from smaller to larger bubbles further causes coarsening of the cells in foam structure (Banhart 2006). The rupture (coalescence) is the disappearance of cell walls during the foaming process because of a sudden

instability of the pressure (Weaire and Hutzler 1999). These events happen simultaneously in liquid foam and interrelated. Under capillary forces, the liquid metal flows from cell walls to edges and results in cell wall thinning and under tensional forces the cell walls rupture, which overall reduce the stability of foams.

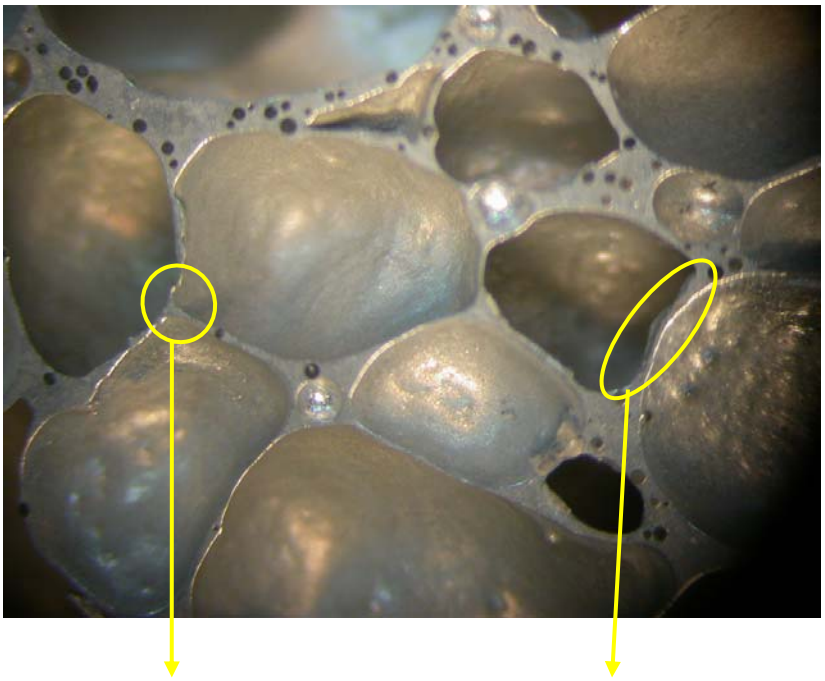

Figure 3.1. Micrograph presenting cell wall and cell edge in foam structure

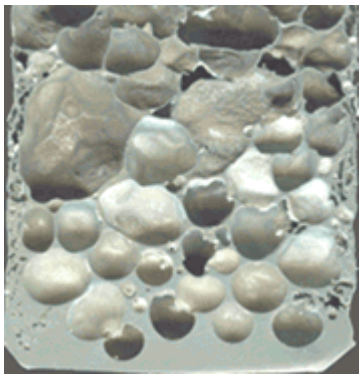

Figure 3.2. Cross-section of an aluminum foam showing thin cell walls, thick cell edges and dense metal layer at the bottom sections

Aqueous liquid foams are primarily stabilized by either surfactants or solid particles or both (Wubben and Odenbach 2004). However, in liquid metal foams only

atoms or at most complexes/clusters made of several atoms can be surface active (Kaptay 2003). Therefore, the surfactants can not be used to stabilize metal foams. However, liquid metal foams can be stabilized by particles. The solid particles accumulate at gas/liquid interface and prevent the bubble-bursting and therefore stabilize the liquid foam (Wubben and Odenbach 2004). Commonly used solid particles include SiC, Al_2O_3, MgO and alloying elements (Leitlmeier et al. 2002, Degischer et al. 2002, Wang and Shi 2003, Babcsan, et al. 2004, Esmaeelzadeh, et al. 2006). The particles in liquid can effectively stabilize the foam, if they are partially wetted by the liquid metal (Figure 3.3). The non-wetted particle will be found in the gas phase, while fully wetted particles in the liquid. Partially wetted particles sit at gas/liquid interface increase the surface viscosity of the cell wall, leading to reductions in the amount of liquid metal flow from cell faces to the cell edges. The effective arrangements of the particles also tend to reduce the pressure differences between cell edge and cell wall which leads to cell rupture. The effectiveness of the several different particle arrangements of the solid particles on the stability of liquid metal foams has been recently analyzed by Kaptay (2003) and shown in Figure 3.4. According to Kaptay's analysis, the particle configuration (e) in Figure 3.4 forms the most stable foams, while (b) the least stability.

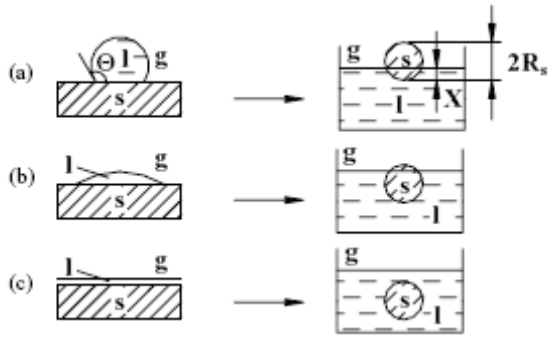

Figure 3.3. (a) non-wetted particle, (b) partially wetted particle and (c) fully-wetted particle (Source: Kaptay 2003)

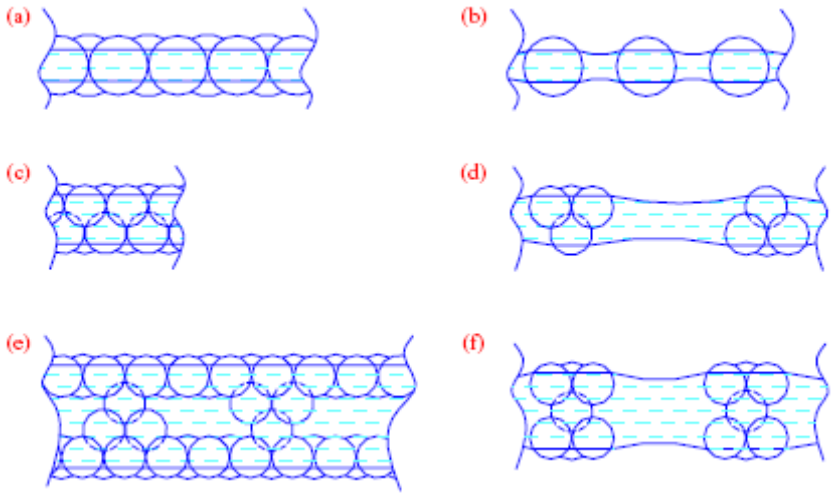

Figure 3.4. Schematic of the different arrangement of the stabilizing particles on the cell walls (Source: Kaptay 2003)

3.2. Stability of Al Foams

In closed-cell Al foam processing, which are currently manufactured by several different processes, liquid foam is stabilized by the addition of ceramic particles to the liquid metal either in-situ or ex-situ.

In Cymat foam, the liquid metal is foamed by injecting gases (e.g. air or nitrogen) into the melt and the liquid foam is stabilized by adding 8-20 μm size SiC particles (Jin, et al. 1992, Andrews, et al. 2001). The stabilization was found to be a function of particle volume fraction and the distance traveled by the bubbles (Leitlmeier, et al. 2002). Figure 3.5 shows stable foam processing in Cymat method as a function of distance traveled by bubbles and SiC volume fraction. At low traveling distances and low SiC volume contents, the bubbles are bursted and the stability was lost as depicted in Figure 3.5, while the stability is achieved at long traveling distances and high volume content of SiC particles. It was found that minimum distance traveled by the bubble in a melt containing roughly 10 wt% SiC was ideal for foam stabilization. Nitrogen blown foams were less stable than air or oxygen blown foams. For oxygen containing foams the thickness of the cell walls was more homogeneous. Oxygen created a dense oxide layer on the cell wall surface and kept the SiC particles away from the gas/metal interface as shown in Figure 3.6. The oxide films were found to be 30 nm thick.

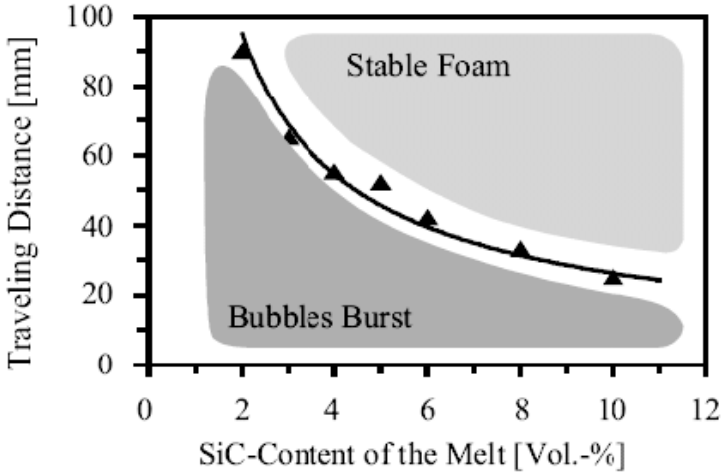

Figure 3.5. Criterion to obtain stable Al foams (alloy A356, T = 727 °C) (Source: Leitlmeier, et al. 2002)

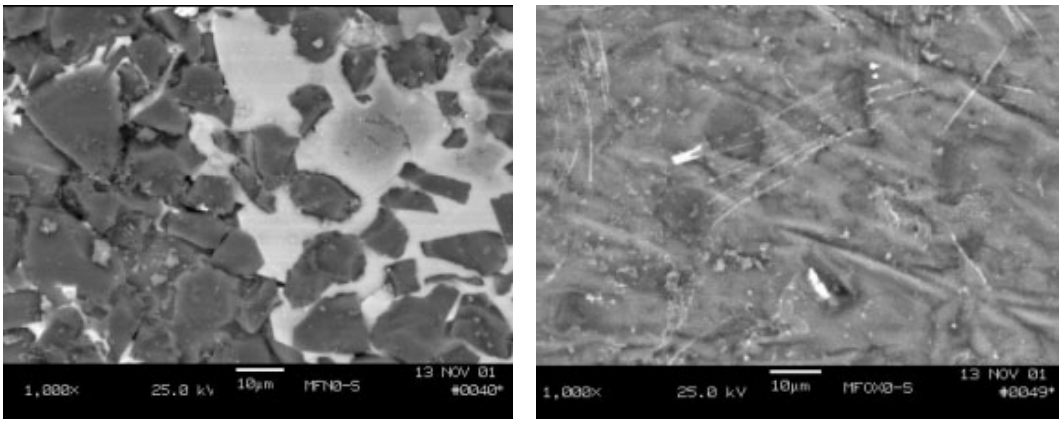

(a) (b)

Figure 3.6. Back-scattered scanning electron microscope (SEM) image of SiC particles at the cell wall surface of F3D20S-foam manufactured by blowing (a) nitrogen and (b) air (Source: Leitlmeier, et al. 2002)

Wang and Shi (2003) investigated the effect of SiC (1, 7, 14 and 20 μm) and Al_2O_3 (3.5, 5 and 10 μm) particles, foaming temperature and gas flow rate on the cell sizes and cell wall thicknesses of Al foams in Alcan foam processing route. Cell sizes and cell wall thicknesses increased with increasing particle size and particle volume fractions, while the cell wall thicknesses decreased with increasing foaming temperature. The cell wall thicknesses varied between 45 to 80 μm depending on the particle size and volume fraction. The cell sizes increased, while cell wall thicknesses decreased with increasing gas flow rates. It was noted in the same study that, the

presence of particles in liquid foam increased the bulk viscosity of the composite melt; hence, reduced the liquid flow from cell faces to cell edges. The particles at liquid/gas interface further reduced the capillary pressure difference between cell edge and cell wall. Both were noted to be effective in stability of the composite foam. Low concentration of large particles could not cover adequate cell surface hence lead to unstable foam; while high concentration of small particles increased the viscosity of the melt significantly so that the air injection could not foam the composite melt. The effects of melt (pure Al) viscosity (adjusted by the Ca-addition and melt stirring time) and holding time on the cell structure of Alporas foams were studied by Song et. al (2000). With the increasing melt viscosity, the metal foam stability increased and the cell size decreased. It was further emphasized that too high viscosity might prevent the homogenous dispersion of the foaming agent. For large cell size, holding time increased and the amount of foaming agent decreased. Yang and Nakae (2000) investigated the foaming behavior of liquid A356 Alloy with the addition of 0.5 to 4 wt% TiH_2 foaming additions and at various temperatures. The liquid viscosity was adjusted by Al powder addition. Increasing the amount of foaming agent until about 1 wt% TiH_2 addition increased the porosity, while foaming efficiency decreased with increasing amount of foaming agent over 1 wt%. The optimum foaming agent addition amount was determined 1 wt% by considering cell uniformity and foaming efficiency. At low foaming temperatures, less than 630 °C, sufficient gas release for foaming did not occur while foaming at temperatures above 650 °C, resulted in rapid bubble coalescence. The optimum foaming temperature was given in the range of 630-650 °C for studied melt alloy.

In foaming of powder compact process, foam stabilization was ascribed to the metal oxide filaments, which are the remnants of the thin oxide layer on the aluminum powders and/or the solid component of the particular alloy (Al-rich phase in the Al-Si eutectic) (Banhart 2000). The early stage pore formation in AA6061 Al and Al-7%Si powder compacts was further investigated by synchrotron-radiation tomography (Helfen, et al. 2005). The pores in the former alloy formed dominantly around the blowing agent, while in the latter alloy the pores preferentially initiated around Si particles. Gergely and Clyne (2000) modelled the drainage in the standing foams of relatively thick cell faces. The model emphasized that the small initial cell size and high initial porosity level inhibited the drainage; the attention should be given to the rapid

foaming processes and cell wall stabilization using a foaming agent that would oxidize the cell faces. In another study, the oxygen content of the starting Al powders increased by pre-heat treatment in order to see the effect of oxygen content on foam expansion (Asavavisithchai and Kennedy 2006). The oxide content increased with the duration of the heat treatment. It was shown that there is an optimum oxygen content which leads to maximum expansion in compact (Figure 3.7). The foam made of Al powder containing 0.333 wt% oxide was shown to be the most stable. The addition of relatively small amount (0.6 wt%) of Mg particles in powder compacts was found to enhance the wetting of Al_2O_3 particles (Figure 3.8) and promoted higher expansions (Figure 3.9) (Asavavisithchai and Kennedy 2006). Aluminum foams were also prepared with the additions of Cu, Mg, Si and Ni, containing different types of particles (Al_2O_3 and SiC) in various volume fractions (10–30 %) (Babcsan, et al. 2004, Babcsan, et al. 2006). The alloying elements Si and especially Mg were found to decrease cell wall thickness.

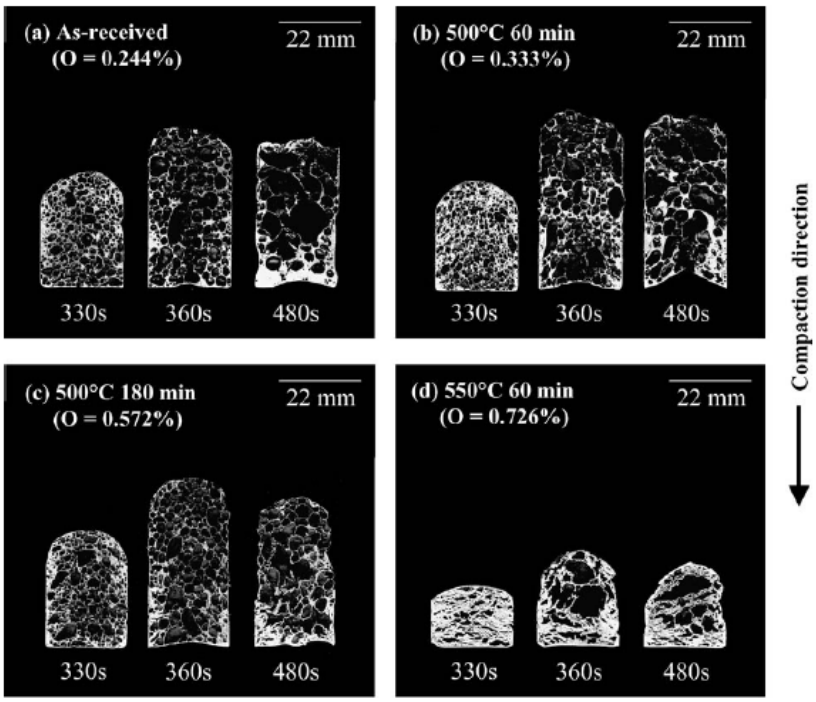

Figure 3.7. Cross sections of Al foams made using different Al powders: (a) as-received, (b) powder heat treated at 500 °C for 60 min, (c) powder heat treated at 500 °C for 180 min, and (d) powder heat treated at 550 °C for 60 min (Source: Asavavisithchai and Kennedy 2006)

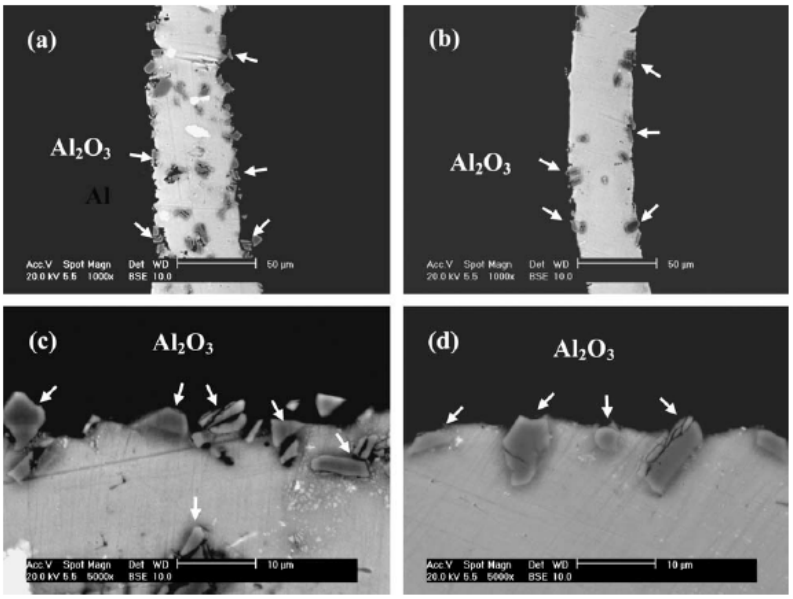

Figure 3.8. SEM micrographs showing the attachment of Al_2O_3 particles at the cell wall surfaces for (a) and (c) Al–6 wt%Al_2O_3 and (b) and (d) Al–6 wt%Al_2O_3–0.6wt.%Mg foams (Source: Asavavisithchai and Kennedy 2006)

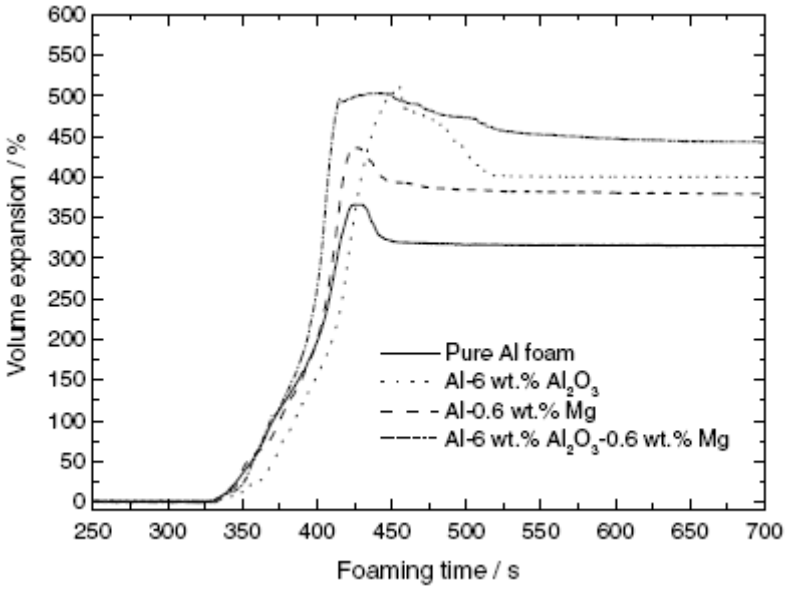

Figure 3.9. Effect of Mg and Al_2O_3 additions on the expansion of Al foams (Source: Asavavisithchai and Kennedy 2006)

It has been recently shown that TiB_2 addition to the Al powder compacts in the foaming from powder compact process, although, increased the plateau stresses of Al foams, it was not effective in long-term foam stabilization (Kennedy and Asavavisitchai

2004). Contrary to TiB_2-addition, SiC_p-addition of 3 wt% was shown to improve the foam stability of Al powder compacts (Kennedy and Asavavisithchai 2004).

The present report is a further investigation of the effect of particle addition on the foaming and quasi-static crushing behavior of Al powder compacts. For that purpose, Ti6Al4V/Al MMC and Al powder compacts were prepared and foamed. Ti6Al4V are known to be wetted by liquid Al and therefore a good model particle in order to see the effect of wetted particles on the expansion, stability and mechanical properties of foamed Al powder compacts. The effect of Ti6Al4V-addition on the foaming behavior was determined by comparing the expansions of Al compacts processed under the same conditions. Compression testing on the prepared composite and Al foams was conducted in order to determine the effect of Ti6Al4V-addition on the crushing behavior.

CHAPTER 4

EXPERIMENTAL

4.1. Materials and Compact Preparation

The specifications of materials; aluminum powder, TiH_2 (blowing agent) and spherical Ti6Al4V used to prepare foamable compacts are listed in Table 4.1. The average particle size of the Al was 34.64 μm and the size of TiH_2 particles were less than 37 μm. Ti6Al4V powder was manufactured by Phelly Materials Company, with a particle size range of 30 to 200 micrometers. The particles were spherical in shape (Figure 4.1.a) and the microstructure is consisted of acicular needle-like alpha (α) (Figure 4.1.b), which is known as martensitic α (Javier Gil, et al. 2007). This type of microstructure can form as a result of quenching after heat treatment above the beta (β)–transition temperature (1050 ^{o}C). The powder was sieved to particle size range of 30-45, 45-56, 56-90, 90-106, 106-160 and 160-200 micrometers in order to determine the effect of particle size on the foaming behavior of Al compacts.

Table 4.1. Specifications of raw materials. D is the particle size and (X%) is the percentage of the particles smaller than the given value

Powders	Size (μm)	Density (g/cm^3)	Purity	Measured mean diameter (μm)	D (10%) (μm)	D (50%) (μm)	D (90%) (μm)
Al powder	< 74	2.702	99%	37.13	17.32	34.64	69.28
TiH_2 (Merck)	< 37	3.76	>98%	–	–	–	–
Ti6Al4V (Phelly)	30-200	4.42	–	–	–	–	–

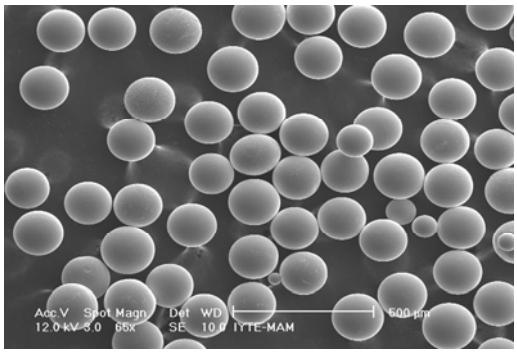

(a)

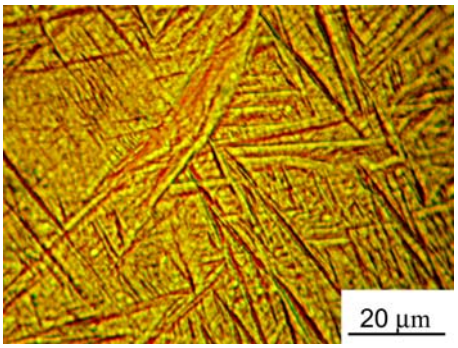

(b)

Figure 4.1. (a) SEM picture of spherical Ti6Al4V powder and (b) Optical microscope micrograph showing the acicular needle-like alpha (α) microstructure of the powder

The steps of the foam preparation method is schematically shown in Figure 4.2. The process starts with the mixing of appropriate amounts of basic ingredients (Al powder, TiH_2 and Ti6Al4V) inside a plastic container, which was rotated on a rotary mill for 2 hours in order to form a homogeneous powder mixture. Compacts with a diameter of 30 mm and a thickness about 8 mm were cold compacted from the powder mixture inside a stainless steel die (Figure 4.3), under varying pressures to reach a relative density near 98%. In order to assess the effect of Ti6Al4V powder addition on Al foam, Al compacts without Ti6Al4V addition were also prepared and foamed under same conditions. The foaming was performed in a vertical tube furnace. The sizes, applied pressures and final relative densities of the compacts are listed in Table 4.2. For particle containing compacts, a higher compaction pressure is applied in order to increase the relative density to the level of Al compacts with no particle addition. In Table 4.3, the statistical analysis of the relative density of the prepared compacts are given. The mean relative density varies about 97% for the compacts with particle addition and 98% for Al compacts with no particle addition.

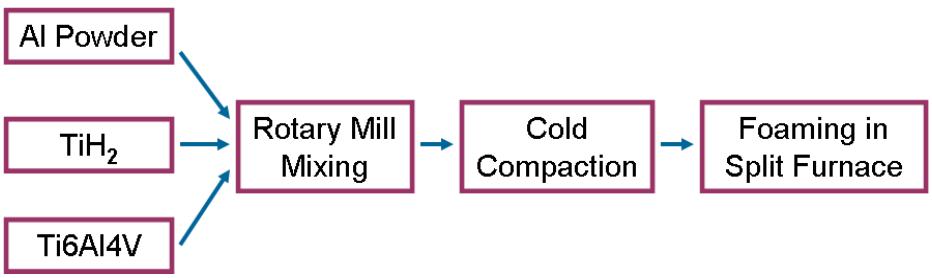

Figure 4.2 Foaming process

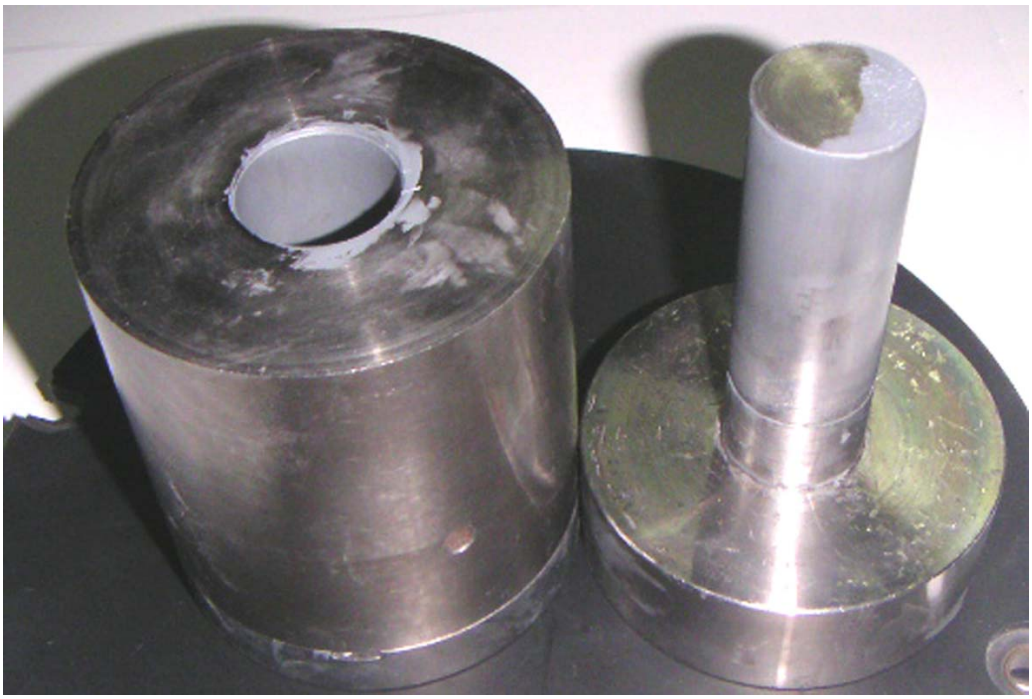

Figure 4.3. Compaction die for foamable compact preparation

Table 4.2. Processing parameters of the compacts prepared for foaming experiments

Sample Code	m(g)	h(mm)	d(g/cm^3)	Relative density (%)	Compaction Pressure (MPa)
PAL-1	15.085	8.05	2.638	97.6	185
PAL-2	14.890	7.97	2.619	97.8	185
PAL-3	14.958	7.93	2.653	98	185
PAL-4	14.988	7.93	2.669	98.7	185
PAL-5	15.108	7.98	2.669	98.7	185
P0.0.1	14.918	7.93	2.648	98.00	185
P0.0.2	15.063	8.01	2.644	97.8	185
P0.0.3	14.956	8.02	2.644	97.8	185
P0.0.4	14.910	7.97	2.644	97.8	185
P0.0.5	14.945	7.97	2.645	97.9	185
ST-(30-45)-0.5-1	14.744	7.85	2.651	97.0	200
ST-(30-45)-1-1	14.719	7.83	2.647	96.9	200
ST-(30-45)-1-2	14.780	7.82	2.657	97.3	200
ST-(30-45)-1-3	14.790	7.94	2.648	97.0	200
ST-(30-45)-1-4	14.844	7.90	2.646	96.9	200
ST-(30-45)-1-5	14.923	7.92	2.654	97.2	200
ST-(30-45)-1-6	14.918	7.92	2.647	96.9	200
ST-(30-45)-1-7	14.907	7.89	2.660	97.4	200
ST-(30-45)-1-8	14.881	7.88	2.658	97.3	200
ST-(30-45)-1-9	14.642	7.76	2.653	97.1	200
ST-(30-45)-1-10	14.873	7.88	2.658	97.3	200
ST-(30-45)-2-1	14.749	7.79	2.670	97.1	217
ST-(30-45)-2-2	14.749	7.78	2.665	97.0	217
ST-(30-45)-3-1	14.780	7.72	2.668	96.5	252
ST-(30-45)-4-1	14.758	7.62	2.693	96.8	261
ST-(30-45)-5-1	14.795	7.67	2.709	96.8	261
ST-(30-45)-5-2	14.824	7.68	2.708	96.8	261
ST-(30-45)-5-3	14.786	7.70	2.705	96.7	261
ST-(45-56)-5-1	14.842	7.72	2.709	96.8	261
ST-(45-56)-5-2	14.821	7.71	2.710	96.9	261
ST-(45-56)-5-3	14.862	7.73	2.708	96.8	261
ST-(45-56)-5-4	14.767	7.66	2.725	97.4	261
ST-(56-90)-5-1	14.817	7.70	2.712	96.9	261
ST-(56-90)-5-2	14.833	7.71	2.717	97.1	261
ST-(56-90)-5-3	14.834	7.71	2.717	97.1	261
ST-(90-106)-5-1	14.771	7.69	2.712	96.9	261
ST-(90-106)-5-2	14.741	7.66	2.714	97.0	261
ST-(90-106)-5-3	14.823	7.70	2.715	97.0	261
ST-(106-160)-5-1	14.819	7.70	2.715	97.0	261
ST-(106-160)-5-2	14.854	7.71	2.712	96.9	261
ST-(106-160)-5-3	14.843	7.71	2.708	96.8	261
ST-(106-160)-5-4	14.603	7.58	2.708	96.8	261
ST-(160-200)-5-1	14.824	7.67	2.712	96.9	261
ST-(160-200)-5-2	14.770	7.64	2.707	96.7	261
ST-(160-200)-5-3	14.840	7.69	2.712	96.9	261
ST-(160-200)-5-4	14.793	7.66	2.712	96.9	261
ST-(160-200)-5-5	14.771	7.67	2.717	97.0	261
ST-(160-200)-5-6	14.801	7.68	2.718	97.1	261
ST-(160-200)-5-7	14.911	7.72	2.726	97.4	261
ST-(160-200)-5-8	14.759	7.66	2.717	97.0	261
ST-(160-200)-5-9	14.847	7.69	2.725	97.3	261
ST-(160-200)-5-10	14.863	7.69	2.724	97.3	261
ST-(160-200)-5-11	14.891	7.70	2.718	97.1	261
ST-(160-200)-5-12	14.874	7.71	2.717	97.0	261
ST-(160-200)-5-13	14.885	7.71	2.714	96.9	261
ST-(160-200)-5-14	14.897	7.70	2.714	96.9	261
ST-(160-200)-5-15	14.862	7.68	2.722	97.2	261

Table 4.3. Variation of relative density of the compacts

	Al	ST-(30-45) 5 wt%	ST-(30-45) 1 wt%	ST-(45-56) 5 wt%	ST-(56-90) 5 wt%	ST-(90-106) 5 wt%	ST-(106-160) 5 wt%	ST-(160-200) 5 wt%
Minimum	97.59	96.69	96.90	96.80	96.90	96.90	96.80	96.69
Maximum	98.69	96.80	97.40	97.40	97.09	97	97	97.40
Mean	**98.01**	**96.77**	**97.13**	**96.97**	**97.03**	**96.96**	**96.87**	**97.04**
Median	97.85	96.80	97.149	96.85	97.09	97	96.85	97

4.2. Foaming Set-Up

In order to assess the effect of particle addition on the expansion of the powder compact, an experimental set-up, which measures the linear expansion of the compact during foaming was used. The schematic of the foaming set-up is shown in Figure 4.4. and Figure 4.5 shows the pictures of the parts of the foaming set-up. The experimental set-up consists of a vertical split furnace, a linear expansion measurement system and a foaming mold which accomodates the compact. The cold compact was inserted inside a stainless steel mold with an inner diameter of 3 cm and a height of 8 cm (Figure 4.6). The bottom of the mold was closed tightly and the compact was placed at the bottom. The linear expansion measuring system consists of a linear variable displacement transducer (LVDT), rod, wires and pulleys. In a typical experiment, the furnace was initially heated to 750 ^{o}C. The mold accommodating the compact was then inserted into the furnace with the help of an elevator system. The rod which was connected to linear expansion measuring system was lowered and the steel plate attached to the end touched to compact's upper surface. As soon as the mold was inserted, the furnace temperature decreased to 640 ^{o}C. Within 10-15 minutes, the furnace temperature rose to 730 ^{o}C as the mold was heated up and the foaming started. As the foaming proceeded the plate moved up and pushed the linear expansion measuring wire to the backward with the help of two pulleys as seen in Figure 4.5.b. The LVDT which was assembled to the end of the wires measured the movement of the wire and hence the linear expansion of the compact. The measurements were taken with the help of a data logger which was directly connected to the LVDT. Finally the data were transferred to a personal computer. The linear expansion data (mm) was then converted to linear expansion (LE) using the following equation:

$$LE = \frac{expansion}{initial\ length} \tag{4.1}$$

A linear expansion of 2 implies that compact expanded two times of its initial length.

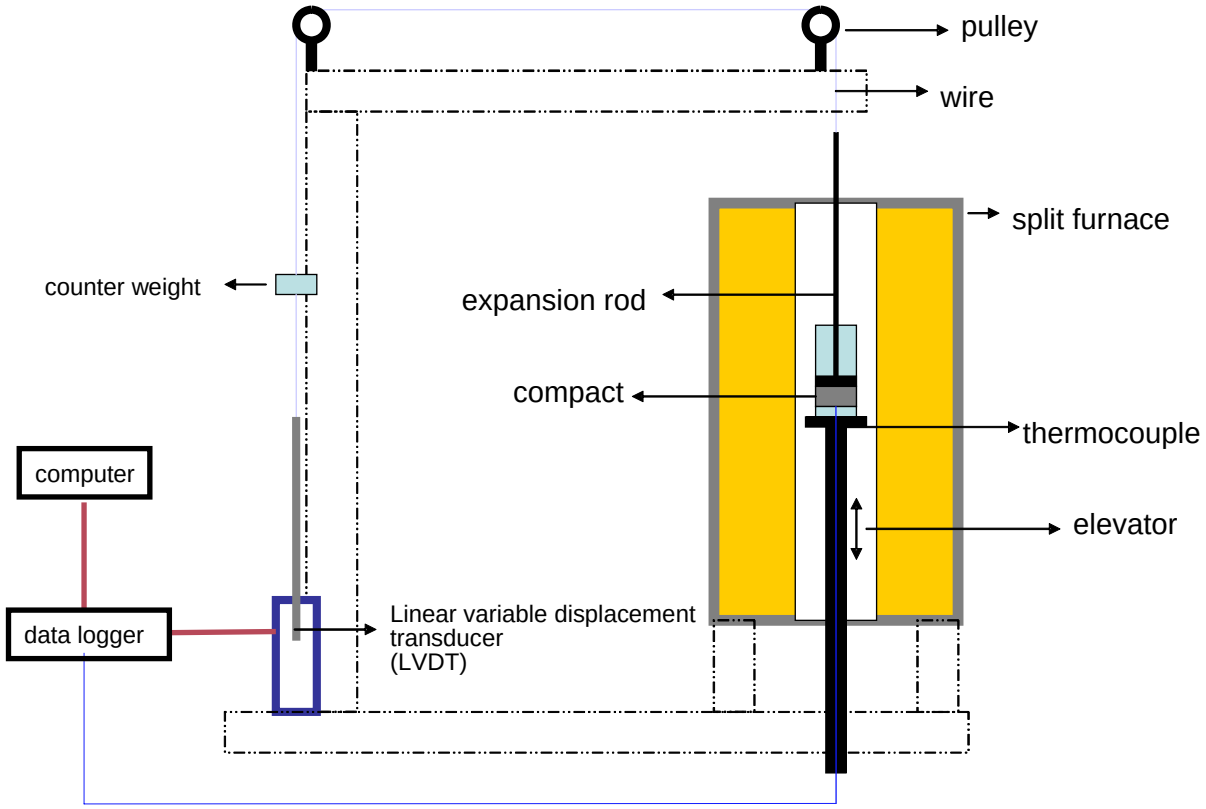

Figure 4.4. Schematic of foam expansion-measurement set-up

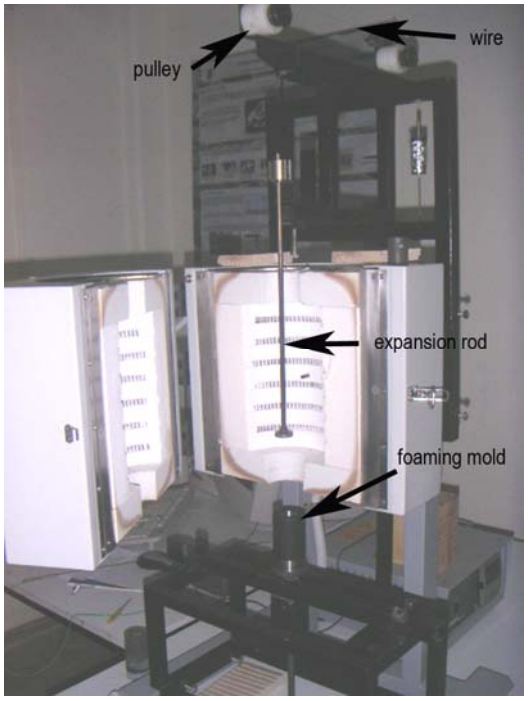

(a)

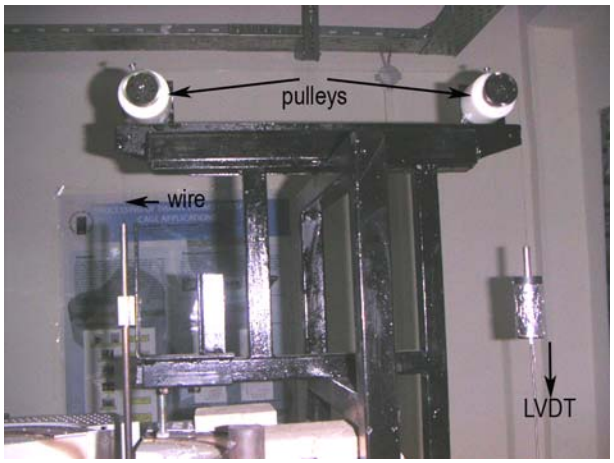

(b)

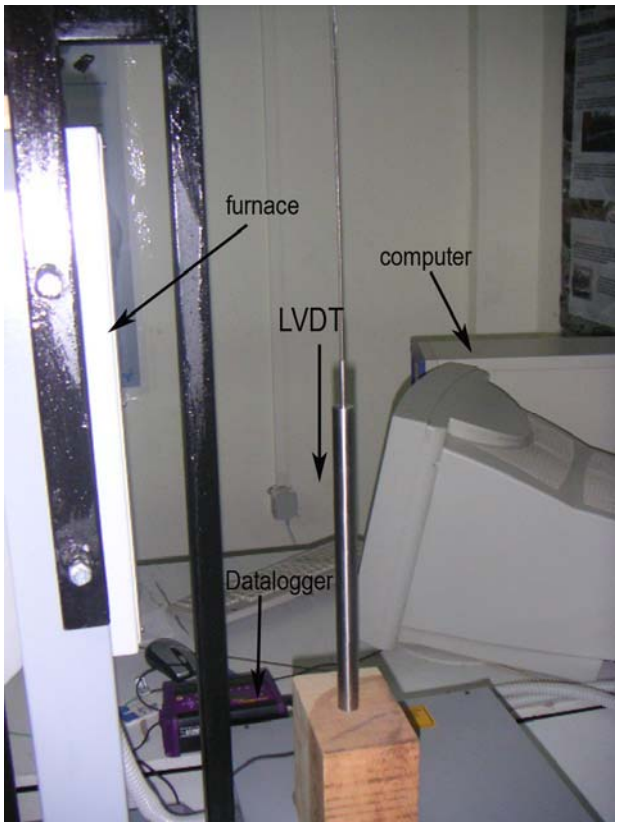

(c)

Figure 4.5 Foaming experimental set up (a) general view, (b) pulleys and (c) LVDT, data logger and computer

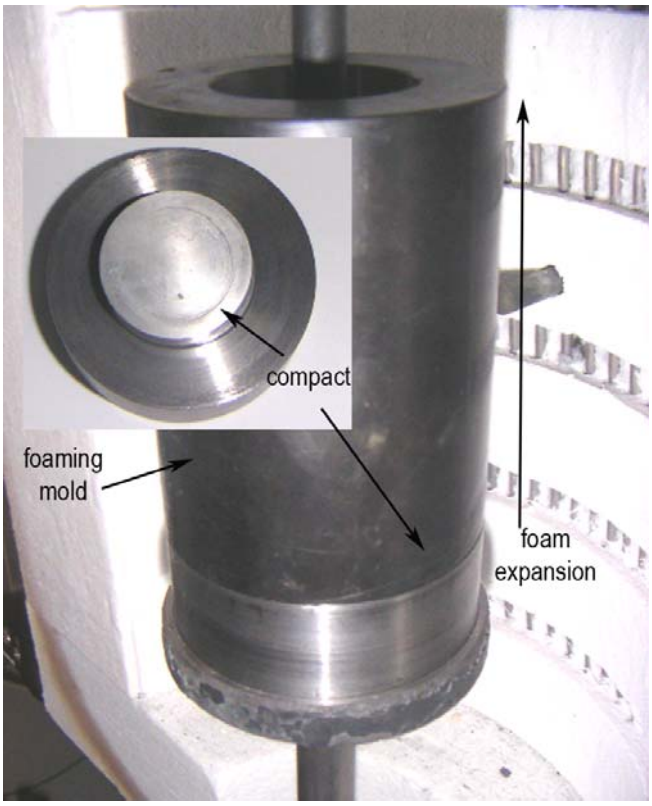

Figure 4.6. Foaming mold and position of the compact

Inital experiments were performed in order to control the correctness of expansion experiments. Various types of pulleys and wires were tried. The pulleys and wire combination which provided the lowest friction were selected. A special EDM Wire was used in the expansion measurement set-up. The electrically measured expansion data were further compared with the mesurements made on the quickly cooled sample. A good agreement was found between the measurements, confirming the accuracy of the linear expansion measurements made in this study.

Two types of measurements were made in the foaming experiments. In the first, the compacts were foamed for 15 minutes and then cooled at room temperature. In the second, the compacts were foamed partially at various times such as 100, 150, 200, 300, 400 and 500 seconds and then taken from the furnace quickly with the elevator system and then quenched with water. The mold prevented the liquid foam from contacting to the water. All procedure continued, taking from the furnace and quenching in water, for 10-15 seconds. Therefore the microstructure of the quenched foams showed the foam structure of 10-15 seconds further in the measured expansion-time data.

4.3. Microscopy

Various kinds of microscopic analysis techniques were applied to foamed compacts. Sectioning of foams, parallel to the expansion axis was done using an electrical discharge machine in order to prevent cells from damaging. The cross-sections were ground and polished for microscopic analysis. The grinding and polishing processes were done gently, again, preventing extensive cell wall deformation. The polished cross-sections were etched before microscopic analyses using Kroll's reagent (3 cm^3 of HF and 6 cm^3 of HNO_3 in 100 ml of H_2O). Polished foam cross-sections were scanned in order to analyze the cells sizes. Microscopic analyses were further performed on the tested composite samples using optical microscope (OM) and a Philips XL30-SFEG scanning electron microscope (SEM) with an EDX analyzer. ScionImage image analyzing software was used to make measurements from the micrographs of the foam samples.

4.4. Mechanical Testing

Quasi-static compression tests were conducted in a displacement controlled SHIMADZU AG-I universal testing machine with a displacement rate of 2.5 mm s^{-1} using an eccentric compression upper test platen. Sizes and densities of the test samples are listed in Table 4.3. Length/diameter ratio was taken as 1.5. These samples were core dirilled from the foamed compacts through the foaming direction as shown in Figure 4.7. The drilling was performed using an electrical discharge machine. The test samples were extracted from the mid sections in order exclude the drainaged sections in compression testing. During compression testing, the test platens were lubricated in order to reduce the radial frictional forces. Few of the samples' deformation were video recorded in order to extract the deformation mechanism involved in the crushing. The stress and strain were calculated using the following equations:

$$\sigma = \frac{P}{A_o} \tag{4.2}$$

$$\varepsilon = \frac{\delta}{L_o} \tag{4.3}$$

where P, A_o, δ and L_o are the load, initial cross-sectional area, displacement and initial length of the sample respectively.

Table 4.4. Sizes, densities and masses of the foam samples for compression test

Sample Code	**Initial height (mm)**	**Mass (mg)**	**Diameter (mm)**	**Density (g/cm^3)**
ST-(160-200)-5-6	22.00	1948	15.40	0.476
ST-(160-200)-5-7	21.15	2291	15.40	0.582
ST-(160-200)-5-13	23.45	1567	15.40	0.359
ST-(160-200)-5-14	22.40	1139	15.40	0.273
ST-(160-200)-5-15	22.00	1617	15.40	0.395
ST-(30-45)-1-4	23.60	579	15.40	0.132
ST-(30-45)-1-5	23.00	1075	15.40	0.251
ST-(30-45)-1-7	22.20	891	15.40	0.216
ST-(30-45)-1-8	22.75	730	15.40	0.173
ST-(30-45)-1-9	22.10	935	15.40	0.228

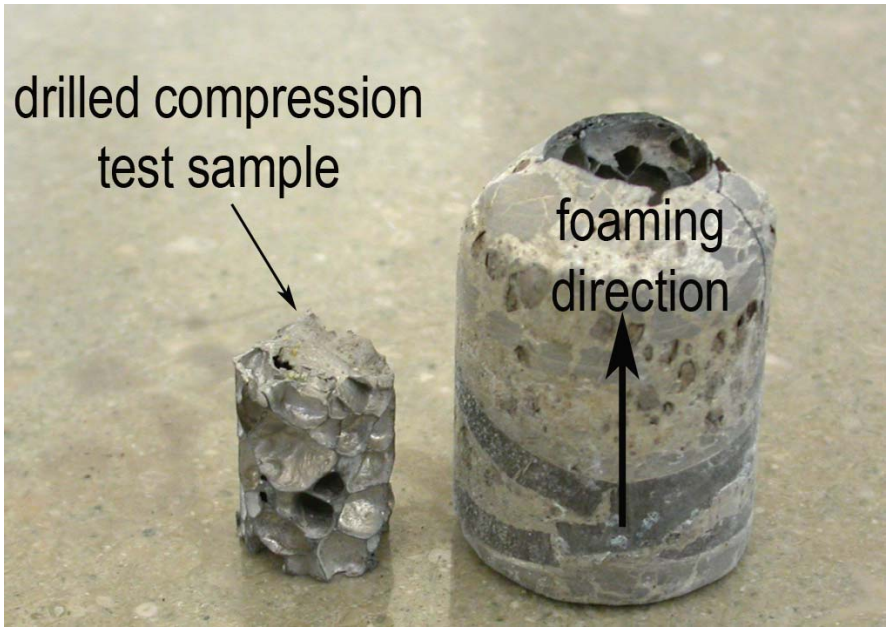

Figure 4.7. Drilled compression test sample and foam sample after drilling

CHAPTER 5

RESULTS

5.1. Pure Al Compacts

A typical linear expansion-time and temperature-time graph of an Al powder compact (precursor) with 1% TiH_2 foaming agent addition is shown in Figure 5.1. The expansion-time curve may be considered in 4 regions as labeled in Figure 5.1. In the first and second regions, 1 and 2, the expansion increases almost linearly with time, although the rate of expansion is higher in the second region. After maximum expansion, LE_{max}, the expansion decreases in region 3. In region 4, the expansion remains to be nearly constant and the expansion in this region is labeled as LE (Figure 5.1). These regions are characteristics of the foamable Al precursors and observed in all compacts. During foaming experiments, although the furnace is fixed to 750 ºC; when the cold mold accommodating the foamable compact is inserted, the temperature drops to a lower temperature. During a typical foaming duration, the temperature rises to 730 ºC as depicted in Figure 5.1. The increase in the expansion rate of the compact in the second region is due to the melting of the compact. Before the melting temperature (673 ºC), the compact expansion starts at temperatures of 650 ºC, corresponding to region 1 in Figure 5.1.

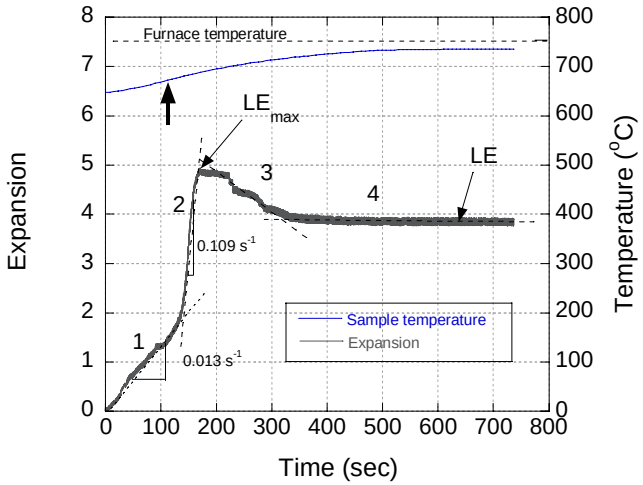

Figure 5.1. Typical expansion-time and temperature-time graph of Al compact

Figure 5.2 shows the expansion-time graphs of the foaming of Al precursors. Despite the variations between the expansion values of the compacts, the expansion behavior is almost the same, showing the characteristic expansion behavior as stated earlier. It is noted in Figures 5.1 and 5.2 that, the foam expansions are initially rather quick, reaching a maximum expansion in 147-169 sec and leveling after 300 sec. The rate of expansion in Region 2 (0.109 s^{-1}) is about 10 times higher than that of Region 1 (0.013 s^{-1}). It is also seen in Figure 5.1 that the transition from Region 1 to Region 2 occurs at an expansion of 2 and roughly at 125 sec. The values of LE_{max} and LE are further shown in Figure 5.2 and vary between 4.13 and 4.86 and 3.25 and 3.86. Higher is the LE_{max} and lower is the LE, as seen in Figure 5.2.

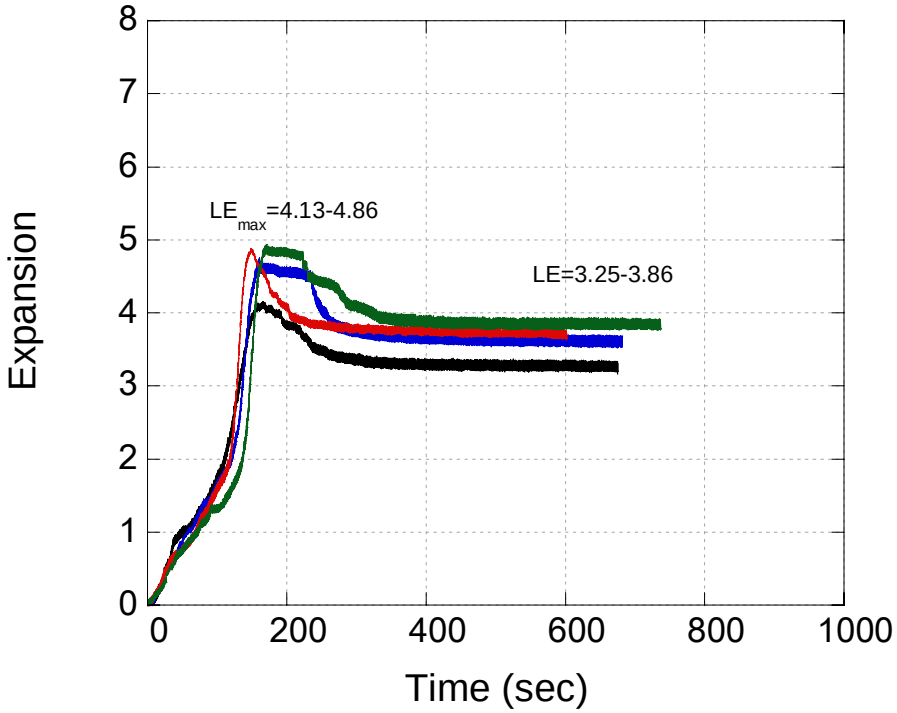

Figure 5.2. Expansion-time graphs of Al compacts

In order to determine the foam evolution including cell size, cell wall thicknesses and the extent of foam drainage, foams were taken from the furnace after prescribed furnace holding times and then quenched in water. These tests were called interrupted foaming tests. Figure 5.3 shows the resultant expansion-time graphs of such interrupted-foaming experiments. Figure 5.4 shows the general and cross-sectional views of the foam samples taken from the furnace after a certain furnace holding time, respectively. The final heights of the foam samples in these figures confirm clearly that the linear expansion increases until the maximum expansion. Cell size increases as the

furnace holding time increases, particular cells are bigger in the upper sections of the foam cylinders. The drainage, the accumulation of Al metal at the bottom of foamed compacts, is clearly seen to increase as the furnace holding time increases in Figure 5.4.b. Another effect of longer furnace holding times is the thickening of the cell walls located at the bottom sections of the foam cylinders. The foam cell collapse is further seen at the upper sections of the foam cylinder after 200 sec furnace holding time. In summary increasing furnace holding time in Al foamable compacts (a) increases cell size, (b) intensifies drainage and cell wall thickening at the bottom sections, (c) promotes cell wall collapse at the upper sections and (d) induces a nonhomogeneous cell size distribution in the foam cylinder. One can also detect from Figure 5.4.a that the earlier cells are elliptical as the lateral crack like features are formed on the foam sample surfaces. These are the cracks formed on the oxide layer on surface of the foam samples.

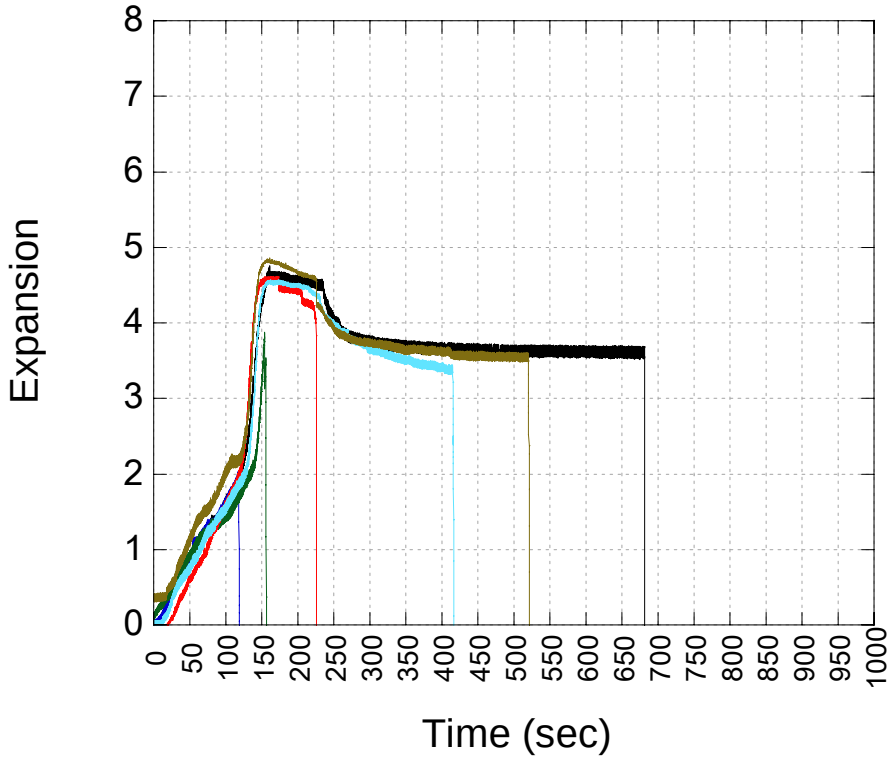

Figure 5.3. Expansion-time graphs of foamable Al compacts in interrupted-foaming

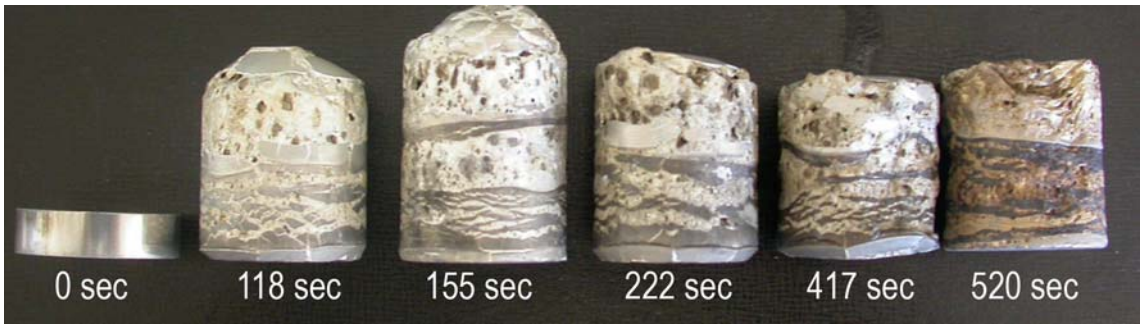

(a)

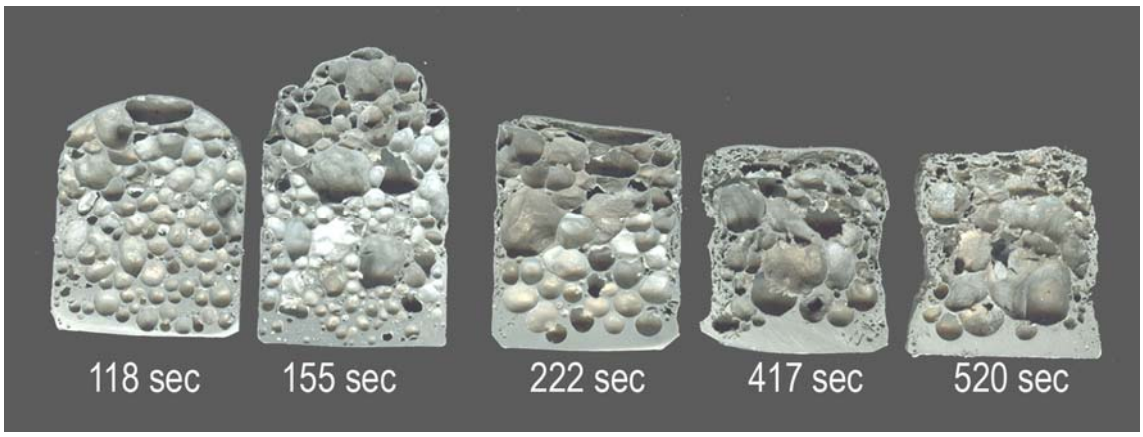

(b)

Figure 5.4. Pictures of foamed samples until about various furnace holding times; (a) general view and (b) cross-sectional view

5.2. Effects of 30-45 micrometers Size Particles

The expansion-time graphs of 5 wt% 30-45 μm size Ti6Al4V-Al powder compacts are shown in Figure 5.5 together with the representative expansion-time graph of Al compacts. The addition of 5 wt% 30-45 μm size Ti6Al4V powder greatly reduces LE_{max} and LE as compared with Al compacts without particle addition. The values of LE_{max} and LE for these compacts are relatively low, 2.15-2.60 and 1.274, respectively. Essentially, following the Region 1, the graphs show fluctuations in expansion values and as the time increases the fluctuations decreases. These fluctuations are related to the reaction between liquid Al and solid Ti6Al4V particles and were elaborated in discussion section.

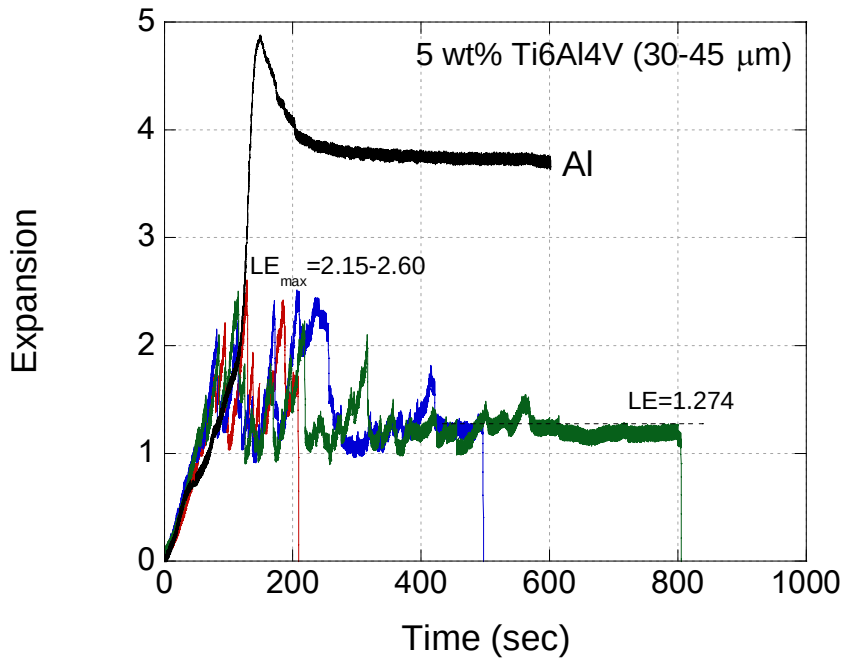

Figure 5.5. Expansion-time graphs of 5 wt% 30-45 μm size Ti6Al4V-Al compacts

In order to see the effect of particle weight fraction on the expansion behavior of Al compacts, compacts having particle wt% of 0.5, 1, 2, 3 and 4 were prepared and foamed in the furnace with the same processing parameters. The expansion-time graphs of 30-45 μm size Ti6Al4V-Al powder compacts of varying weight percents are shown in Figure 5.6. The expansion behavior of 0.5 and 1 wt% Ti6Al4V powder-added Al compacts are very much comparable with that of Al compacts as seen in the same figure. However, the expansion decreases sharply when Ti6Al4V powder weight percent increases over 2 %. The final expansions fluctuate around 1 (Figure 5.6). Figure 5.7 shows the cross-sections of 5 wt% 30-45 μm Ti6Al4V-Al powder compacts foamed until various furnace holding times. The initial large cells at 208 sec disappear at longer furnace holding times. This proves the cell collapse with increasing furnace holding times. It is also noted in the same figure that the cell size distribution is very heterogeneous. The fluctuations in expansion-time graphs are believed to be a result of the collapsing of grown large cells which are identified at the early stages of the foaming process. Figure 5.8 shows the pictures of the foamed 30-45 μm size Ti6Al4V-Al powder compacts containing various weight percentages of Ti6Al4V particles. These samples were foamed until about 800 sec. The effect of weight percentage of particles on the final expansion is clearly seen in this figure. After 1 wt% of the particles addition, the expansion of the foam decreases greatly.

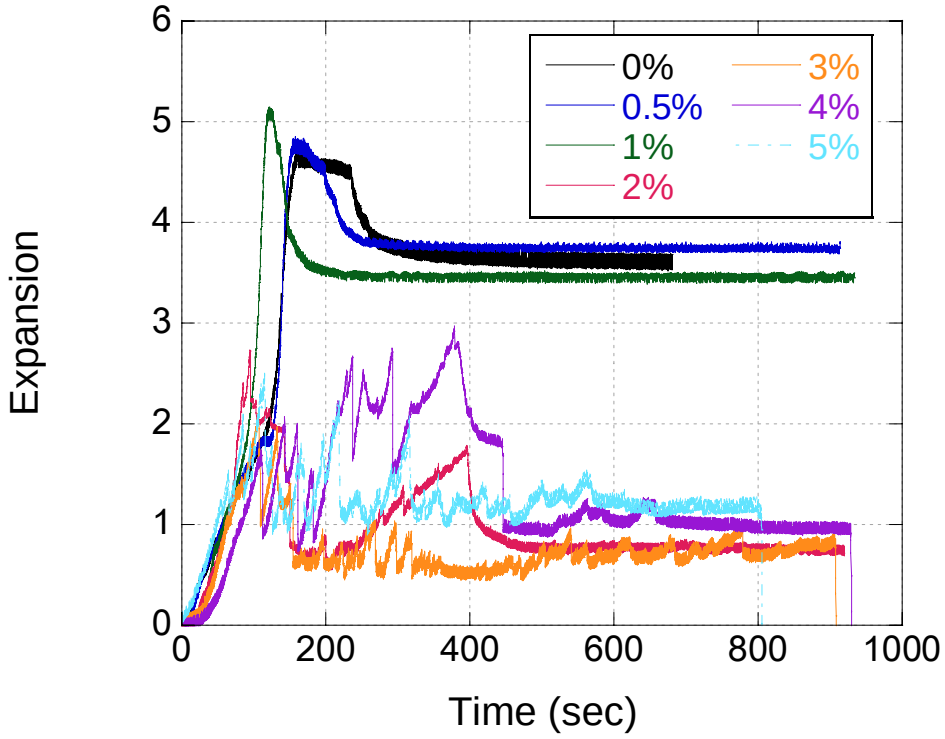

Figure 5.6. Expansion-time graphs of Al compacts containing different wt% of 30-45 μm size Ti6Al4V powder

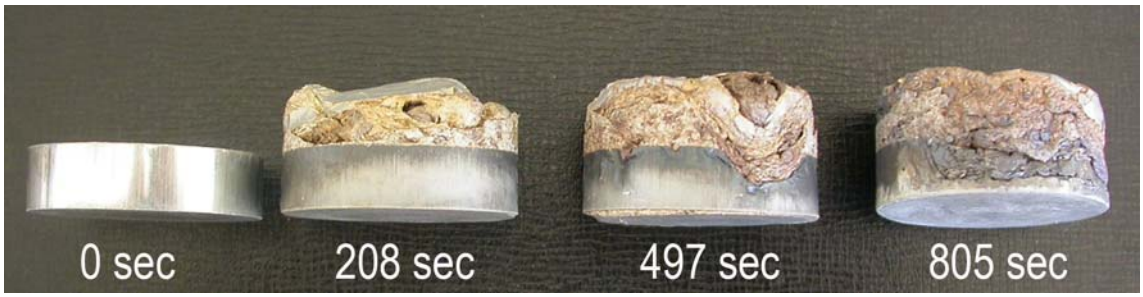

(a)

(b)

Figure 5.7. Pictures of 5 wt% 30-45 μm size Ti6Al4V-Al compacts foamed until about various furnace holding times (a) general view and (b) cross-sectional view

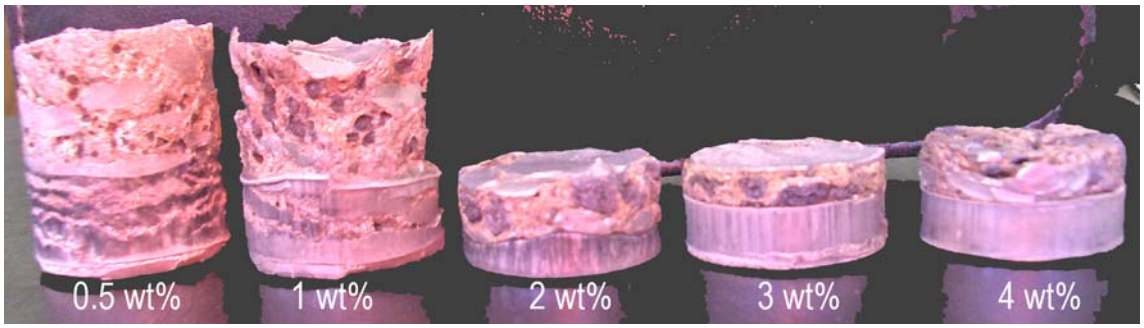

Figure 5.8. Pictures of foamed 30-45 μm size Ti6Al4V-Al compacts

5.3. Effects of 45-56 micrometers Size Particles

The expansion-time graphs of 5 wt% 45-56 μm size Ti6Al4V-Al powder compacts are shown in Figure 5.9. The addition of 5 wt% 45-56 μm size Ti6Al4V results in LE_{max} and LE values varying between 2 and 3 and 1-1.5, respectively. The final expansions are again very low and fluctuate around 1, the same as those of 5 wt% 30-45 μm size Ti6Al4V-Al powder compacts.

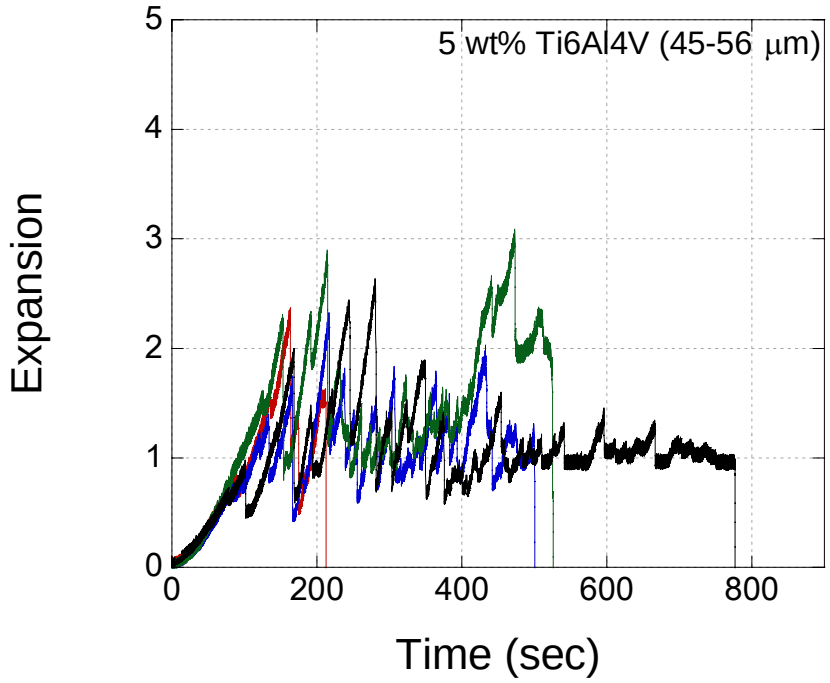

Figure 5.9 Expansion-time graphs of 5 wt% 45-56 μm size Ti6Al4V-Al compacts

5.4. Effects of 56-90 micrometers Size Particles

The expansion-time graphs of 5 wt% 56-90 μm size Ti6Al4V-Al powder compacts are shown in Figure 5.10. LE_{max} and LE values in 5 wt% 56-90 μm size Ti6Al4V powder compacts is also very low, 1 and 2, respectively. In these compacts, contrary to 5 wt% 30-45 and 45-56 μm size Ti6Al4V-Al powder compacts; the expansions show initially no sharp fluctuations until about 300 sec. The expansion increases to a maximum value of about 2 at about 400 sec; thereafter it decreases to a value of 1 after 500 sec. This expansion behavior is quite different from those of the earlier compacts containing smaller size of Ti6Al4V particles.

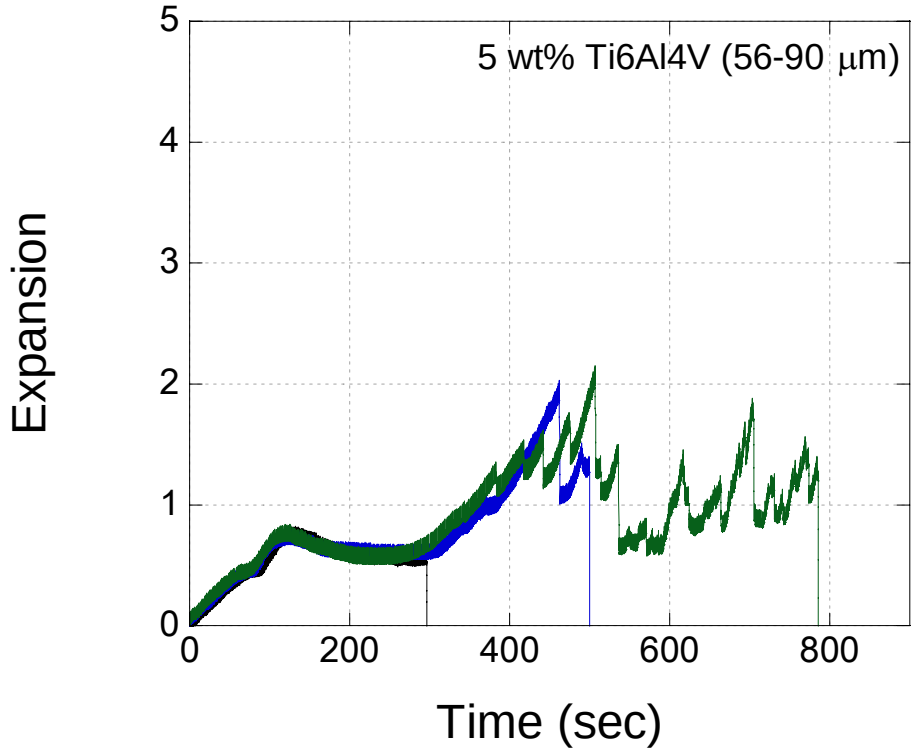

Figure 5.10. Expansion-time graphs of 5 wt% 56-90 μm size Ti6Al4V-Al compacts

5.5. Effects of 90-106 micrometers Size Particles

The expansion-time graphs of 5 wt% 90-106 μm size Ti6Al4V-Al powder compacts are shown in Figure 5.11. Initially, the expansions are around 1.5-2 at above 150 sec and decrease gradually to 1; thereafter increase above 2. The expansion

behavior of 5 wt% 90-106 μm size Ti6Al4V-Al powder compacts is very similar to that of 56-90 μm size Ti6Al4V-Al powder compacts.

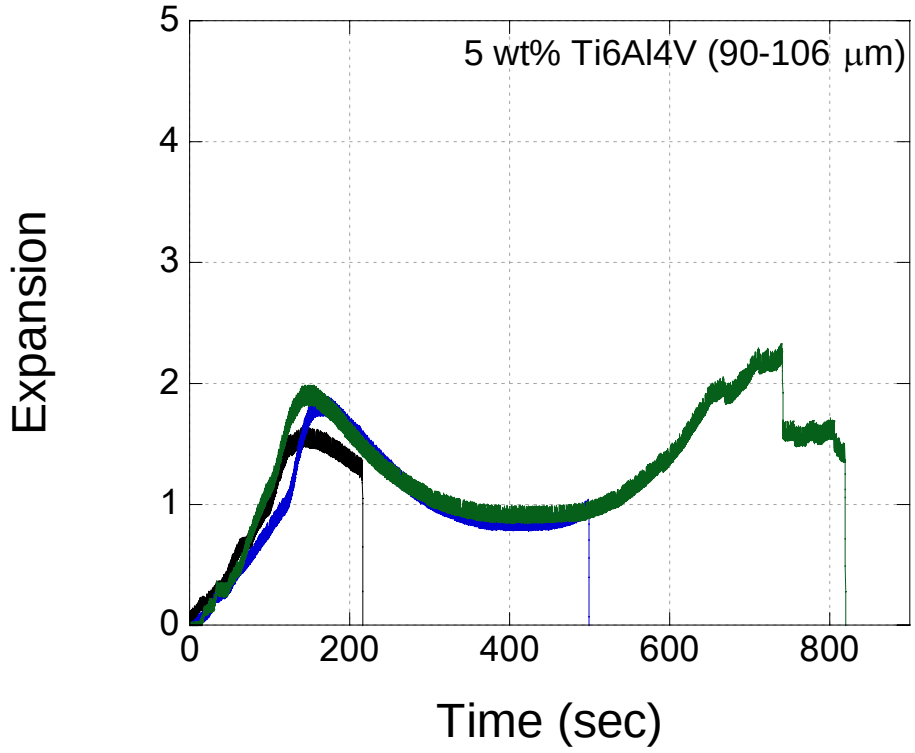

Figure 5.11. Expansion-time graphs of 5 wt% 90-106 μm sized Ti6Al4V-Al compacts

Figure 5.12 shows general view and cross-sections of the foamed 5 wt% 90-106 μm size Ti6Al4V-Al powder compacts until about various furnace holding times. At 200 sec, the cells are elongated normal to the compaction direction and Ti6Al4V particles are collected in the mid sections of the foamed compact. At increasing furnace holding times, 820 sec, the cells become more elliptical but the cell size distribution is still very heterogeneous. The cell collapse at the upper sections of foam cylinder is also visible in Figure 5.12.b. Drainage is clearly seen at longer furnace holding times but the thickness of the drained region is narrow when compared with Al compacts at similar furnace holding times.

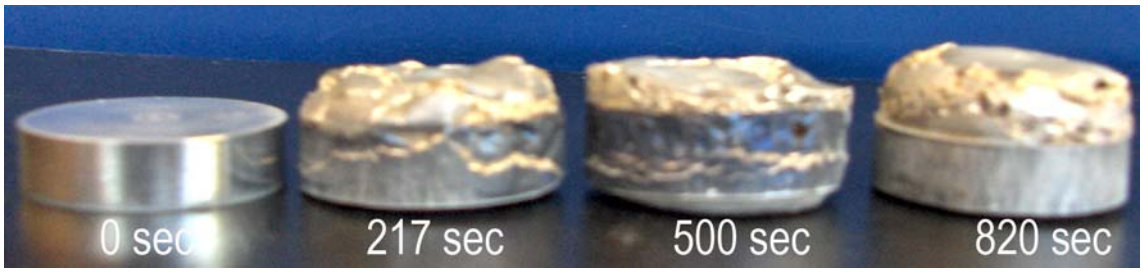

(a)

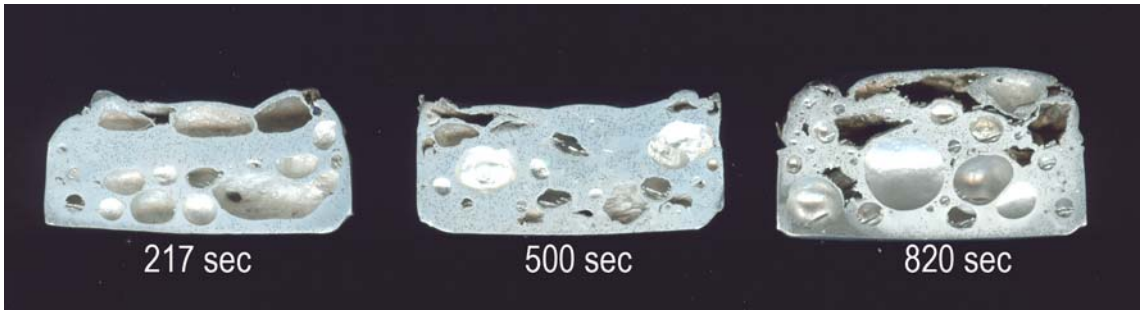

(b)

Figure 5.12. Pictures of 5 wt% 90-106 μm size Ti6Al4V-Al compacts foamed until about various furnace holding times (a) general view and (b) cross-sectional view

5.6. Effects of 106-160 micrometers Size Particles

The expansion-time graphs of 5 wt% 106-160 μm sized Ti6Al4V-Al powder compacts are shown in Figure 5.13. Initially the expansions are relatively high; 2.5-3 at above 150 sec, it gradually decreases to 2 after 150 sec; thereafter it gradually increases to a value of 2 at 800 sec furnace holding time. The expansion behavior is very similar to those of 56-90 and 90-106 μm size Ti6Al4V-Al compacts. Figures 5.14.a and 5.14.b show the general view and cross-sections of the foamed compacts until about various furnace holding times respectively. At 200 sec, the cells are slightly elongated normal to the compaction direction and the cells become more spherical at the bottom sections at furnace holding time of 500 sec. The cell collapse at the upper sections is visible but the extent of cell collapse is relatively reduced as compared with 56-90 and 90-106 μm size Ti6Al4V-Al compacts. It is also noted in Figure 5.14.b that drainage is greatly reduced at longer holding times as compared with Al compacts.

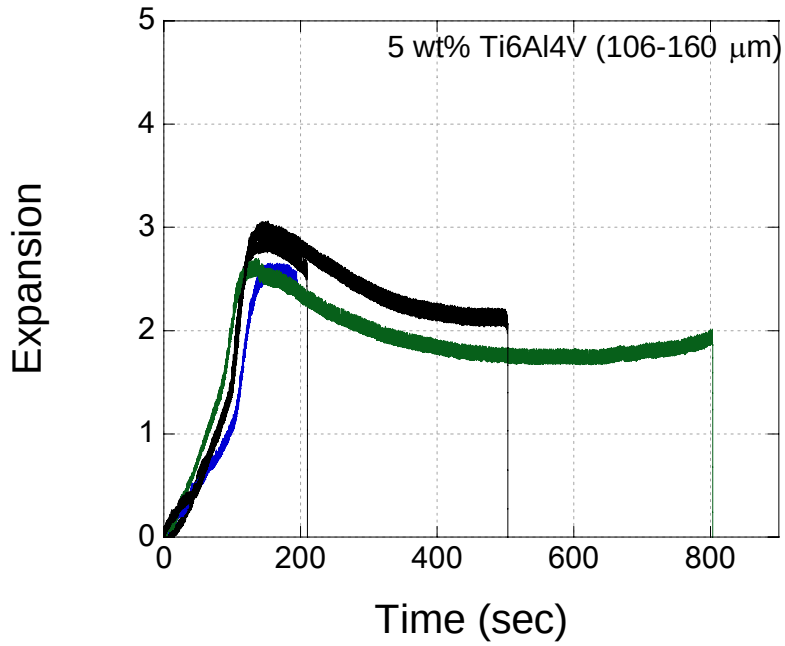

Figure 5.13. Expansion-time graphs of 5 wt% 106-160 μm size Ti6Al4V-Al compacts

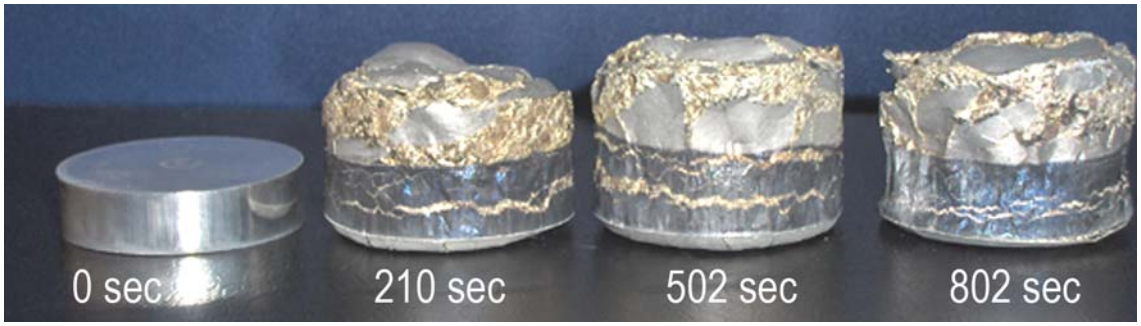

(a)

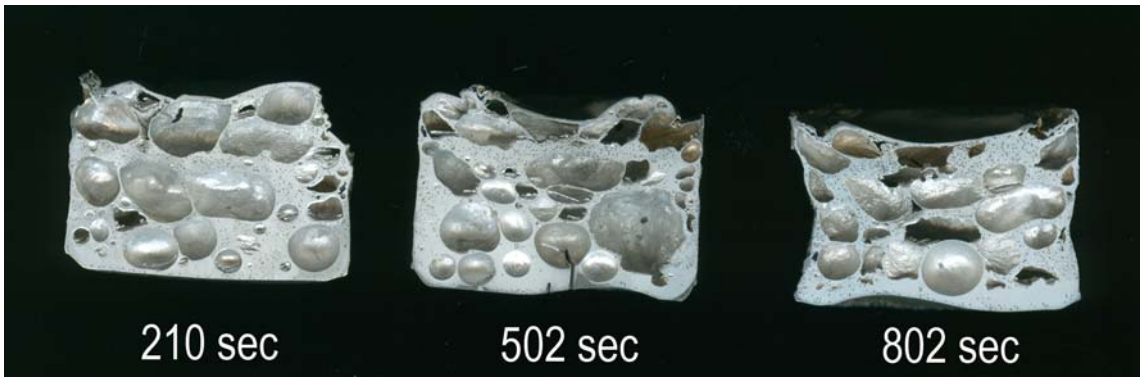

(b)

Figure 5.14. Pictures of 5 wt% 106-160 μm size Ti6Al4V-Al compacts foamed until about various furnace holding times: (a) general view and (b) cross-sectional view

5.7. Effects of 160-200 micrometers Size Particles

The expansion-time graphs of 5 wt% 160-200 μm size Ti6Al4V-Al powder compacts are shown in Figure 5.15. The expansion behavior of these compacts show very much resemblance with that of Al compacts. Regions 1 and 2 are clearly seen in the initial region of the expansion curve in Figure 5.15. LE_{max} and LE values vary between 3-3.92 and 2.18-2.46, respectively. These values are smaller than those of Al compacts, 4.13-4.86 and 3.25-3.86. It is noted that the compact reaches LE_{max} within 80-100 sec, earlier than Al compacts. Similar to Al compacts after maximum expansion at about 100 sec, the expansion values decrease. Figures 5.16.a and 5.16.b show the general view and cross-sections of the foamed 5 wt% 160-200 μm size Ti6Al4V-Al powder compacts until various furnace holding times respectively. The initial high expansion at about 100 sec is clearly seen in Figure 5.16.b. Although, cell collapse is seen at upper regions of the foam cylinder in Figure 5.16.b, the drainage is greatly reduced at longer furnace holding times as compared with Al compacts. It is also noted that the initial nearly equi-axed cells are elongated normal to compaction axis at longer furnace holding times. Compared with Al compact foams, the cell size distribution in these compacts are much more homogeneous at longer furnace holding times (400 sec), showing the effect of Ti6A4V particle addition on the kinetic stability of cells.

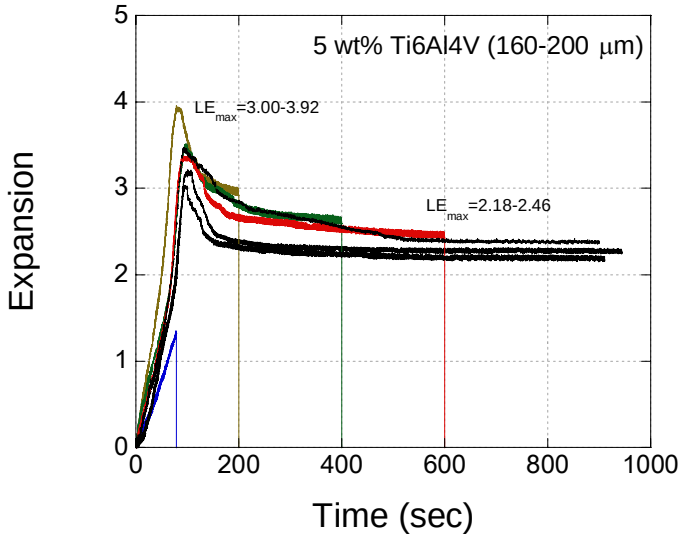

Figure 5.15 Expansion-time graphs of 5 wt% 160-200 μm size Ti6Al4V-Al compacts

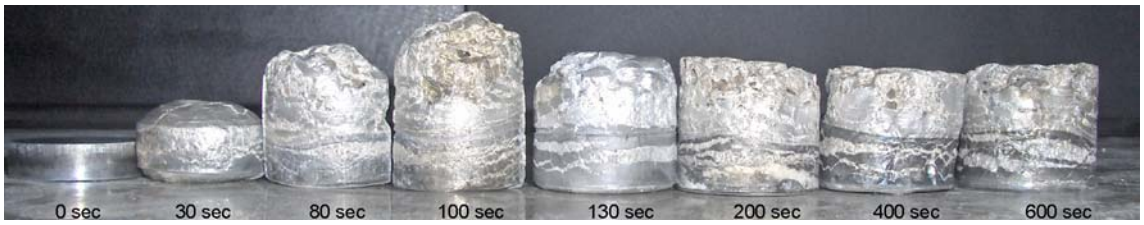

(a)

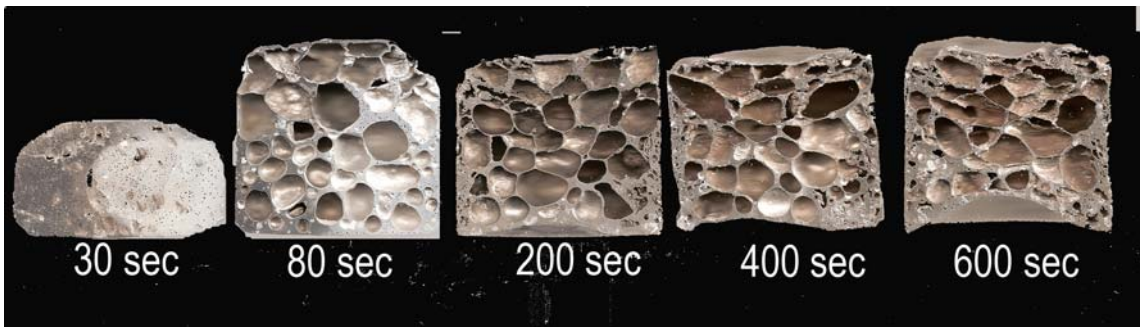

(b)

Figure 5.16. Pictures of 5 wt% 106-160 μm size Ti6Al4V-Al compacts foamed until about various furnace holding times (a) general view and (b) cross-sectional view

5.8. Comparison of The Expansions of Ti6Al4V-added Al Compacts with Pure Al Compacts

The expansion-time graphs of representative 5 wt% Ti6Al4V-Al powder compacts are shown in Figure 5.17 together with that of Al compact for comparison. Increasing particle size at constant weight percentage of the particles increases the expansion values, while the expansion values of compacts with particle addition are lower than those of pure Al compacts as shown in Figure 5.17. It is also noted in the same figure that the LE fluctuations disappear for the particles addition with sizes larger than 90-106 μm. The rate of expansion in the initial rising part of the expansion-time curves is noted to increase with increasing particle size at the same weight percentage. Figures 5.18.a and 5.18.b show the cell structures of foamed Al compact and Ti6Al4V-Al compacts after furnace holding times of 200 and 500 sec, respectively. At both furnace holding times, 200 and 500 sec, the foams of 160-200 μm size Ti6Al4V-Al compacts show more homogeneous cell size distribution than the foams of Al compact. The reduced extent of drainage is also seen in 106-160 and 160-200 μm size Ti6Al4V-

Al compacts as compared with Al compacts. However, the cell growth in Ti6Al4V particle-added foamed compacts is relatively low as compared with Al compact.

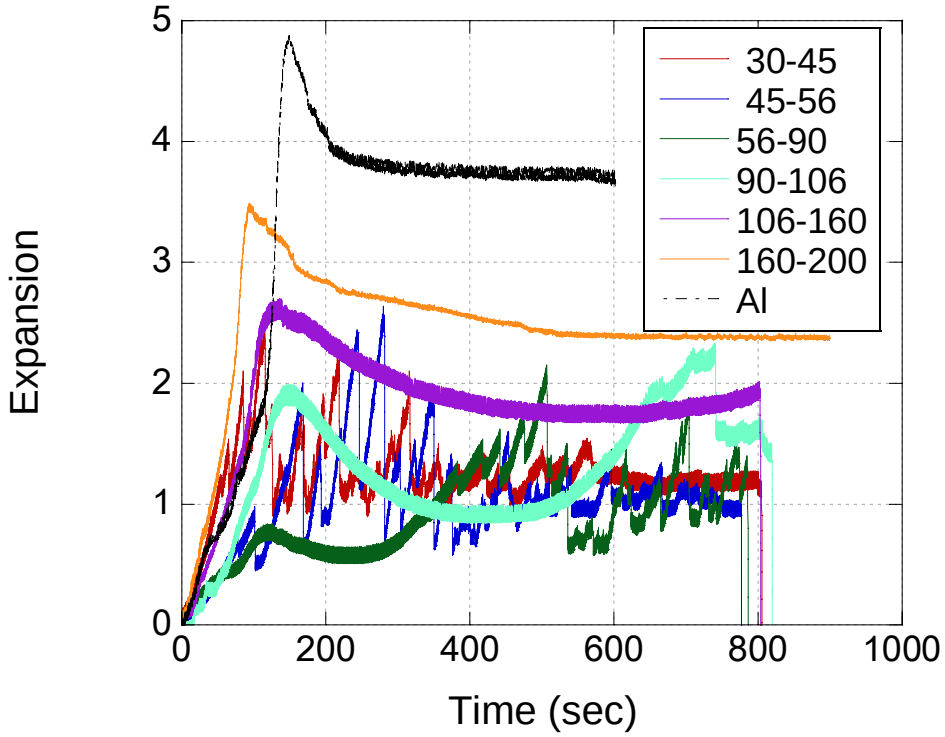

Figure 5.17. Expansion-time graphs of 5 wt% 160-200 μm size Ti6Al4V-Al compacts

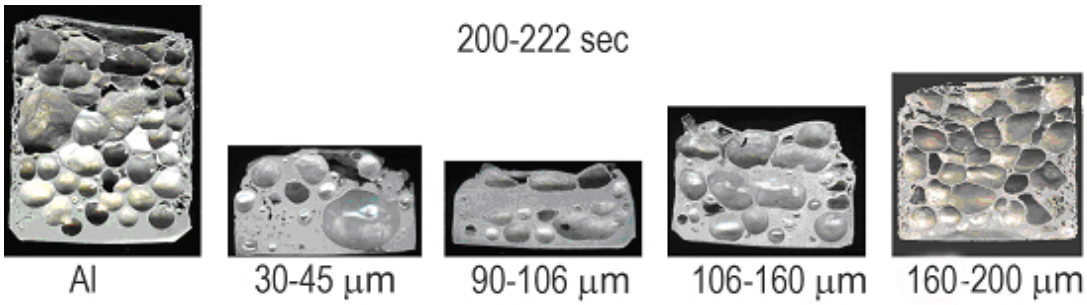

(a)

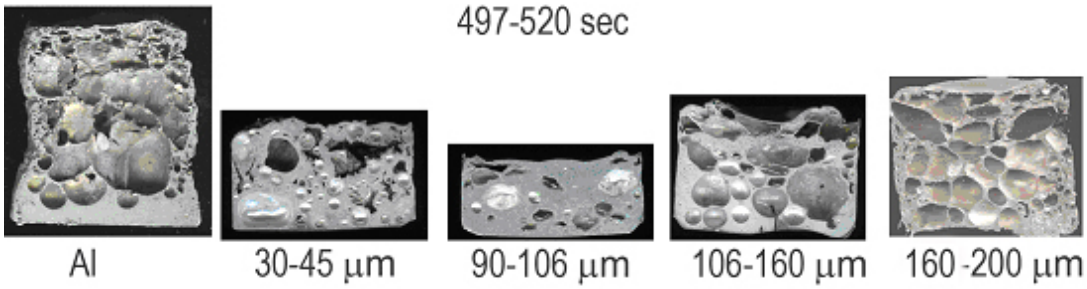

(b)

Figure 5.18. Comparison of the cross-sections of foams taken at similar furnace holding times: (a) 200-222 sec and (b) 497-520 sec

In order to see the effect of particle addition on the cell size of the compacts as a function of furnace holding time, the number of cells and the cell sizes of the foams taken from the furnace after prescribed holding times were measured using Scion Image program. In Figures 5.19.a and 5.19.b, the typical measurements are shown. The cell sizes were measured horizontally for comparison. The measurements were also started from the bottom of the foam cylinder; therefore, initial cell size measurements belong to the bottom sections and latter measurements belong to the upper sections. The variation of cell diameter, number of cells and average cell diameters of the Al and 160-200 μm size Ti6Al4V-Al foamed compact samples are shown in Figures 5.20.a and 5.20.b, respectively, while in Figure 5.20.c average cell diameters and number of cells of Al and 160-200 μm size Ti6Al4V-Al foamed compact samples are shown together for comparison. As the furnace holding time increases, the number of cells decreases, while average cell size increases for both types of foamed compacts as depicted in Figures 5.20.a and 5.20.b. However, the growth of cell diameter in Al compacts is higher with increasing furnace holding times. Initially, the number of cells is also higher in Al compacts and later decreases below that of Ti6Al4V-Al compacts. In Ti6Al4V-Al

compacts, the increase of the average cell diameter and decrease of the number of cells are more gradual than Al compacts, showing increased kinetic stability of compacts with particle addition.

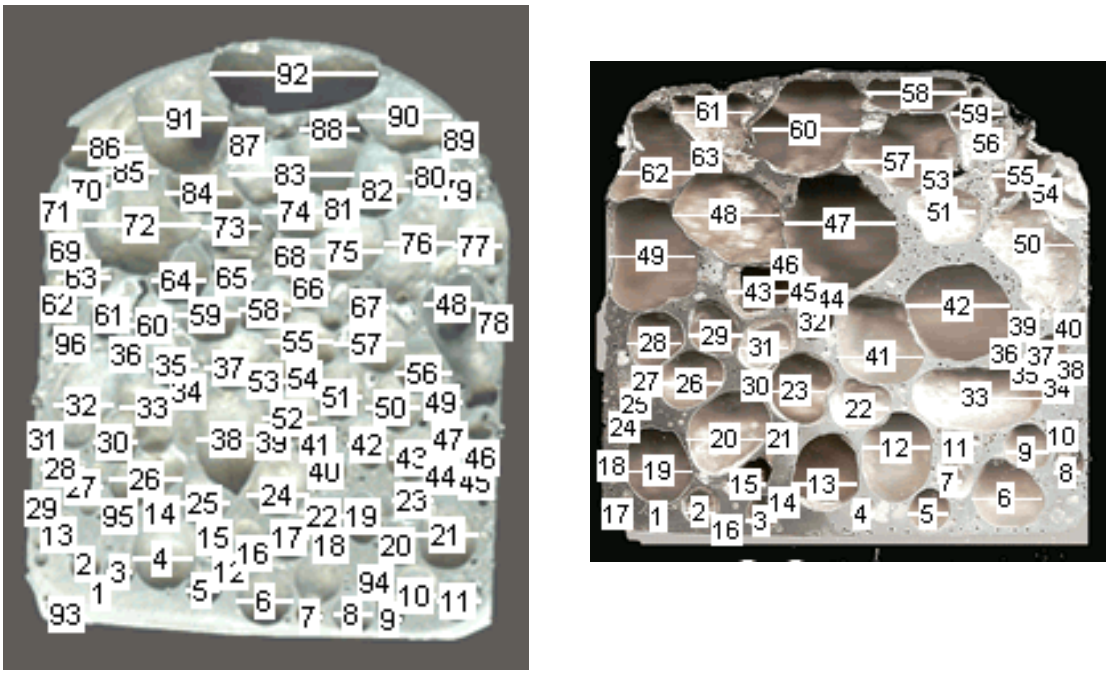

(a) (b)

Figure 5.19. Examples for the cell size measurements in (a) Al and (b) 160-200 μm size Ti6Al4V-Al foam samples

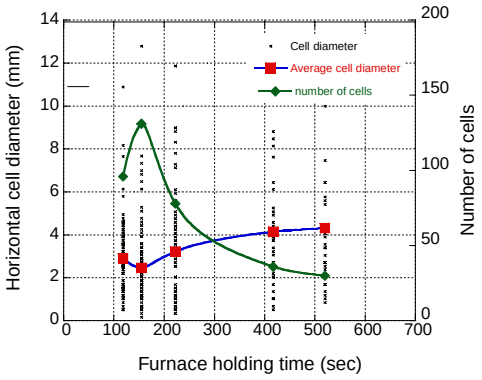

(a)

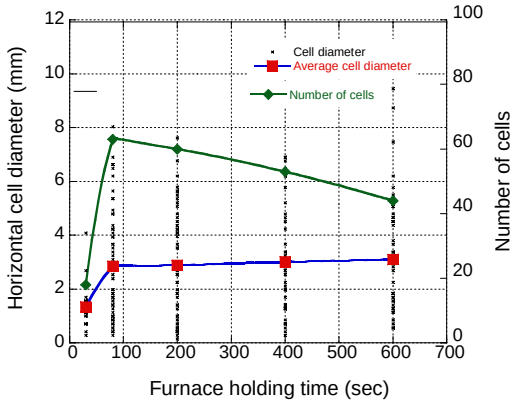

(b)

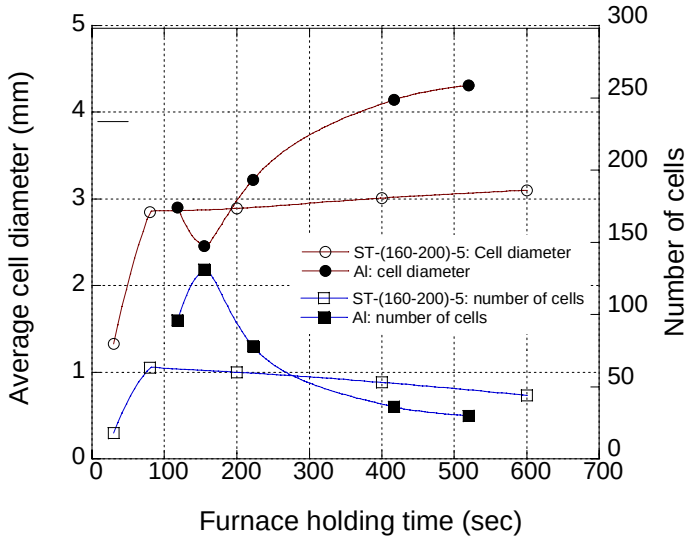

(c)

Figure 5.20. Cell diameter and number of cells vs. furnace holding time for (a) Al and (b) 160-200 μm size Ti6Al4V-Al foam samples and (c) comparison of average cell diameter and number of cells of Al and 160-200 μm size Ti6Al4V-Al foam samples

5.9. Microscopic Observation of Foam Structures

5.9.1. The Composition and Thickness of The Reaction Layer

During foaming, Ti6Al4V particles react with liquid Al and form a reaction layer around Ti6Al4V particle. The reaction layer thickness increases with increasing

furnace holding times. Figures 5.21.a, 5.21.b and 5.21.c show the reaction layer around Ti6Al4V particles in the 160-200 μm size Ti6Al4V particle added foam precursors with furnace holding times of 100, 200 and 600 sec, respectively. Sequentially, the thicknesses of the reaction layers are about 3, 6 and 15 μm for 100, 200 and 600 sec. EDX analyses of a reaction layer next to a Ti6Al4V particle are shown in Figures 5.22.a and 5.22.b. The Atomic weight percent of Al phase varies between 21.26 and 24.43, showing the phase formed is nearly corresponding to $TiAl_3$. The XRD analysis of the 160-200 μm (5 wt%) Ti6Al4V particle added foam sample is shown in Figure 5.22.c. XRD spectra clearly show the presence of $TiAl_3$ formation in the compacts. In order to verify the variation of the weight percentage of Ti and Al along the reaction layer, SEM line scanning were conducted. Figures 5.23.a and 5.23.b show the line scan measurement from A to B next to a Ti6Al4V particles and the corresponding variation of Ti and Al as a function of distance, respectively. In Figure 5.23.a, A is located within the particle and B in Al. It is noted in Figure 5.23.b, near B, Ti concentration is almost zero; while near A, Al concentration in Ti6Al4V is relatively small. Since Al is in molten state at foaming temperature, its diffusion rate is higher in Ti6Al4V. The reaction region thickness at 30 sec holding time is relatively thin, 1.2 μm thick (Figure 5.23.b), and wt% of Al and Ti sequentially increases and decreases gradually. When the furnace holding time increases to 90 sec, the thickness of the reaction layer increases to 5 μm, as shown in Figure 5.24. It is also noted that in the reaction layer, wt% of Ti and Al almost constant and 33 and 67%, respectively. The thickness of the reaction layer increases above 15 μm when the furnace holding time increases to 600 sec as shown in Figures 5.25.a and 5.25.b. It is also noted in Figure 5.25.a that the reaction product, $TiAl_3$, was detached from the particle forming precipitates in the Al matrix. The size of Ti-Al alloy particles varies between 1 to 10 μm. In the reaction layer wt% of Al is almost constant at 71% (Figure 5.25.b). Figures 5.26.a and 5.26.b show sequentially SEM line-scan measurement from A to B next to a Ti6Al4V particle and the corresponding variation of Ti and Al as a function of distance of the reaction layer around the Ti6Al4V particle in 1 wt% 30-45 μm size Ti6Al4V particle added foam with a furnace holding time of 900 sec. The reaction of Al-Ti particles is seen in Figure 5.26.a dispersed in the matrix and the line-scan shows a constant wt% of Al of 71% in the reaction layer. These above findings presented that the particles of $TiAl_3$

intermetallic compound is formed during the foaming of the Ti6Al4V added Al compacts.

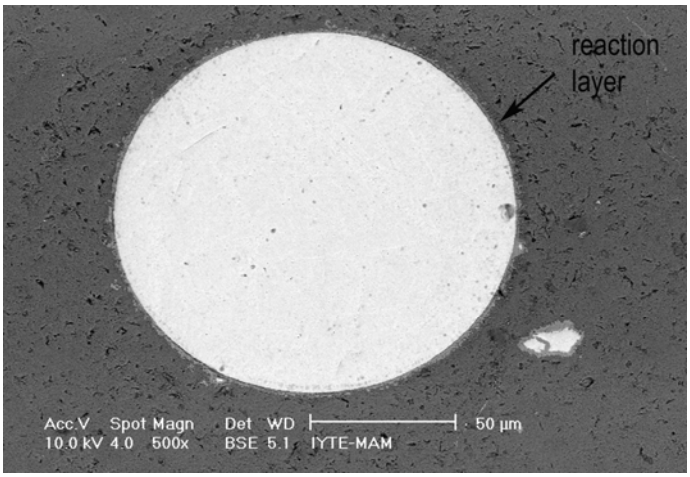

(a)

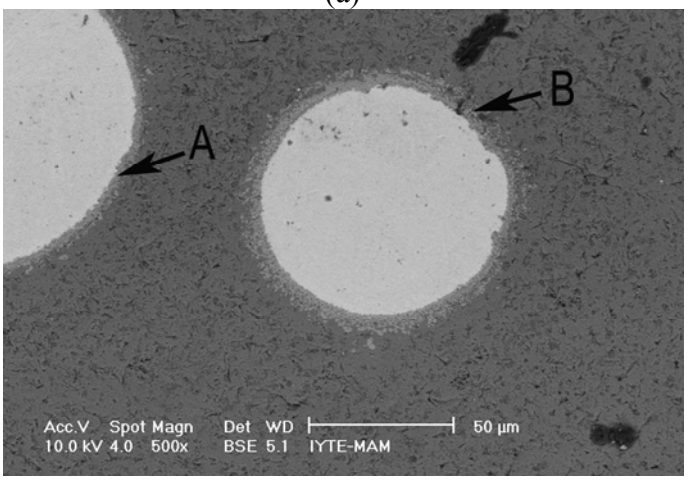

(b)

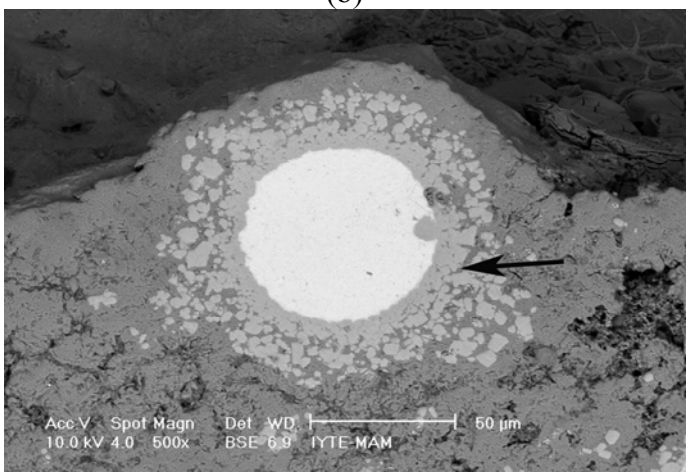

(c)

Figure 5.21. SEM pictures of 160-200 µm size (5 wt%) Ti6Al4V particle added foamed compact samples with furnace holding times of (a) 100, (b) 200 and (c) 600 seconds

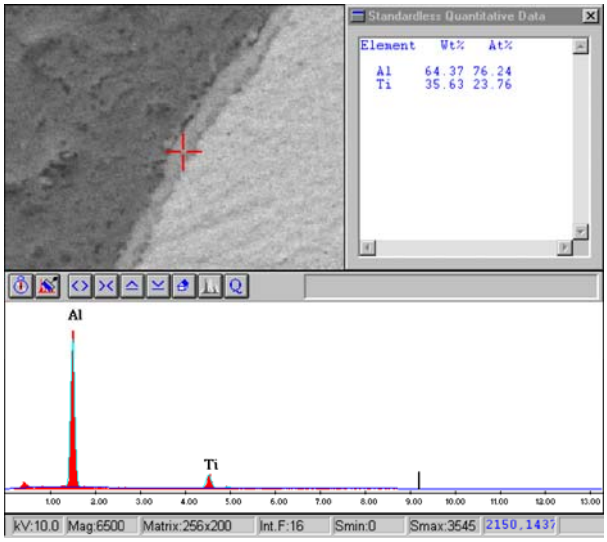

(a)

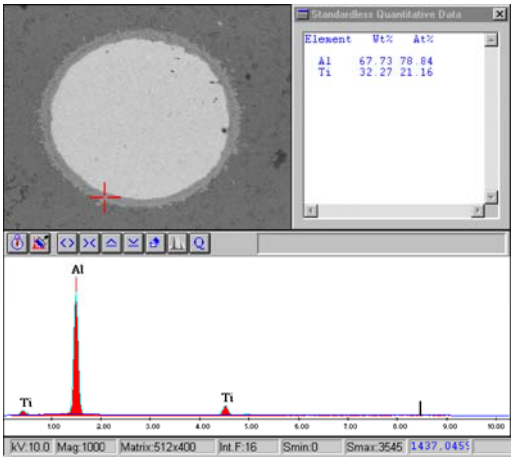

(b)

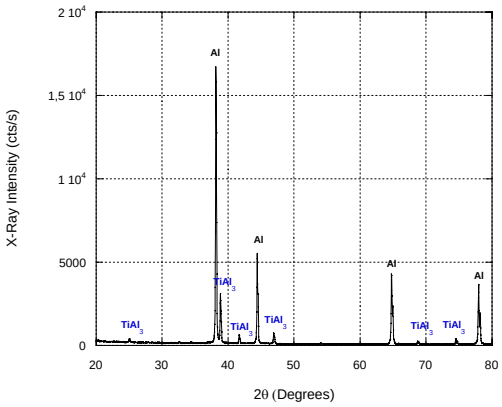

(c)

Figure 5.22. (a) and (b)EDX analysis of the reaction layer and (c) XRD result in a 160-200 μm size (5 wt%) Ti6Al4V particle added foamed compact samples with furnace holding times of 600 seconds

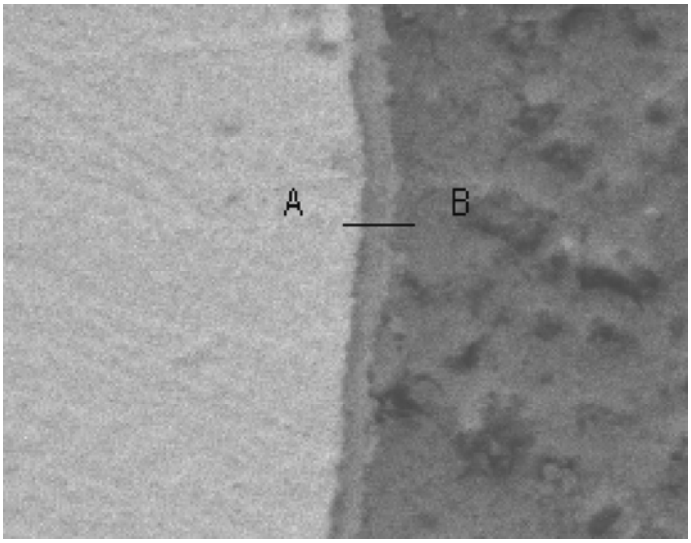

(a)

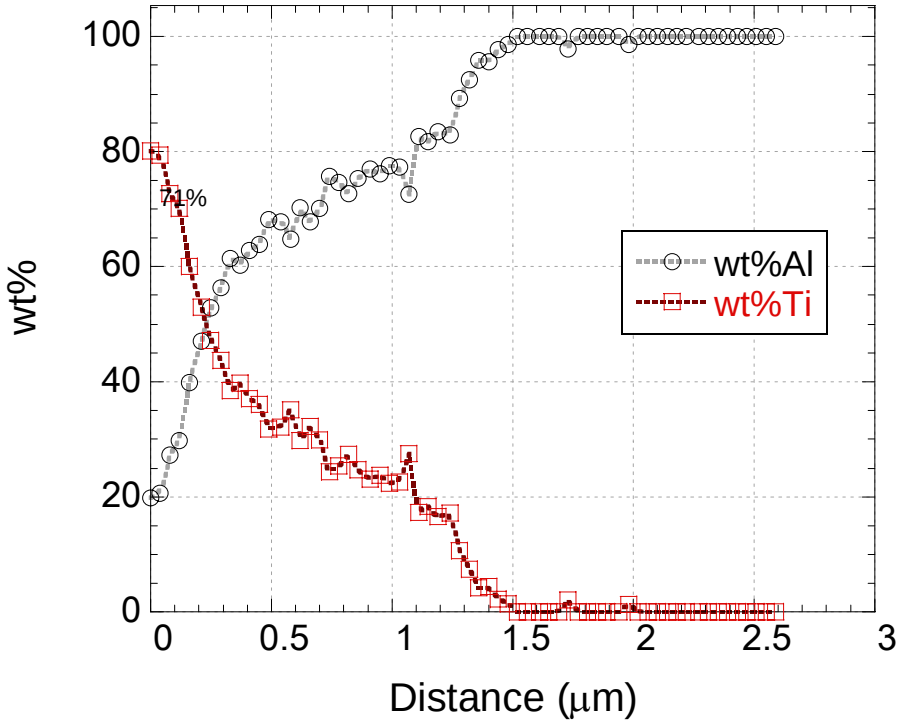

(b)

Figure 5.23. SEM line-scanning of the reaction layer in 160-200 μm size (5 wt%) Ti6Al4V particles added foamed compact samples with furnace holding times of 30 sec; (a) line segment on the reaction layer and (b) variation of the composition with respect to the distance on the reaction layer

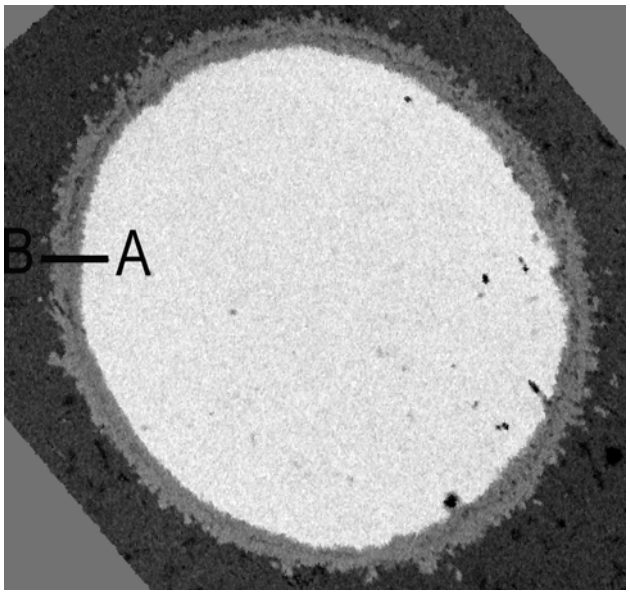

(a)

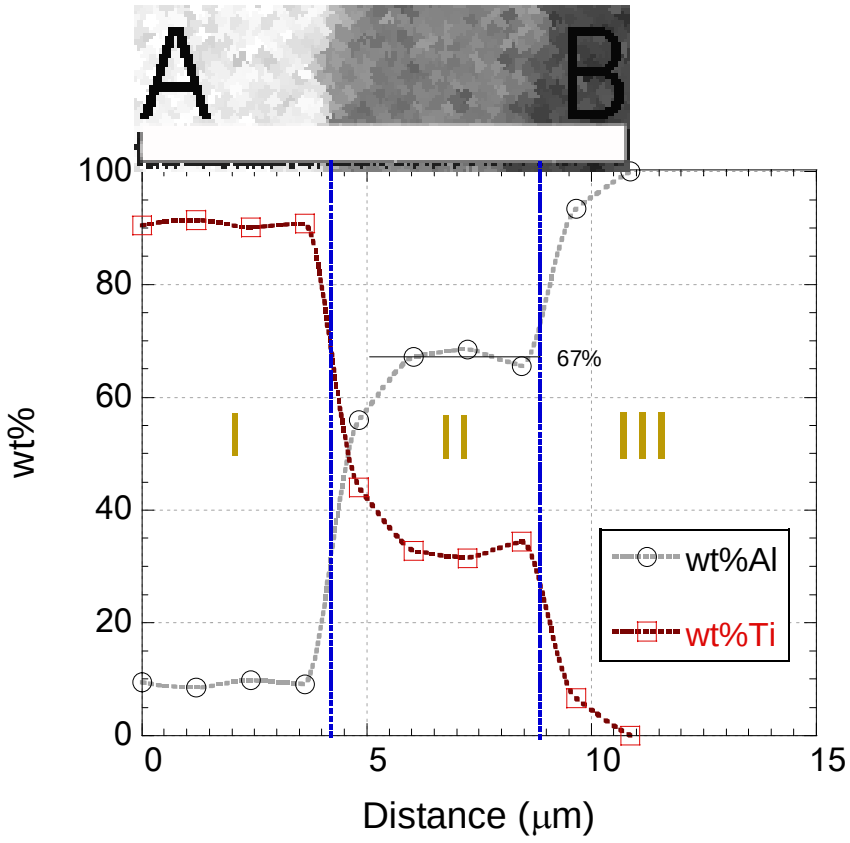

(b)

Figure 5.24. SEM line-scanning of the reaction layer in 160-200 μm size (5 wt%) Ti6Al4V particles added foamed compact samples with furnace holding times of 90 sec; (a) line segment on the reaction layer and (b) variation of the composition with respect to the distance on the reaction layer

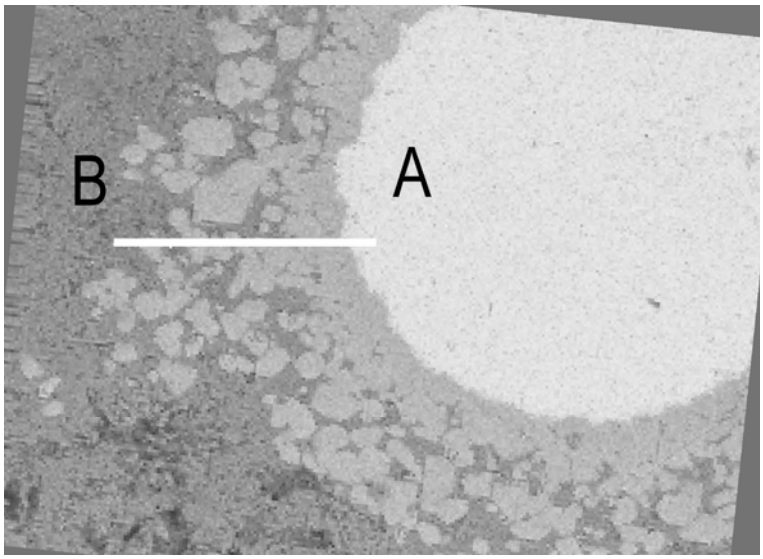

(a)

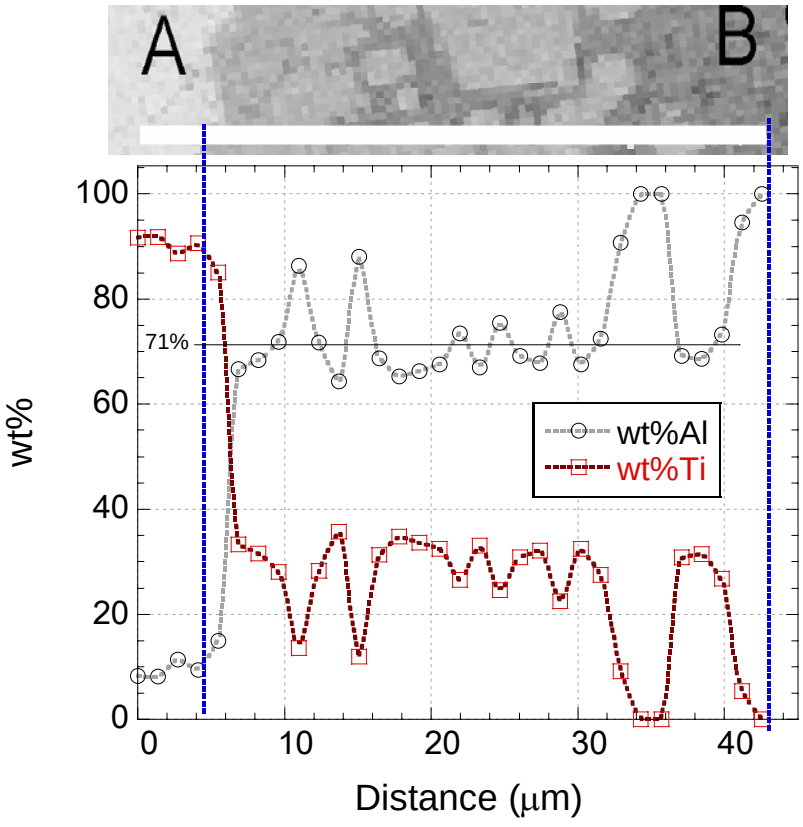

(b)

Figure 5.25. SEM line-scanning of the reaction layer in 160-200 μm size (5 wt%) Ti6Al4V particles added foamed compact samples with furnace holding times of 600 sec; (a) line segment on the reaction layer and (b) variation of the composition with respect to the distance on the reaction layer

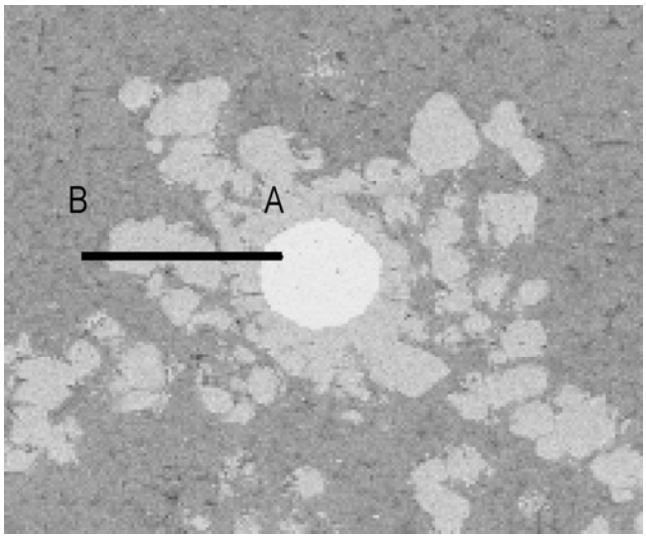

(a)

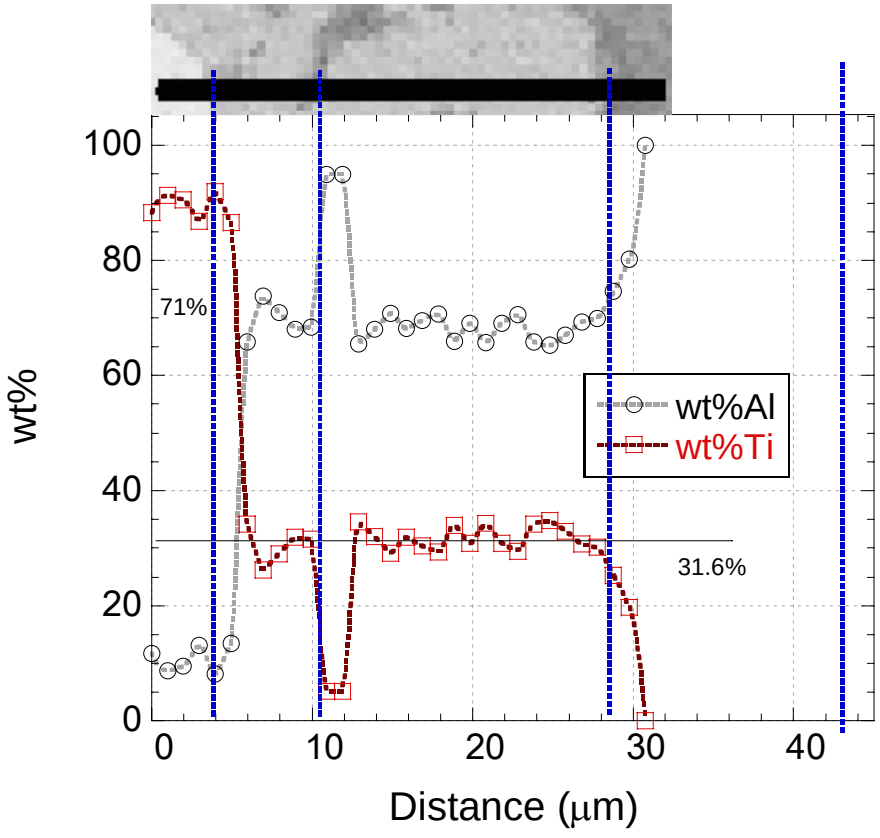

(b)

Figure 5.26. SEM line-scanning of the reaction layer in 30-45 μm size (1 wt%) Ti6Al4V particles added foamed compact samples with furnace holding times of 900 sec; (a) line segment on the reaction layer and (b) variation of the composition with respect to the distance on the reaction layer

5.9.2. Effect of Furnace Holding Time on The Al-Ti Particle Formation

In Figure 5.27, the expansion-time graph of 5 wt% 30-45 μm size Ti6Al4V-Al foam is shown together with SEM pictures corresponding to the furnace holding time. Figure 5.27 clearly shows that, as the furnace holding time increases the amount of Ti-Al particles increases. These particles were formed within the cell edges and cell walls as will be elaborated in discussion section. As the number of particles formed increase, the extent of fluctuations in expansion-time graph decreases. After 600 sec the expansion becomes steady, corresponding to relatively higher number of particle formation ((c) in Figure 5.27).

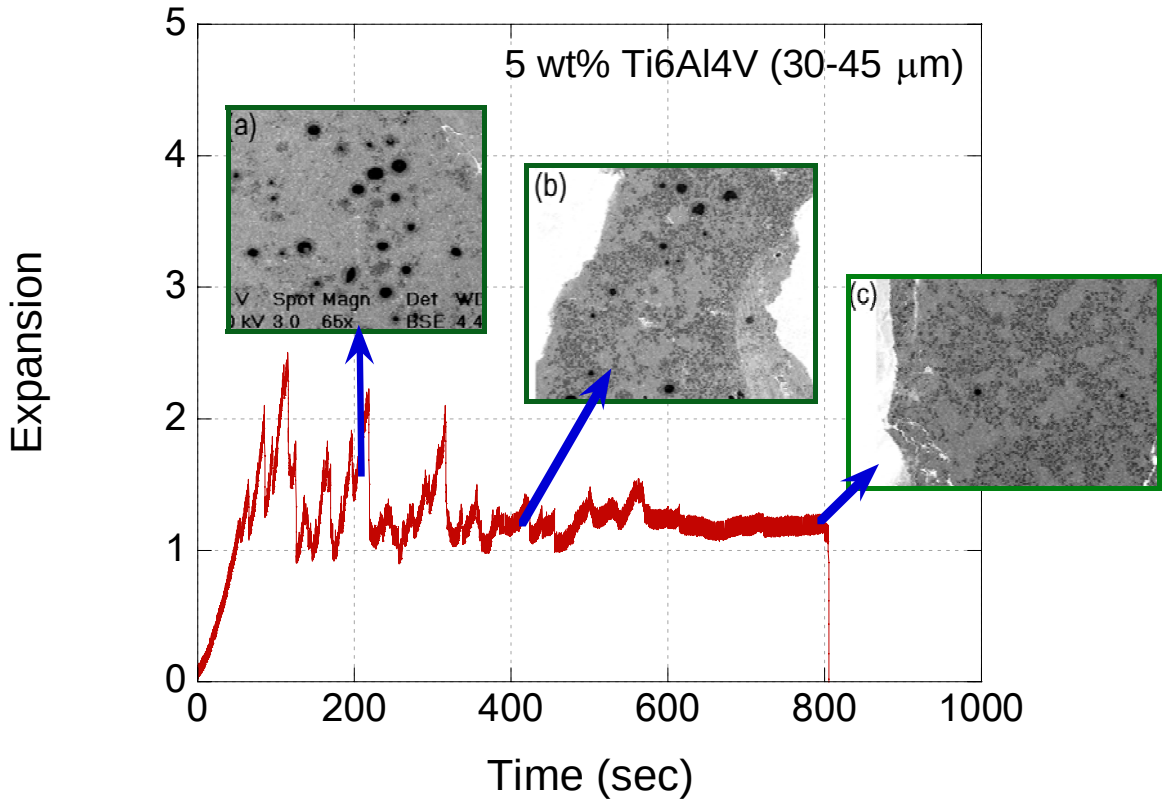

Figure 5.27. SEM images of Ti-Al particle developments in 30-45 μm size (5 wt%) Ti6Al4V particles added foamed compact samples with furnace holding times of (a) 208, (b) 497 and (c) 805 sec

A general observation made from SEM observations is that when Ti6Al4V particle size is relatively small, formed Al-Ti particles disperse throughout the matrix as shown in Figure 5.28.a, with increasing Ti6Al4V particle size, Al-Ti layer pretty much

remain connected to the particle as shown in Figure 5.28.b. In small size Ti6Al4V particles added compacts, Al-Ti particles are bigger in size than the bigger size particles added compacts at the same furnace holding time, which emphasizes the importance of the surface area effect on the reaction rate.

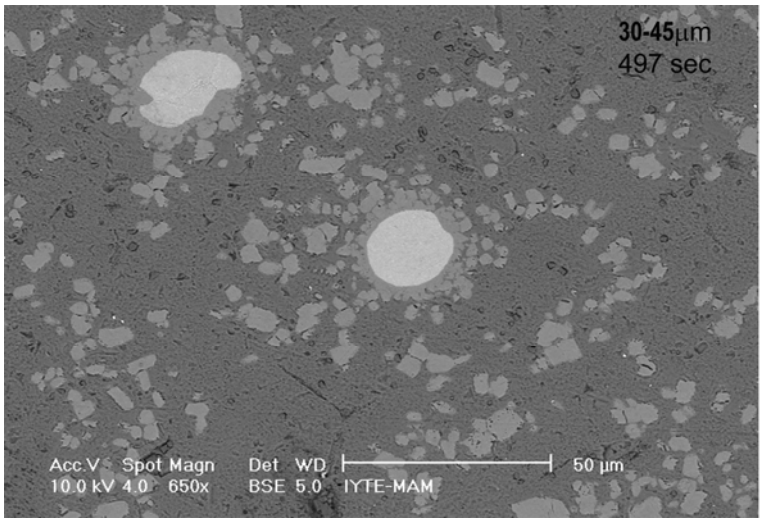

(a)

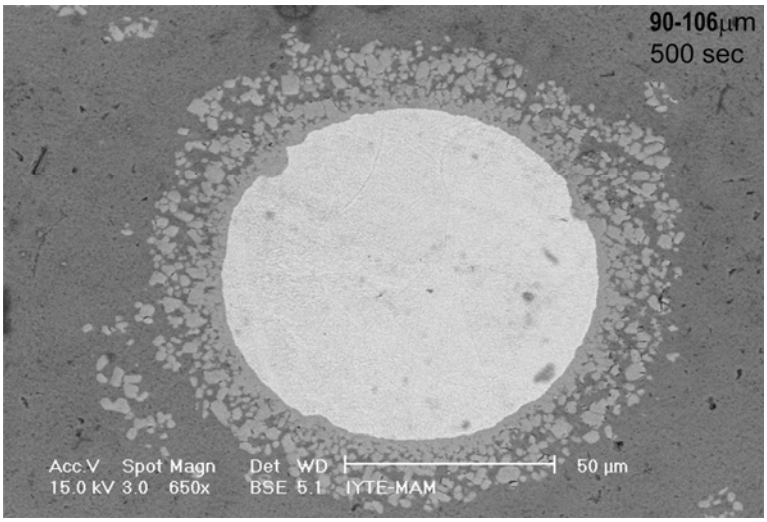

(b)

Figure 5.28. SEM pictures of Ti6Al4V particle added foamed compacts (furnace holding time 500 sec) showing the reaction layer around the particles; (a) 30-45 μm size and (b) 90-106 μm size particles

5.9.3. Cell Morphology and Particle Distribution

Foams of Al and 160-200 μm size Ti6Al4V-Al compacts after 200 sec furnace holding time are shown in Figures 5.29.a and 5.29.b, respectively. The magnified view of the numbered sections on the foam cylinder of Al and 160-200 μm size Ti6Al4V-Al compacts shown in Figures 5.29.a and 5.29.b are sequentially shown in Figures 5.30.a and 5.30.b. The cell edges at the bottom of the foam cylinders (1 in Figures 5.30.a and 5.30.b), are seen in these micrographs to be thicker in Al foams than Ti-particle added foam. Opposite of the Al foam, the cell walls become thicker in particle added foam at the mid and top sections (2 and 3 in Figures 5.30.a and 5.30.b). Another noticeable feature of particle added foams is that the particle concentration is higher at the top sections than the bottom sections (3 in Figure 5.30.b).

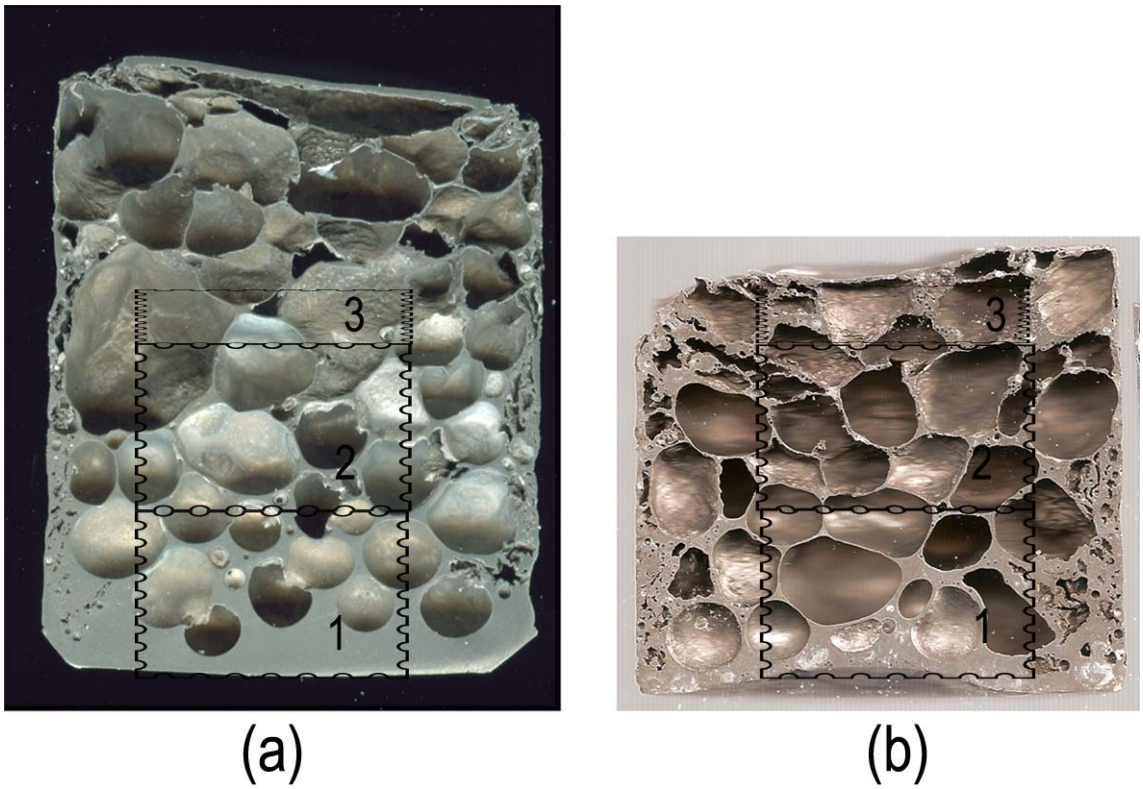

Figure 5.29. Foams of (a) Al and (b) 160-200 μm size Ti6Al4V-Al compacts after about 200 sec furnace holding time

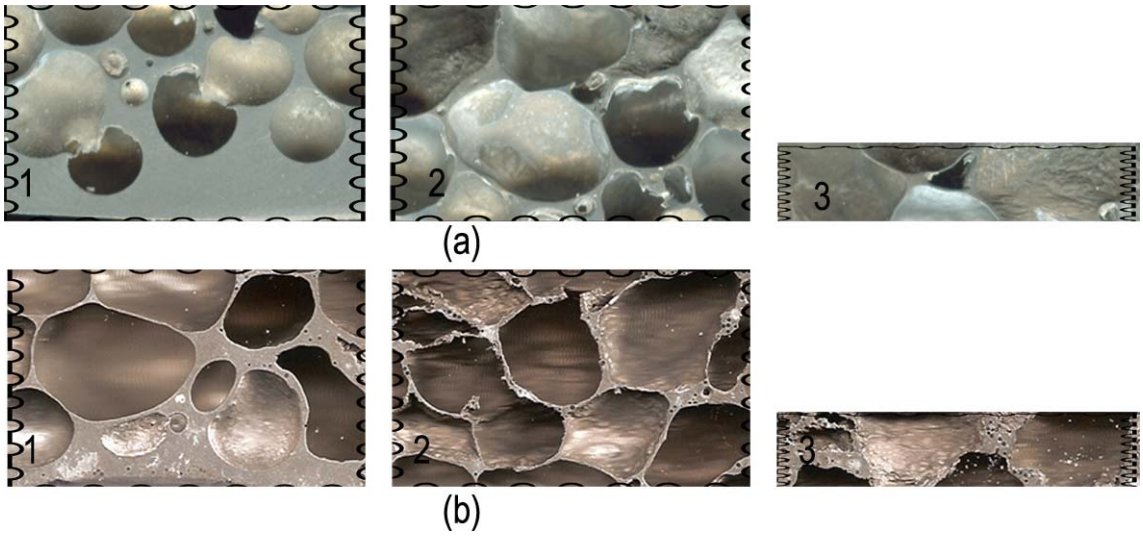

Figure 5.30. Magnified cell structures of foams of (a) Al and (b) 160-200 μm size Ti6Al4V-Al compacts after about 200 sec furnace holding time

Foams of Al and 160-200 μm size Ti6Al4V-Al compacts after about 400 sec furnace holding times are shown in Figures 5.31.a and 5.31.b respectively. The magnified view of the numbered cell sections of the foam cylinders in Figures 5.31.a and 5.31.b are sequentially shown in Figures 5.32.a and 5.32.b. At the bottom sections of the foam cylinders (1 in Figures 5.32.a and 5.32.b), the cell edges are again thicker in Al foams than Ti-particle added foams at longer furnace holding times. The thicker cell walls in particle added foam become more noticed at longer furnace holding times at the top sections (2 in Figures 5.32.a and 5.32.b). A higher particle concentration is also seen in particle added foam at the top sections than the bottom sections (2 in Figure 5.32.b).

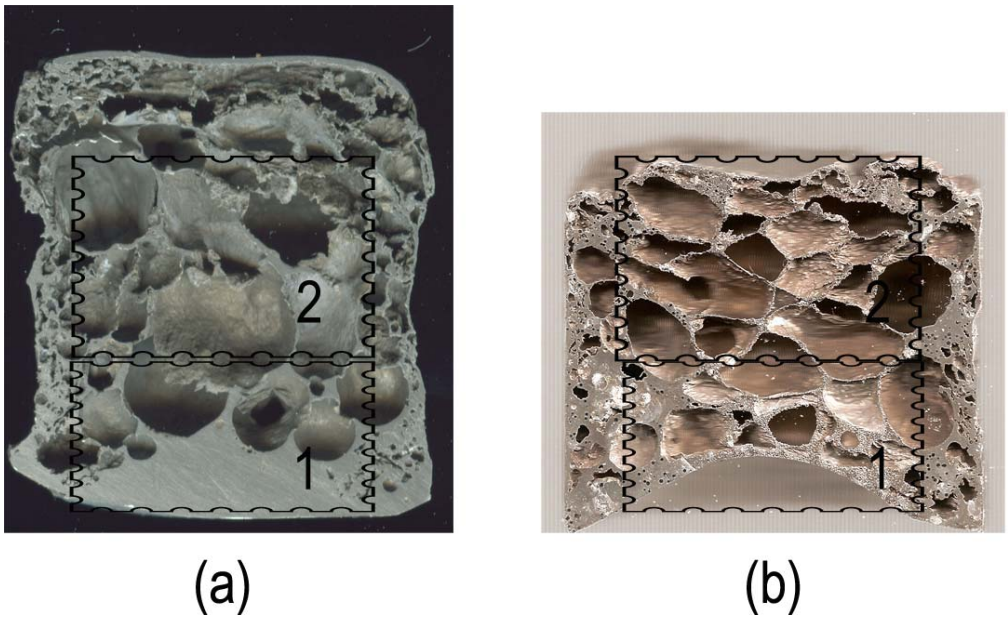

Figure 5.31. Foams of (a) Al and (b) 160-200 μm size Ti6Al4V-Al compacts after about 400 sec furnace holding time

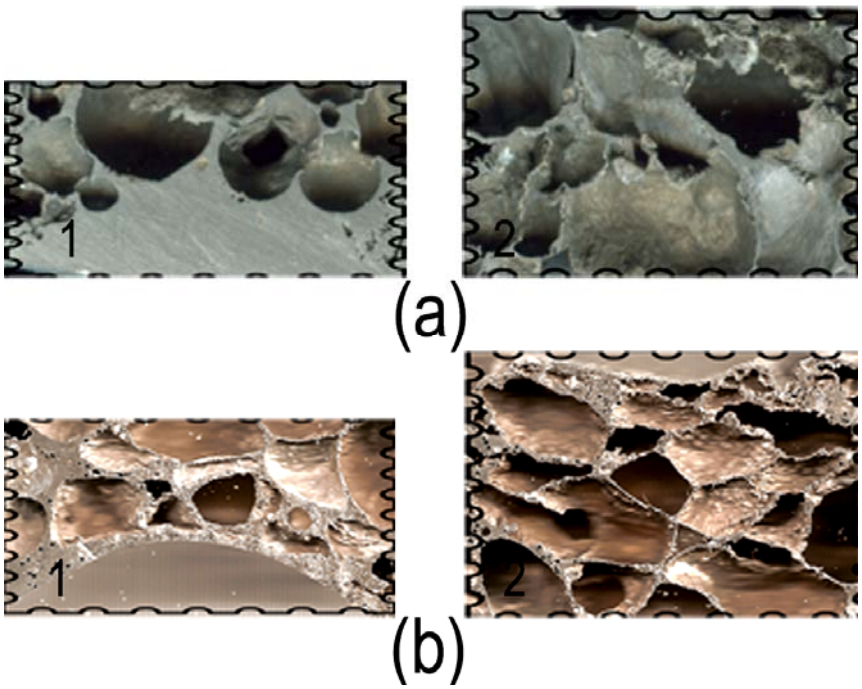

Figure 5.32. Magnified cell structures of foams of (a) Al and (b) 160-200 μm size Ti6Al4V-Al compacts after about 400 sec furnace holding time

Figures 5.33.a and 5.33.b show the cell structure of cross-sections of 160-200 μm Ti6Al4V Al compacts after 200 sec furnace holding time in a foam cylinder and foam sample produced by compaction of the powder in 7x7 cm steel die. In processing

of the second foam sample, the powder mixture was initially cold compacted inside a steel die, 7x7 cm in cross-section, under a pressure of 200 MPa. The compacts having 80% relative density were then open-die hot-forged at a temperature of 350 ºC; resulting with foamable precursor materials with final densities of 98% and thicknesses of approximately 8 mm. Foaming experiments were conducted in a pre-heated furnace at a temperature of 750 ºC. The precursor was inserted into a pre-heated steel mold providing expansion only in the vertical direction. In Figures 5.33.a and 5.33.b, the increased number of particles is seen in mid and top sections. The particles are found in cell wall (a in Figure 5.33.b) and cell edges (b and c in Figure 5.33.b). The particles on the cell walls, although not seen, are noticed inside the cells as shown in d of Figure 5.33.b. In Figures 5.34 (a-f), the particles at cell edges and walls are shown in 160-200 μm size Ti6Al4V-Al foam. Following observation can be concluded from these micrographs: the particles are found in cell edges (a) and cell walls (b-f). The increased thickness in particle located sections of the cell walls are clearly seen in (e) and (f) of Figure 5.34. Observations made from the cell walls further show that Ti6Al4V particles are completely wetted by liquid Al (Figure 5.35).

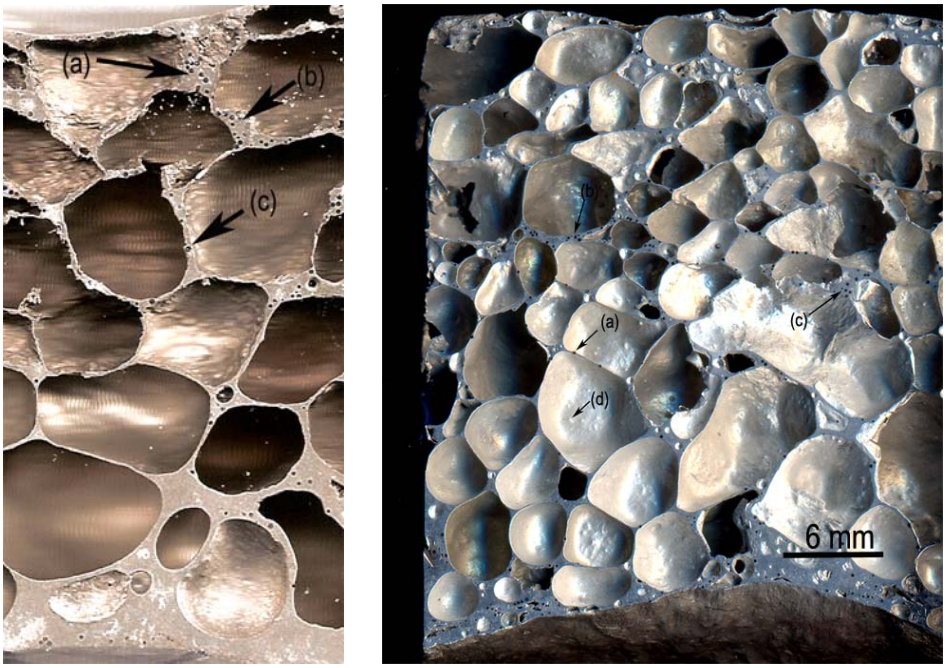

(a) (b)

Figure 5.33. The cell structure of 160-200 μm size Ti6Al4V-Al compacts after 200 sec furnace holding time: (a) foam cylinder (D = 30mm) and (b) 7x7 foam sample, the height cross-sections

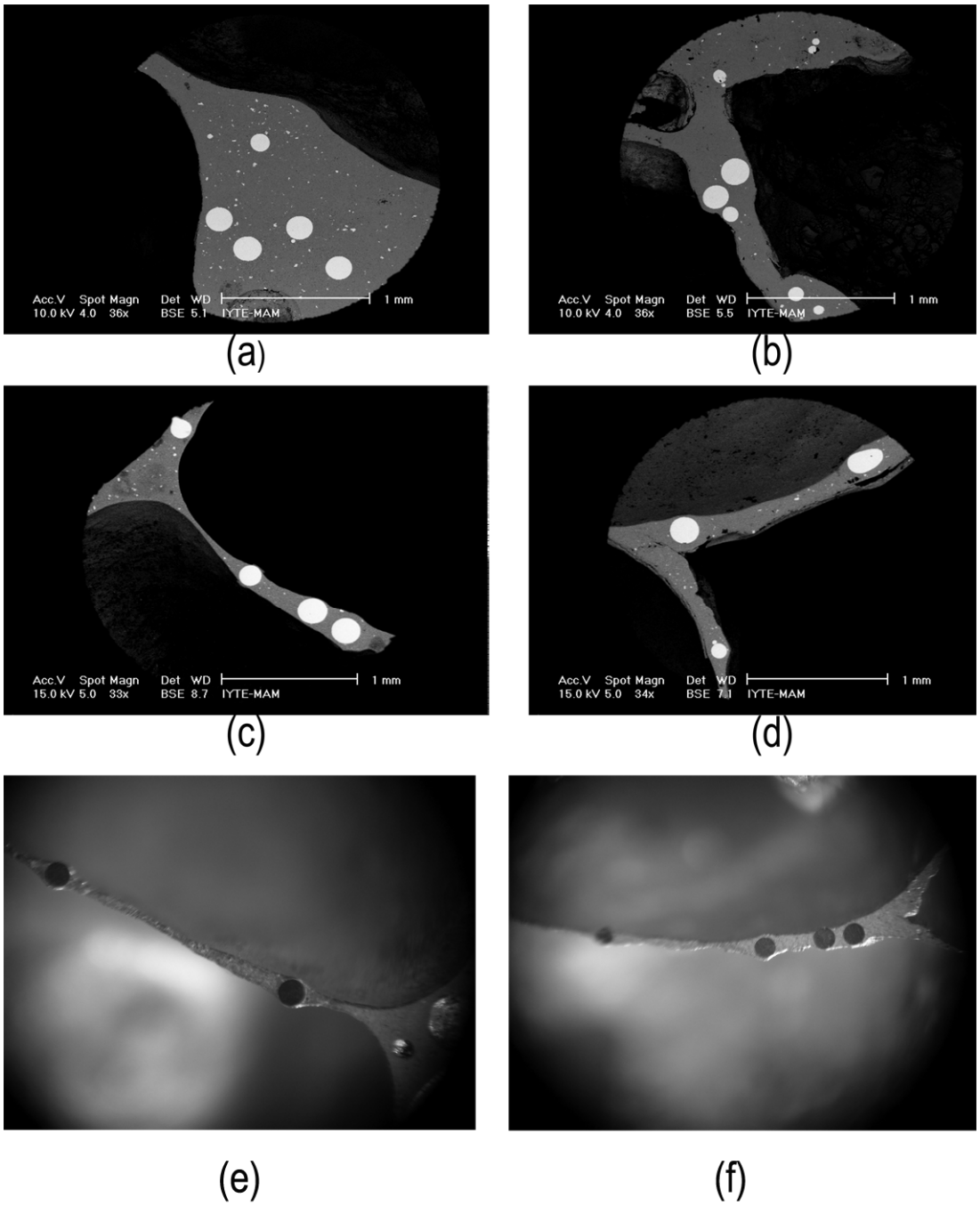

Figure 5.34. Ti6Al4V particles of a 160-200 μm size Ti6Al4V-Al foam after 200 sec furnace holding time: (a) cell-edge and (b-f) cell walls

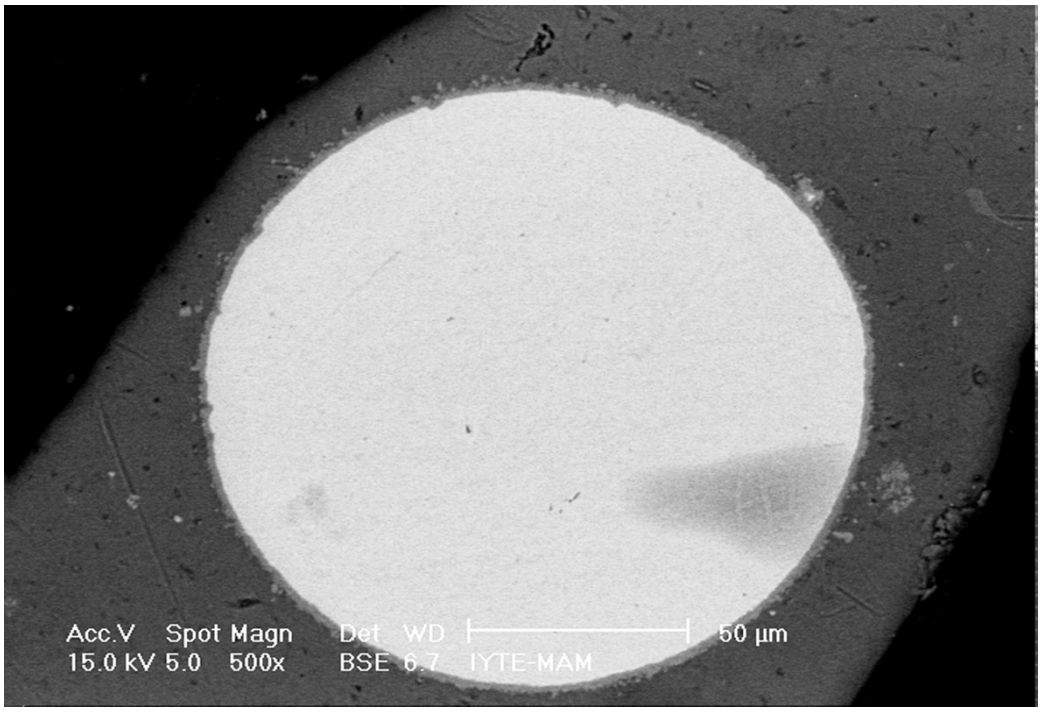

Figure 5.35. Ti6Al4V particle in a cell wall

In some cells, black borders are seen at the cell walls as shown in Figures 5.36.a and 5.36.b. This results from the oxide skin of the starting Al particles. The oxide skin which is not breaking down during compaction, leads to border formation in cells during foaming.

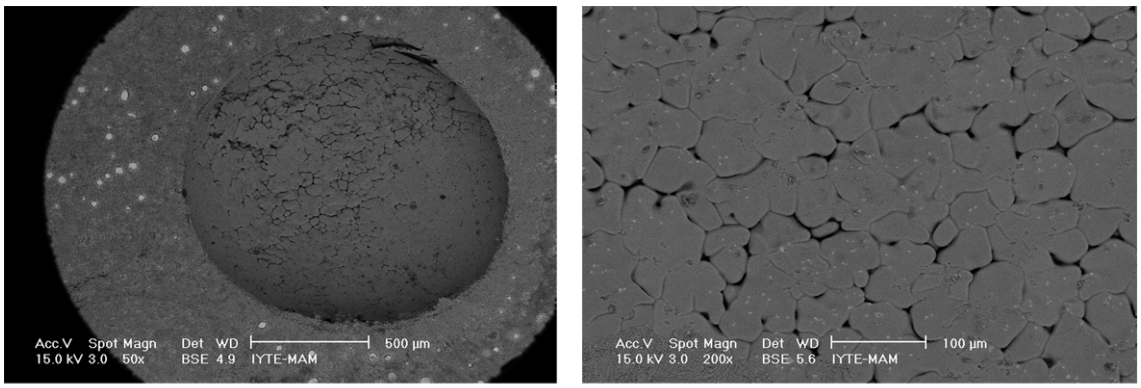

Figure 5.36. Inside of a foam cell wall showing (a) particle boundaries and (b) at higher magnification

5.10. Compression Mechanical Properties

The results of compression tests on small size specimens are shown in Figure 5.37.a for 1 wt% 30-45 μm size Ti6Al4V-Al compact samples. The increasing foam density increases the foam plateau stresses. Figure 5.37.b is the comparison of the 1 wt% 30-45 μm size Ti6Al4V-Al compact samples compression behavior with that of pure Al foams at similar densities. The Al foam samples of 20 mm in diameter and 25 mm in length were previously tested (Kavi, et al. 2004). Therefore, the samples sizes are bigger than those of 1 wt% 30-45 μm Ti6Al4V-Al compact samples. Al foam shows higher initial plateau stresses than those of 1 wt% 30-45 μm Ti6Al4V-Al foam samples. However, at large strains both samples show similar stress values. The increasing foam density also increases the plateau stresses of 160-200 μm Ti6Al4V-Al foam samples (Figure 5.38.a), while Al foam samples show higher plateau stresses than 160-200 μm Ti6Al4V-Al foam samples (Figure 5.38.b). The deformation mode of 160-200 μm Ti6Al4V-Al foam samples are also similar to those of Al foams, composing of (i) cell buckling (Figure 5.39.a) and (ii) cell wall fracture (Figure 5.39.b).

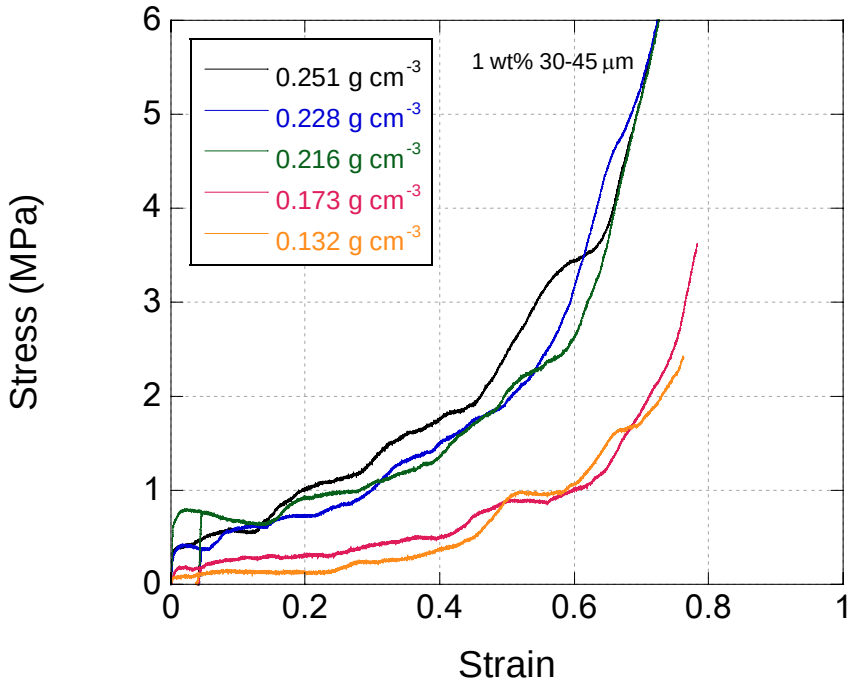

(a)

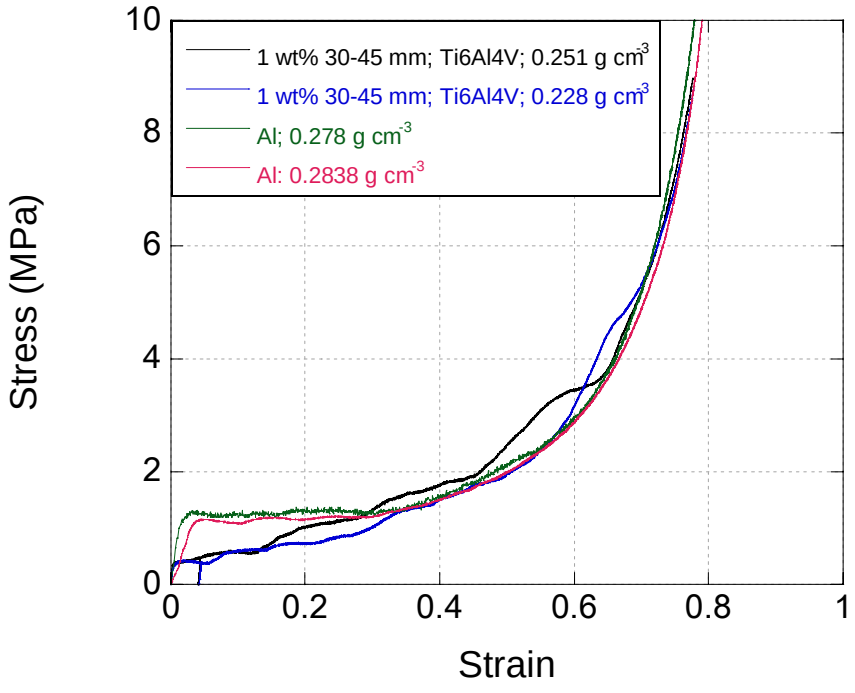

(b)

Figure 5.37. Stress strain curves of (a) 1 wt% 30-45 µm size Ti6Al4V-Al foam at various densities and (b) comparison with Al foam

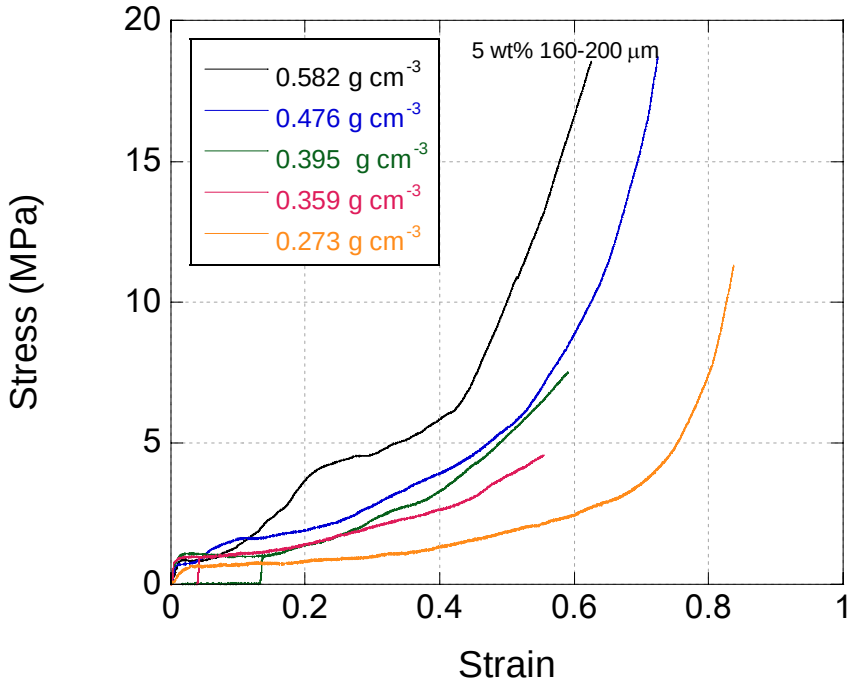

(a)

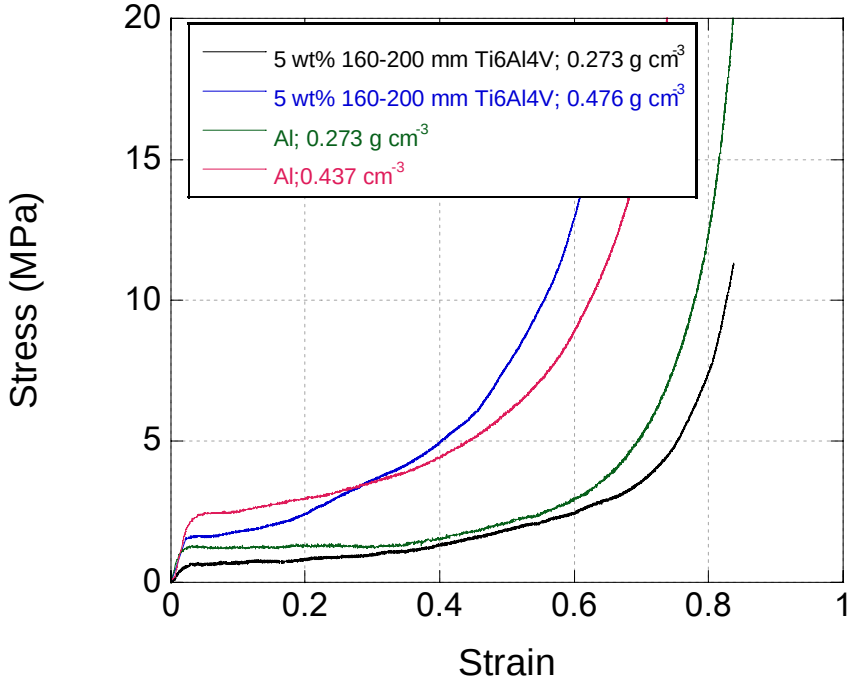

(b)

Figure 5.38. Stress strain curves of (a) 5 wt% 160-200 µm size Ti6Al4V-Al foam at various densities and (b) comparison with Al foam

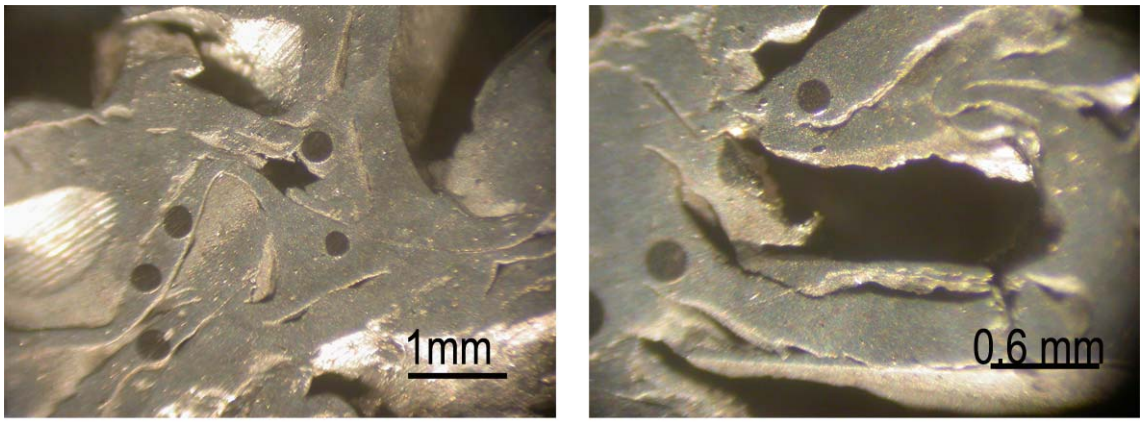

Figure 5.39. Optical micrograph showing deformed (80% strain) structure of 5 wt% 160-200 μm size Ti6Al4V-Al foam; (a) cell wall buckling and (b) cell wall cracking

CHAPTER 6

DISCUSSION

6.1. The Expansions of The Powder Compacts

The foaming is a statistical process: two foaming processes starting with the same compact geometry, composition and foaming conditions such as foaming temperature will not give the same foam expansion (Duarte and Banhart 2000). The variations in blowing agent distribution, composition and compaction pressure; the presence of any impurity in the compact; small variations in the heat transfer between the mold and the furnace and the variations in the frictional forces of the expansion measurement system unavoidably lead to variations in foam expansions in between the tests of the similar compacts. This effect, the variation of the expansion-time curves of the same Al compacts, is clearly seen in Figure 5.2. A similar observation was previously made in the foaming of AlSi7 powder compacts (Duarte and Banhart 2000). This effect is also seen in Al compacts with Ti6Al4V particle addition (Figures 5.5, 5.6, 5.9, 5.10, 5.11, 5.14 and 5.15).

The foaming process, foam expansion, is a relatively quick process and a maximum expansion is reached within 100 seconds (Figure 5.1). It was argued that the measured maximum linear expansions were due to the rapid bursting of the hydrogen in the initial foaming stage after the compact melted (Duarte and Banhart 2000). The initial slow-rate expansion region of the expansion-time curves was due to the expansion of the mushy compact before the complete melting of the compact. After the melting, the compact showed a higher rate of expansion (region 2). Until about the maximum expansions, the cells were observed to be small and in the following regions the cells become larger. Although not detected in this thesis, the anisotropy in the compacted precursor results in compact expansion parallel to the compaction direction by forming crack-like initial cells (Stanzick, et al. 2002).

Several different factors affect the foamability of the powder compacts. These factors may include (i) compaction conditions such as pressure and temperature, (ii) foaming conditions such as foaming temperature and heating rate and (iii) the

microstructure of the compact to be foamed. The effects of the compaction and foaming conditions on the foaming behavior of AlSi7 and 6061 Al compacts were studied previously (Duarte and Banhart 2000, Duarte, et al. 2002). It was found that increasing foaming temperatures increased the foam expansions in both types within the temperature range of 600-800 °C. Increasing temperatures reduced the viscosity and promoted the gas evolutions, leading to increased foam expansions. It was shown in the same study that the volume expansions were saturated at 750 °C for AlSi7 alloy compact, while the viscosity of 6061 Al alloy compact was not sufficient for the efficient foaming until about 800 °C. For the studied Al compacts, the foaming temperature was held between 700-730 °C and the maximum expansions were found to vary between 4.13-4.86. The expansion values were further converted into mm unit for comparison with previous studies. In the present study, 8 mm thick Al compacts showed maximum expansions varying between 32 and 39 mm, while the expansion values of 9 mm AlSi7 compacts were found to be around 45 mm (Banhart 2000). In another study, the maximum volume expansion of Al compacts, compacted at room temperature, found to vary between 3.5 and 4 (Asavavisithchai and Kennedy 2006). These expansion values are comparable with expansion values of the studied Al compacts. The hot forging of the compacts was further found to be effective in increasing compact expansions because higher compaction temperatures resulted in denser compacts, leading to increase in expansions (Duarte and Banhart 2000). The effect of compaction method on the expansion of Al-0.6%TiH_2 powder compacts was further investigated by Asavavisithchai et. al. (Asavavisithchai and Kennedy 2006). It was shown that simple cold compaction of Al powder compacts of >99% dense and containing 0.3-0.4wt% oxygen produced the foam expansions similar to the ones prepared by hot compaction forming processes. The effect of oxygen content of the starting Al powders on the expansion and stability of Al-0.6%TiH_2 powder compacts was investigated by Asavavisithchai and Kennedy (2006). The oxide content of the powder was increased by pre-heat treatment process applied to the powder before consolidation. It was shown that the maximum foam expansion increased with increasing oxygen content, up to 0.333 wt%, while increasing oxygen content above 0.6 wt% level resulted in low expansions but more stable foams. The oxide particles formed clusters of crumpled films, restricting drainage. In the present study no heat treatment was applied to the powder before and during the compaction stage, and the initial oxygen content of the powder is not known. However, it is anticipated that the oxygen content of initial

powder is enough to give comparable expansions and foam stability with studies mentioned above.

The in-situ measured expansion values of the studied Al compacts were further compared with the expansion values measured previously by ex-situ (Guden and Yuksel 2006). These compacts were prepared inside a stainless steel die, heated at 350 °C for 30 min, hot compacted under a pressure of 220 MPa and foamed in a pre-heated furnace at a temperature of 750 °C. By measuring the final length of the foamed compacts, the expansion was calculated. Figure 6.1 shows the comparison of the expansions of Al foams measured by in-situ and ex-situ methods. The ex-situ measurements show similar expansion values with those of in-situ measurements as shown in Figure 6.1. Small discrepancies may naturally arise between the measurements because of the small variations in the densities of the compacts and the shrinkage of the foam during solidification in ex-situ measurements.

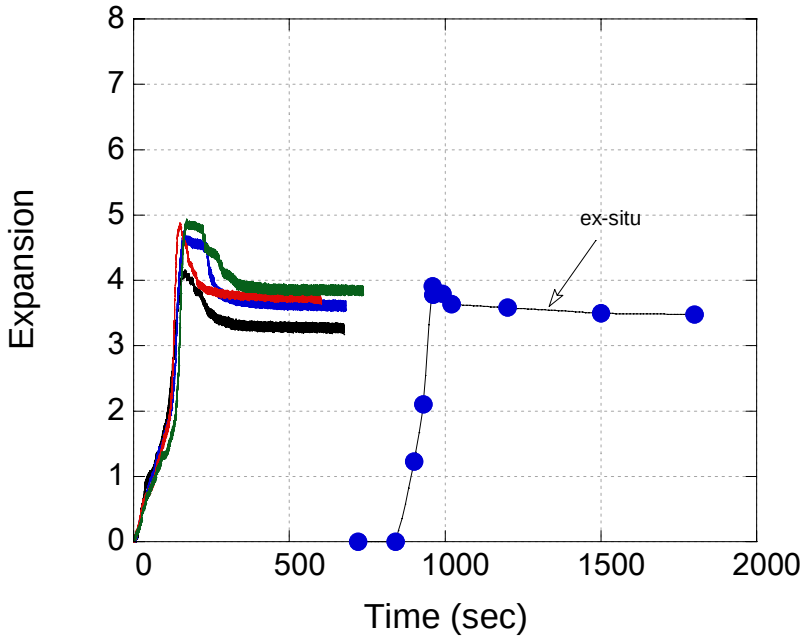

Figure 6.1. Comparison of in-situ and ex-situ expansion measurements of Al compacts

6.2. Foam Evolution

The foam evolution in the foaming of powder compacts may be considered as composing of several stages as shown in Figure 6.2. The foam formation starts in solid state just before melting of the compact. The region 2 is identified as the decay stage

and the region 3 solidification. As the foam forms, the decaying processes become operative/active with cell wall rupture and foam drainage. The cell wall rupture occurs by the thinning of the cell walls: the liquid metal flows from the film surface to the plateau borders under the action of gravity (drainage) and the pressure difference between film and plateau border. It should be noted that although the foam expansion in Region 4 of Figure 5.1 remains constant with time, the foam structure evolution continue as shown in Figure 5.4; drainage reduces the cell wall thickness and forms a dense layer at the bottom and the cell rupture induces larger cells at the top sections of the foam cylinder. Stanzick et. al. (2002) observed the foaming behavior of uniaxially compacted AlSi7 and thixocast AlSi6Cu4 foamable precursors using real time X-ray radioscopy. The cell wall rupture time for both types of precursors was determined around 50 milliseconds. The cell rupture occurred at thicknesses of cell walls below 50 μm. It should be noted that whenever the cell wall thickness reaches this critical value, rupture occurs. The cell rupture time (T) was further approximated by using following relation;

$$T = \frac{b}{2}\sqrt{\frac{c\rho}{\sigma}} \tag{6.1}$$

where, b, c, ρ and σ are the cell wall length, thickness, liquid metal density and surface tension, respectively. Using the typical values of Al in above equation, a rupture time of 1.2 ms was calculated. In external foaming of 20 vol% SiC (10 μm) particle containing melt by argon gas blowing, a rupture time of cell wall of below 33 ms were found (Babcsan, et al. 2005, Babcsan, et al. 2007), proving a fast cell wall rupture occurring in milliseconds. The cell rupture events were further determined as a function of foaming time and shown in Figure 6.3. The rupture events increase greatly with foaming time after an incubation time of 106 sec. The incubation time of 100 seconds is well accord with the present study, corresponding to the maximum expansions at about 125 sec. For the studied foams, therefore, the cell wall rupture is likely to be dominant in regions following the maximum expansion in expansion/time graphs. Any effects which increase the rupture time will increase the stability of the liquid foam. The increase in cell wall thickness, reduction in surface tension and increase in cell material density will induce longer cell rupture times.

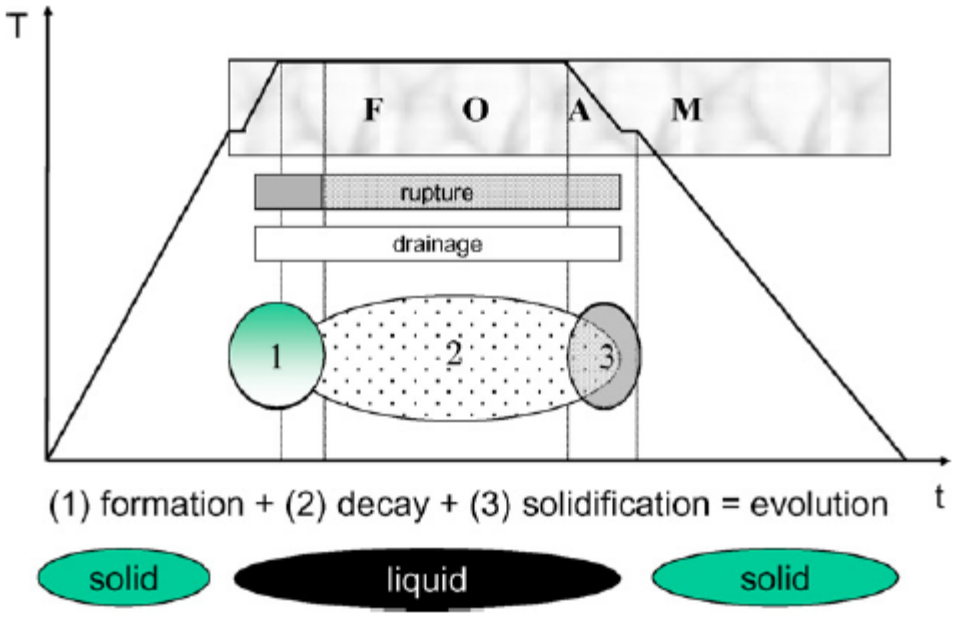

Figure 6.2. Schematic of metal foam evolution (T. temperature and t: time) (Source: Babcsan, et al. 2007)

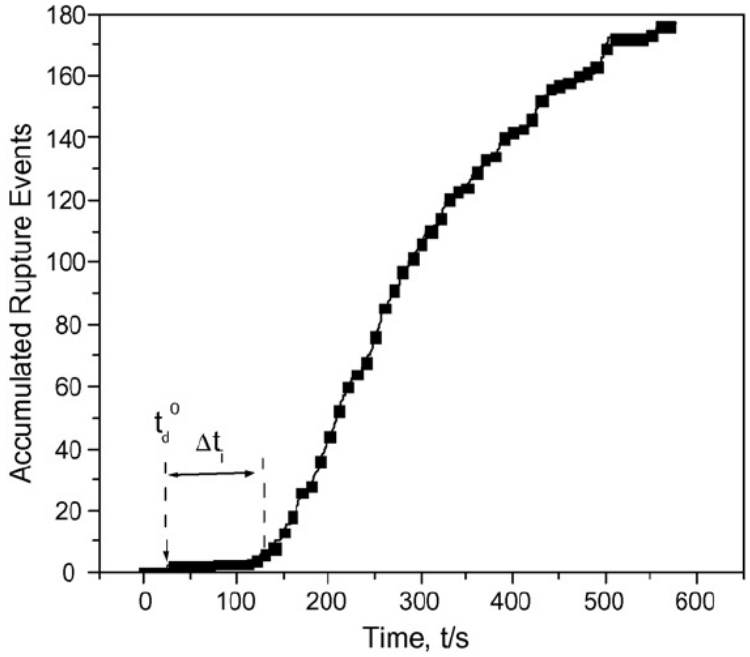

Figure 6.3. Cumulated number of rupture events in foams made from Duralcan MMC by blowing with high purity argon (oxygen content 0.02 vol.%) with argon used as ambient gas above the melt (Source: Babcsan, et al. 2007)

6.3. Effects of Particles on The Expansion of Al Compacts

Haibel et. al. (2006) have recently analyzed the possible stabilization mechanisms operative in foaming of powder compact processes. In the case of no particles on plateau borders and cell walls, the liquid metal on a film (cell wall) connected to the plateau border (cell edge), under the effect of the pressure difference,

$$\Delta P = 2\sigma\left(\frac{1}{R_{PB}} - \frac{1}{R_F}\right) \approx \frac{2\sigma}{R_{PB}} \tag{6.2}$$

flows from the cell walls to the plateau borders (R_{PB} and R_F radius of curvature of plateau border and cell face, respectively). The several different stabilization models were considered in the presence of particles on the cell wall. The partially wetted particles on the cell wall form menisci of radius of $R_F \cong R_{PB}$, which reduces the pressure difference and capillary suction (Figure 6.4.b). In another model, small particles sit at the liquid/gas interface, which give rise to local menisci between adjacent particles, Figure 6.4.c; hence reduce the melt flow from the film to plateau border. Next model, which has become popular recently, is based on the mechanical connection of the particles covering the opposite film surface, which provides repulsive mechanical forces, Figure 6.4.d. Another model is based on the increased viscosity of the melt by the presence of small particles in the film, which immobilized the liquid metal flow (Figure 6.4.e). In the foaming of a metal matrix composite Al-10wt%Si-1wt% Mg/10vol%SiC (13 μm) foamable precursor, it was shown microscopically that most of particles located at metal/gas boundaries and only few were found in the interior of the cell walls. X-ray tomographic analysis of cell walls further showed no evidence of mechanical bridges between the particles of the opposite cell faces. The global distribution of SiC particles in foaming melt was further determined. The particles were found to be predominately located near the liquid/gas interface (37%), while at a 40 μm distance from the liquid/gas interface, the particle concentration dropped to 7%. Finally, a model of foam stabilization, comprising the particle covering the cell faces and increasing apparent viscosity of the melt (Figure 6.4.f) was proposed.

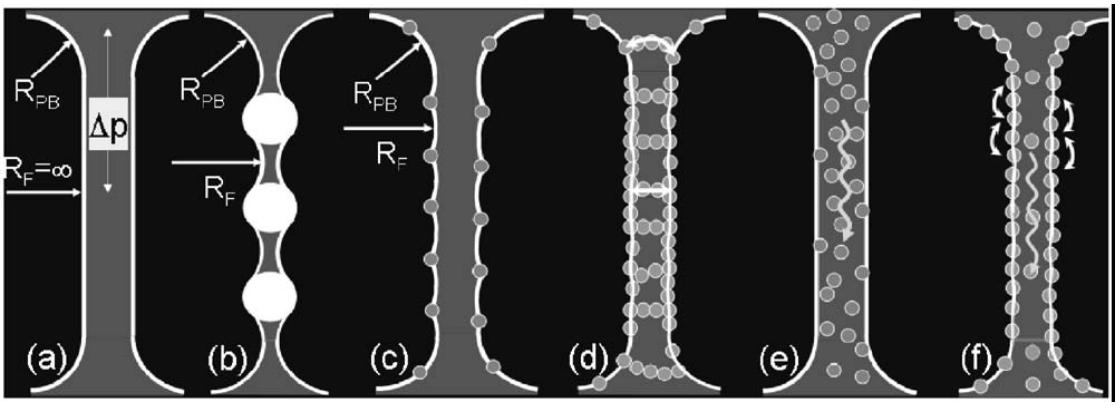

Figure 6.4. (a) Liquid film in a foam. (b–f) Different models for foam stability: (b) adsorbed particles bridged by film (c) interfaces modulated by adsorbed particles (d) particle layers on interfaces mechanically connected by bridges, (e) drainage reduction by particles arrow and (f) the model proposed by Haibel et. al. (Source: Haibel, et al. 2006)

Based on the above foam stabilization models, the effects of Ti6Al4V addition on the expansion and the stability of Al compacts will be discussed. The effects of average particle size on the maximum expansion and expansion values of Al compacts at constant particle weight percent (5 wt%) are shown in Figure 6.5. On the same graph, the average accumulative surface area of the particles is also shown. At low average particle sizes and high cumulative particle surface areas, the expansion and maximum expansion values of Ti6Al4V added Al compacts are relatively low, but increases with increasing average particle size after about 100 μm and/or with decreasing particle surface area. It is also noted that at high average particle size, because of reduced surface area, a reduced amount of reaction product is expected. Ti-particles are wetted by the liquid Al and therefore, the particles and reaction products are found within the cell edges and cell walls. The higher surface area of the smaller particle sizes naturally induces more reaction layer. Ti and the reaction product ($TiAl_3$) increase the apparent viscosity of the foaming compact. At small particle size, due to increased surface area and higher rate of $TiAl_3$ formation, the foam expansions are relatively low. At larger particle sizes, the reduced surface area of the particles and the amount of reaction product, increase the expansion of the compacts. The stability of Ti-added compacts is therefore matched to the model (e) given in Figure 6.4. This has also been confirmed microscopically as no particles found on the cell wall surfaces. It is further noted that, Ti6Al4V particles are also found within the cell walls forming local menisci as shown

in Figure 5.34 and therefore, the model (b) of Figure 6.4, may also be effective in the stability of Ti6Al4V added foams. However, the numbers of these particles are low and this effect is merely seen in foams of large particles.

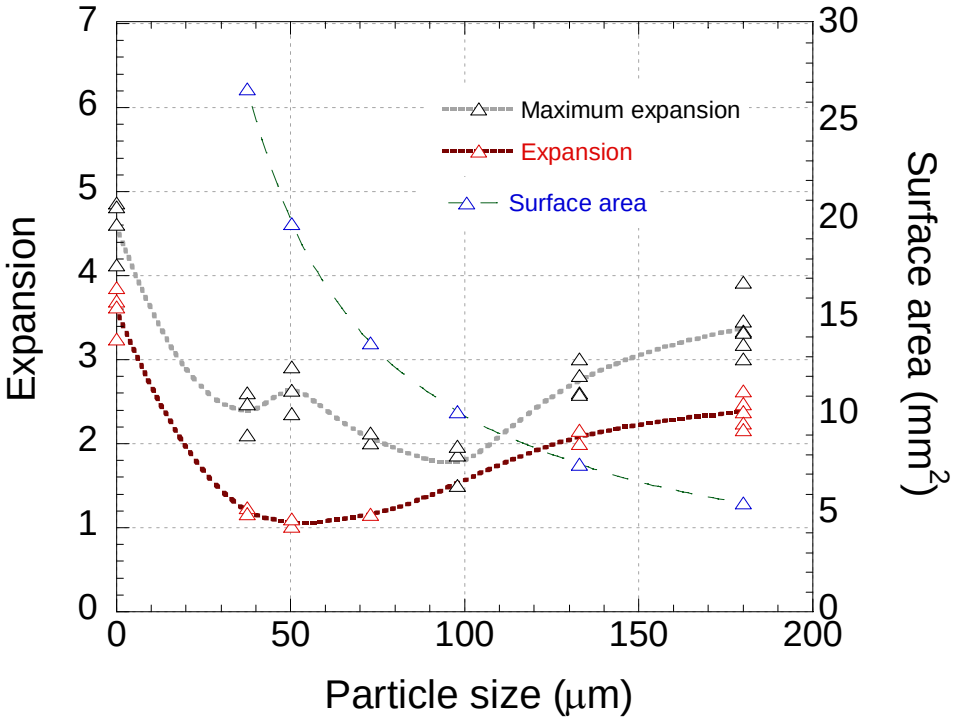

Figure 6.5. Expansions and cumulative surface areas of Ti particles vs. average particle size

The effect of the viscosity on the foaming properties of Al melts was previously studied. Wang and Shi (2003) investigated the effect of SiC (1, 7, 14 and 20 μm) and Al_2O_3 (3.5, 5 and 10 μm) particle addition in Alcan foam processing route. It was noted that, low concentration of large particles could not form an adequate coverage of cell surface hence lead to unstable foam, while high concentration of small particles increase the viscosity of the melt significantly so that the air injection could not foam the composite melt. Gergely and Clyne (2004) modeled the drainage in the standing foams of relatively thick cell faces. The model emphasized that the small initial cell size and high initial porosity level inhibited the drainage; the attention should be given to the rapid foaming processes and cell wall stabilization using a foaming agent that would oxidize the cell faces. The oxidized cell surfaces would reduce the surface viscosity and hence the drainage. Babcsan et. al. (2005, 2007) analyzed the stability of aluminum metal foaming processes ex-situ and in-situ. In foam prepared by Formgrip process, in foams of 13 μm SiC particles, the particles were observed to segregate to the cell

surface, while in foams of 70 μm SiC particles, only small amount of particles observed on the cell surface. The cell wall thicknesses were also found to be quite different: 85-100 μm in foams of 13 μm sized SiC particles and up to 300 μm in foams of 70 μm sized SiC particles. These show that the particle size range is important in stabilization of metal foams and in determining the thicknesses of the cell walls.

In Alporas foams, the size and volume of the oxide inclusions were predicted to be 1 μm and 1 vol%, respectively. For Cymat foam, the particle size and volume fraction for foam stabilization are above 1 μm and 1 vol%, while these are less than 1 μm and 1 vol% in Alporas and Alulight foams. It was also shown that the composition of the melt alloy was effective in particle distribution. Foaming of an AlSi0.8Mg0.8/10vol% Al_2O_3 melts in Alcan process produced thicker cell walls than the alloy contained lower Si/Mg ratio. In three different foaming processes, Cymat, Alporas and Alulight, the foamed alloys were considered by similarity, suspensions (50-100 μm), sols (micrometer size particles) and gels (nano sized particles), respectively. These alloys were foamed through external foaming (gas injection) or internal foaming (blowing agent). Results showed that internal foaming of Alporas alloy produced longer standing foams than Alulight metal alloy. In external foaming, Alcan metal showed the highest and Alulight metal showed lowest foam qualities.

It should be noted that the particles in the cell walls reduces the drainage but also introduces thicker cell walls. For the processing of lighter cell structures, one should consider high foam expansions, through partially wetted particles. The partially wetted particles segregate at liquid/gas interface and reduce the surface tension of the film and increase the surface viscosity. On the other hand, non-wetted particles like TiB_2 are not effective in increasing the foam stability although they increased the foam expansion.

The effect Ti-particle addition on the cell size of foamed Al compacts is shown in Figure 5.20.c for 160-200 μm particles. The particles reduce the foamability of the compacts reflected as the reduced number of cells formed and bigger cell size initially as compared with Al compacts. In Al compacts, the number of cells decreases significantly and the cell size increases greatly with increasing furnace holding time, while cell size and number of cells show small dependence to furnace holding time in Ti-added compacts. The reduced number of cells basically shows the reduced foamability, while the almost invariant cell size and number of cells shows increased

stability in Ti-added compacts. As stated earlier, the partially wetted particles are effective in preventing bursting of the cells by forming a cover on the surface of the cell wall, while in Ti-added compacts, only oxide remnants of the powder particles or oxide might form through oxidation might be found at liquid/gas interface. The initial powder used in the preparation of the powder compacts used for foaming experiments, contains thin oxide films which previously covered the surface of the metallic powder particles. The compaction process breaks oxide layer skin. These thin oxide films are converted to broken oxide filaments with a size between 4 and 100 nm with an average of 20 nm (Babcsan, et al. 2005).

It should be noted that the relative density of the compacts may have an important effect on the foam expansions. Low relative densities lead to early escape of the gas, resulting in lower expansions. The average relative densities of powder compacts foamed are listed in Table 4.3. The average relative density of Al compacts are about 1% higher than those of Ti6Al4V added compacts. The use of higher compaction pressures in Ti6Al4V-Al powder compaction resulted in compact failures. One sample was therefore prepared through hot compaction. The foam structure of the hot consolidated powder compact foam however showed good agreements with foams of cold consolidated powder compacts (Figures 5.33.a and 5.33.b).

6.4. Mechanical Behavior

The compression mechanical properties of foams are function of foam density and the material, which they are made of. Ti-added foams, similar to other closed cell foams, show collapse stresses, which increase with increasing foam density (Figures 5.37.a and 5.37.b). However, Ti-added foam samples showed lower collapse stresses than those of Al foam, as seen in Figures 5.37.b and 5.38.b. In the compression tests, relatively small size samples were used, 15 mm in diameter. A typical Ti/Al foam sample contained only 8-9 cells with a cell size of 3 mm. Al foams used for comparison had the diameter of 20 mm, containing more than 20 cells. Few studies on the effect of specimen size on the compression behavior of Al foams have been found in the literature. Andrews et. al. (2001) showed that Young Modulus and compressive strength of closed-cell Al foams (4.55 mm cell size) increased with relative sample size and reached a plateau level after the sample size of 6 and 5 cells, respectively. For bulk

compression properties, therefore, nearly 20 cells are required. Rakow and Waas (2005) further showed that the samples containing 18 or more cells showed bulk shear properties of Al foam. If the number of cells less than this critical number of cells, the measured compressive strength will be lower than that of the bulk foam. The reduced compressive flow stresses of Ti-added foams as compared with Al foams are likely to occur due to specimen size effect. In order to further verify the above, the collapse strength of Al foams produced by the same process is compared with the published ones. Wang et. al. (2005) reported the plateau stresses of Al foams 0.2 and 1.29 MPa for the foam densities of 0.11 and 0.22 g/cm^3. Mukai et. al. (1999) reported 1.5 MPa collapse strength for Alporas foam of 0.25 g/cm^3. For the present Al foams used for comparison had collapse stress of 1.24MPa at a foam density of 0.27 g/cm^3. Small discrepancies might arise between the collapse strength of foams produced using different methods and Al alloys.

6.5. Summary and Future Studies

Adding Ti6Al4V particles of various sizes into Al compacts showed reduced foamability, but increased stability at large particle sizes. For the particle sizes of 160-200 μm, the foams showed more homogenous cell size distribution and significant reductions in drainage. Several different studies however showed that foaming behavior is also function of foaming temperature. Yang and Nakae (2000) investigated the foaming behavior of liquid A356 Alloy with the addition of 0.5 to 4 wt% TiH_2 foaming agent at various temperatures. At low foaming temperatures, less than 630 °C, sufficient gas release for foaming did not occur while foaming at temperatures above 650 °C, resulted in rapid bubble coalescence. The optimum foaming temperature was given in the range of 630-650 °C for studied melt alloy. Duarte and Banhart (2000) showed experimentally that the optimum foaming temperatures for AlSi7 and Al6061 alloys were quite different. The effect of foaming temperature, therefore, should be investigated on the foaming behavior of Ti-added Al powder compacts.

Other parameters that might affect the foamability include the volume fractions and the sizes of Ti particles added. It was shown in this thesis that, at lower volume fractions of 30-45 μm particles, the foam expansion increased and reached to the expansion values of Al compacts. The effect of particle volume fractions should

therefore be further investigated through systematical microscopic studies. Currently, the lowest particle size of Ti6Al4V powder available is in the range of 30 μm. These powders are produced by melt atomization process. The lower sizes of the powder may be produced through ball milling of the atomized powders and used in Al compact foaming with smaller size Ti6Al4V particles.

The lower compression strength of the foam produced should be also subjected to further investigations by preparing larger size specimens. $TiAl_3$ precipitates would be expected to produce stronger cell walls and this should be cleared out. In an attempt, larger size Ti6Al4V compacts were prepared through hot compaction process. These compacts will be foamed for the extraction of larger test specimens.

The oxygen content of the starting powders should be measured in order to assess more accurately the effect of oxide skin remnants of the powder on the compact expansion and foaming stability. This may help to differentiate the expansion and stability of powder compacts contributed merely by the addition of Ti6Al4V particles. In addition, the size and the amount of the reaction product ($TiAl_3$) should be determined as a function of foaming temperature and furnace holding time. In a separate experimental study, the increased viscosity of the Al melt with addition of Ti6Al4V particles at a constant temperature as function of the time may be determined. This may give useful information about the variation of the melt viscosity with the amount of the reaction products, which may later be used in the optimization of the foaming of Al compacts with Ti6Al4V particle addition.

Finally, the effect of relative density differences between Al and Al/Ti6Al4V compacts on the foaming behavior should be further investigated with the use of one of the hot consolidation methods.

CHAPTER 7

CONCLUSIONS

The foaming behavior of 30-200 μm size Ti6Al4V particles added Al powder compacts was investigated. The compacts were prepared at various compaction pressures to give final relative densities of ~97%. In order to determine the effect of particle-addition on the foaming behavior of Al compacts; Al compacts without particle addition prepared with the same method were also foamed. Foaming experiments were performed using an in-situ foam expansion measuring system at 700-730 ºC. Small compression test samples were further core drilled from foamed Ti6Al4V-Al compact samples and tested at quasi-static strain rates. The results of compression tests were compared with those of Al compact foams without particle addition. Followings are concluded:

1. The linear expansion measurements showed agreement with previous studies on the similar Al compacts. In-situ expansion measurements were also in agreement with the ex-situ expansion measurements on the same Al compacts.
2. Al compacts showed the characteristic expansion-time curve, composing of 4 distinct regions: slow rate of expansion in solid state, followed by a higher rate of expansion after melting of the compact till maximum expansion, a reduced expansion region following the maximum expansion and finally a constant expansion region.
3. The expansion of 5 wt% Ti6Al4V added compacts was relatively low at small particle sizes, 30-45 μm, 45-56 μm and 56-90 μm, and increased with increasing particle size till 160-200 μm. At highest particle size, Ti6Al4V added compacts showed expansion-time graphs, similar to Al compacts, but with lower expansion values.
4. Foam expansions on 30-45 μm size Ti6Al4V-added compacts with various weight percentages of particles showed that when the wt% of particles lower than 2wt%, the expansion behavior of the compact became very similar to that of Al compact.
5. Microscopic studies have shown that Ti6Al4V addition reduced the drainage as compared with Al compacts without particle addition.

6. In foaming of Ti6Al4V-Al powder compacts, the liquid Al reacted with Ti6Al4V particles and formed $TiAl_3$ particles. The size of these particles varied with the size of the initial Ti6Al4V particles, but in the range of 1- 10 μm. In small size particle-added foams (30-45 and 45-56 μm) $TiAl_3$ particles dispersed through cell walls and cell edges, but with increasing particle size, these particles were found next to the Ti6Al4V particles.

7. The reduced drainage and lower foam expansions in the foaming of Ti6Al4V-added compacts were discussed based on the foam stabilization models in the literature. Ti6Al4V particles and the reaction product of $TiAl_3$ increased the apparent viscosity of the foam; hence, reduced the flow of liquid metal from cell wall surfaces to plateau borders. The reduced foamability of the compacts in small particle size Ti6Al4V addition was attributed to the relatively high viscosities, due to the higher cumulative surface area of the particles and higher rate of reaction between liquid Al and Ti6Al4V.

8. In comparison with Al compacts, 160-200 μm Ti6Al4V-added compacts showed lower number of cells with relatively smaller cell sizes and showing a more stable foaming process.

9. Compression tests conducted on the small sized samples of foamed Ti6Al4V-added compacts showed lower compression stresses than those of Al compact foam samples tested previously. The lower compression strength measured in Ti6Al4V-added foams was attributed to the small specimen sizes, which could not show the bulk mechanical properties.

REFERENCES

Andrews, E. W., Gioux, G., Onck, P. and Gibson L. J. 2001. Size effects in ductile cellular solids. Part II: experimental results. *International Journal of Mechanical Sciences* 43(3): 701-713.

Andrews, E. W., Huang, J. S. and Gibson, L. J. 1999. Creep behavior of a closed-cell aluminum foam. *Acta Materialia* 47(10): 2927-2935.

Asavavisithchai, S., and Kennedy, A. 2006. The effect of Mg addition on the stability of Al–Al2O3 foams made by a powder metallurgy route. *Scripta Materialia* 54: 1331-1334.

Asavavisithchai, S., and Kennedy, A. 2006. Effect of powder oxide content on the expansion and stability of PM-route Al foams. *Journal of Colloid and Interface Science* 297: 715-723.

Asavavisithchai, S., and Kennedy, A. 2006. The effect of compaction method on the expansion and stability of aluminium foams. *Advanced Engineering Materials* 8(9): 810-815.

Babcsan, Moreno, F. G., Leitlmeier, D. and Banhart, J. eds. 2006. *Solidification and Gravity Iv: Liquid-metal foams - feasible in-situ experiments under low gravity:* Zurich-Uetikon: Trans Tech Publications Ltd.

Babcsan, N., Leitimeier, D. and Banhart, J. 2005. Metal foams - high temperature colloids - Part I. Ex situ analysis of metal foams. *Colloids and Surfaces a-Physicochemical and Engineering Aspects* 261(1-3): 123-130.

Babcsan, N., Leitlmeier, D., Degischer, H. P. and Banhart, J. 2004. The role of oxidation in blowing particle-stabilised aluminium foams. *Advanced Engineering Materials* 6(6): 421-428.

Babcsan, N., Moreno, F. G. and Banhart, J. 2007. Metal foams - High temperature colloids - Part II: In situ analysis of metal foams. *Colloids and Surfaces a-Physicochemical and Engineering Aspects* 309(1-3): 254-263.

Banhart, J. 2000. Manufacturing routes for metallic foams. *Jom-Journal of the Minerals Metals & Materials Society* 52(12): 22-27.

Banhart, J. 2000. Manufacture, characterisation and application of cellular metals and metal foams. *Progress in Materials Science* 46(6): 559-U3.

Banhart, J. 2003. Aluminum foams: On the road to real applications. *Mrs Bulletin* 28(4): 290-295.

Banhart, J. 2006. Metal foams: Production and stability. *Advanced Engineering Materials* 8(9): 781-794.

Banhart, J., Baumeister, J. and Weber, M. 1996. Damping properties of aluminium foams. *Materials Science and Engineering a-Structural Materials Properties Microstructure and Processing* 205(1-2): 221-228.

Baumeister, J., Banhart, J. and Weber, M. 1997. Aluminium foams for transport industry. *Materials & Design* 18(4-6): 217-220.

Baumeister, J. and Schrader, H. 1992. Methods for Manufacturing Foamable Metal Bodies. *US Patent* No.5151246.

Baumgartner, F., Duarte, I. and Banhart, J. 2000. Industrialization of powder compact foaming process. *Advanced Engineering Materials* 2(4): 168-174.

Beals, J. T. and Thompson, M. S. 1997. Density gradient effects on aluminium foam compression behaviour. *Journal of Materials Science* 32(13): 3595-3600.

Duarte, I. and Banhart, J. 2000. A study of aluminium foam formation - Kinetics and microstructure. *Acta Materialia* 48(9): 2349-2362.

Duarte, Mascarenhas, J., Ferreira, A. and Banhart, J. eds. 2002. *Advanced Materials Forum I: the evolution of morphology and kinetics during the foaming process of aluminium foams*. Zurich-Uetikon: Trans Tech Publications Ltd.

Esmaeelzadeh, S., Simchi, A. and Lehmhusc, D. 2006. Effect of ceramic particle addition on the foaming behavior, cell structure and mechanical properties of P/M AlSi7 foam. *Materials Science and Engineering* 290-299.

Gama, B. A., Bogetti, T. A., Fink, B. K., Yu, C. J., Claar, T. D., Eifert, H. H. and Gillespie, J. W. 2001. Aluminum foam integral armor: a new dimension in armor design. *Composite Structures* 52(3-4): 381-395.

Gergely, V. and Clyne, B. 2000. The FORMGRIP process: Foaming of reinforced metals by gas release in precursors. *Advanced Engineering Materials* 2(4): 175-178.

Gergely, V. and Clyne, T. W. 2004. Drainage in standing liquid metal foams: modelling and experimental observations. *Acta Materialia* 52(10): 3047-3058.

Gibson, L. and Ashby, M. F. eds. 1997. *Cellular Solids: Structure and Properties*. Cambridge. Cambridge University Press 2nd ed.

Gibson, L. J. 2000. Mechanical Behaviour of Metallic Foams. *Annual Reviews Material Science* 30: 191-227.

Guden, M. and Yuksel, S. 2006. SiC-particulate aluminum composite foams produced from powder compacts: foaming and compression behavior. *Journal of Materials Science* 41(13): 4075-4084.

Haibel, A., Rack, A. and Banhart, J. 2006. Why are metal foams stable?. *Applied Physics Letters* 89(15).

Hanssen, A. G., Langseth, M. and Hopperstad, O. P. 1999. Static crushing of square aluminium extrusions with aluminium foam filler. *International Journal of Mechanical Sciences* 41(8): 967-993.

Helfen, L., Baumbach, T., Pernot, P., Cloetens, P., Stanzick, H., Schladitz, K. and Banhart, J. 2005. Investigation of pore initiation in metal foams by synchrotron-radiation tomography. *Applied Physics Letters* 86(23).

Javier Gil, F., Planell, J. A., Padras, A. and Aparicio, C. 2007. The effect of shot blasting and heat treatment on the fatigue behavior of titanium for dental implant applications. *Dental Materials* 23(4): 486-491.

Jin, I., Kenny, L. D. and Sang, H. 1992. Stabilized Metal Foam Body. *U.S. Patent*. No.5112697.

Kaptay, G. 2003. Interfacial criteria for stabilization of liquid foams by solid particles. *Colloids and Surfaces a-Physicochemical and Engineering Aspects* 230(1-3): 67-80.

Kathuria, Y. P. 2001. Laser assisted foaming of aluminum. *Advanced Engineering Materials* 3(9): 702-705.

Kavi, H., Toksoy, A. K. and Guden, M. 2006. Predicting energy absorption in a foam-filled thin-walled aluminum tube based on experimentally determined strengthening coefficient. *Materials & Design* 27(4): 263-269.

Kavi, H., Yüksel, S., Tanoglu, M. and Guden, M. 2004. Crushing behavior of aluminum foam filled aluminum tubes. *Proceeding in 10th Denizli Material Symposium & Exhibition*. 14-16 April pp. 42-49.

Kennedy, A. and Asavavisitchai, S. 2004. Effects of TiB_2 particle addition on the expansion, structure and mechanical properties of PM Al foams. *Scripta Materialia* 115-119.

Kennedy, A. and Asavavisithchai., S. 2004. Effect of Ceramic Particle Additions on Foam Expansion and Stability in Compacted Al-TiH_2 Powder Precursors. *Advanced Engineering Materials* 6(6): 400-402.

Kenny, L. D. 1996. *Aluminium Alloys: Their Physical and Mechanical Properties: mechanical properties of particle stabilized aluminum foam*. Pts 1-3. Zurich-Uetikon: Transtec Publications Ltd.

Kitazono, K., Sato, E. and Kuribayashi, K. 2004. Novel manufacturing process of closed-cell aluminum foam by accumulative roll-bonding. *Scripta Materialia* 50(4): 495-498.

Kobashi, M. and Kanetake, N. 2002. Processing of intermetallic foam by combustion reaction. *Advanced Engineering Materials* 4(10): 745-747.

Kraynik, A. M., Loewenberg, M. and Reinelt, D. A. 1999. Foam Microrheology. *Proceeding in 15th Annual Meeting of the Polymer Processing Society (PPS)'s*. 1 September. Hertogenbosch (NL).

Kunze, H. D., Baumeister, J., Banhart, J. and Weber., M. 1993. P/M Technology for the Production of Metal Foams. *Powder Metallurgy International* 25(4): 182-185.

Leitlmeier, D., Degischer, H. and Flankl, H. J. 2002. Development of a foaming process for particulate reinforced aluminum melts. *Advanced Engineering Materials* 4(10): 735-740.

Miyoshi, T., Itoh, M., Akiyama, S. and Kitahara, A. 2000. ALPORAS aluminum foam: Production process, properties, and applications. *Advanced Engineering Materials* 2(4): 179-183.

Mukai, T., Kanahashi, H., Miyoshi, T., Mabuchi, M., Nieh, T. G. and Higashi, K. 1999. Experimental study of energy absorption in a close-celled aluminum foam under dynamic loading. *Scripta Materialia* 40(8): 921-927.

Mukai, T., Miyoshi, T., Nakano, S., Somekawa, H. and Higashi, K. 2006. Compressive response of a closed-cell aluminum foam at high strain rate. *Scripta Materialia* 54(4): 533-537.

Raj, R. E. and Daniel, B. S. S. 2007. Aluminum melt foam processing for light-weight structures. *Materials and Manufacturing Processes* 22(4): 525-530.

Rakow, J. F. and Waas, A. M. 2005. Size effects and the shear response of aluminum foam. *Mechanics of Materials* 37(1): 69-82.

Ramamurty, U. and Kumaran, M. C. 2004. Mechanical property extraction through conical indentation of a closed-cell aluminum foam. *Acta Materialia* 52(1): 181-189.

Ryan, G., Pandit, A. and Apatsidis, D. P. 2006. Fabrication methods of porous metals for use in orthopaedic applications. *Biomaterials* 27(13): 2651-2670.

Simone, A. E. and Gibson., L. J. 1997. Efficient structural components using porous metals. *Materials Science and Engineering a-Structural Materials Properties Microstructure and Processing* 229(1-2): 55-62.

Simone, A. E. and Gibson, L. J. 1998. Effects of solid distribution on the stiffness and strength of metallic foams. *Acta Materialia* 46(6): 2139-2150.

Song, Z. L., Ma, L. Q., Wu, Z. J. and He, D. P. 2000. Effects of viscosity on cellular structure of foamed aluminum in foaming process. *Journal of Materials Science* 35(1): 15-20.

Stanzick, H., Klenke, J., Danilkin, S. and Banhart, J. 2002. Material flow in metal foams studied by neutron radioscopy. *Applied Physics a-Materials Science & Processing* 74: 1118-1120.

Wang, D. Q. and Shi, Z. Y. 2003. Effect of ceramic particles on cell size and wall thickness of aluminum foam. *Materials Science and Engineering a-Structural Materials Properties Microstructure and Processing* 361(1-2): 45-49.

Wang, D. Q., Xue, W. W., Meng, X. J. and Shi, Z. Y. 2005. Cell structure and compressive behavior of an aluminum foam. *Journal of Materials Science* 40(13): 3475-3480.

Weaire, D. and Hutzler, S. 1999. *The Physics of Foams*. Oxford: Oxford University Press.

Wubben, T. and Odenbach, S. 2004. On the stabilization mechanisms in liquid metallic foams. *Proceedings in Applied Mathematics and Mechanics* 4: 270-271.

Yang, C. C. and Nakae, H. 2000. Foaming characteristics control during production of aluminum alloy foam. *Journal of Alloys and Compounds* 313: 188-191.

Yu, C. J., Eifert, H. H. Banhart, J. and Baumeister, J. 1998. Metal foaming by a powder metallurgy method: Production, properties and applications. *Materials Research Innovations* 2(3): 181-188.